Development and Applications of New Platforms for Electrochemical Sensors

by

Tanyu Wang

A dissertation submitted to the Graduate Faculty of
Auburn University
in partial fulfillment of the
requirements for the Degree of
Doctor of Philosophy

Auburn, Alabama
August 4, 2012

Keywords: electrochemical sensors, immunoassay,
molecularly imprinted polymers, bipolar electrochemistry

Approved by

Curtis Shannon, Chair, Professor of Chemistry
Christopher Easley, Assistant Professor of Chemistry
Wei Zhan, Associate Professor of Chemistry
Aleksandr Simonian, Professor of Material Engineering

Abstract

The primary goal of this dissertation is to develop electrochemical sensors based on novel platforms for applications in medical diagnostics, food safety, and environmental management. Attempts have been made to integrate recognition elements, including biological moecules and synthetic materials, with electrodes through various surface modification strategies, and achieve sensitive, selective, yet low-cost electrochemical sensors for protein quantitation and small molecule detection.

Chapter 1 presents a detailed literature review on electrochemical sensors and two types of recognition elements most commonly applied: biological molecules and synthetic materials. Specifically, the properties of aptamers, antibodies, and molecularly imprinted polymers (MIPs), their applications in electrochemical sensing, and the current stage of research are discussed in detail. Furthermore, a brief insight into bipolar electrochemistry and the suitability of employing bipolar electrode in electrochemical analysis is introduced.

Chapter 2 presents the development of an electrochemical proximity assay (ECPA). ECPA combines the proximity effect and the electrochemical method for detection of insulin. The detection principle and strategy for obtaining base-line level background are discussed. The model system, first generation of ECPA composed of aptamers, and the system with antibody-oligonucleotide conjugates are illustrated in depth.

Chapter 3 describes a MIP-based electrochemical sensor for chiral molecule recognition. The synthesis of MIP particles, characterization, and their incorporation with glassy carbon electrodes by conventional coating method are presented. The results for detection of (+)-catechin and its comparison with results obtained using LC-MS are discussed.

Chapter 4 presents a surface imprinting method for fabrication of MIP thin films on electronic transducers. This study employs the self-assembled monolayer technique and unique “click” chemistry for simple, yet efficient surface modification. Detailed fabrication process and applications of sensor in hydroquinone detection are provided.

Chapter 5 deals with the development of an electrochemical oxygen sensor based on ECL quenching in a bipolar format. The principles of bipolar electrochemistry, bipolar device fabrication, and ECL quenching are presented. The validation of using ECL quenching as a direct reporter of dissolved O_2 concentration is discussed.

Chapter 6 summarizes the findings of research. The recommended future work of projects is stated.

Acknowledgments

I would like to express my deepest gratitude to my advisor Dr. Curtis Shannon for being such a great mentor and a generous supporter during the entire course of my PhD research. His penchant for electrochemistry and surface science has been such an inspiration and encouraged a productive environment for creative research. His many thoughtful suggestions, both at scientific and personal level, will always be remembered in my entire professional career. I would like to offer my sincere gratitude for the incredible contributions from my committee members, Dr. Christopher Easley, Dr. Wei Zhan, Dr. ZY Cheng, and Dr. Aleksandr Simonian, in the direction of helpful insights and valuable suggestions for my research projects and for the preparation of this dissertation. Dr. Easley has been a constant source of support in providing important guidance for my research, especially for our collaboration project. He has been extremely helpful and encouraging to my professional development as well. Dr. Vince Cammarata is one of the best teachers during my graduate study at Auburn. I will always remember his dedication to teaching and remarkable ability to impart knowledge to the next generation. Dr. David Stanbury has been a very generous presence to provide instrumentation for square wave voltammetry. I would like to acknowledge Dr. Yonnie Wu for his support in providing valuable technical inputs for my research and his help in LC-MS. Dr. Anne Gorden has been very supportive in my research and provided many valuable collaboration opportunities. I would like to recognize the generous support and

patience from Dr. Rik Blumenthal for his guidance in administration. I also want to show my gratitude towards Dr. Michael Squillacote for his help in many aspects during my graduate study. I would not be where I am without his selfless devotion.

I have received so much support from the faculty, administration assistants, and friends at the Chemistry Department. My colleagues in our research group have been very helpful at various stages of my study at Auburn and I would like to thank each one of them, Dr. Tsunghsueh Wu, Dr. Anand Sankarraj, Dr. Chaokang Gu, Dr. Hongxia Zhang, Dr. Junhua Xin, Dr. Sridevi Ramakrishnan, Dr. Rajakumari Ramasamy, Ms. Weiping Li, Ms. Axline Sangapi, and Ms. Yajiao Yu. I would like to express my deep gratitude to Mr. Jiaming Hu, who deserves special mention for being such a great research partner and supporter in the ECPA project. I would like to pay tribute to all the other members in Dr. Easley's group, Dr. Joonyul Kim, Mr. Kennon Deal, Ms. Leah Goodwin, Ms. Cheryl DeJournette, and Ms. Jessica Crumbley, for their kind help and assistants.

I would like to thank my parents and family members for their generous support for my education ever since I was a kid. They have been one of the most important sources of encouragement and love. Last but not least, I am extremely grateful to my husband, Yuancheng Li, for his many sacrifices, unconditional love, and constant support during the years of my graduate study. I dedicate my work to all the ones I love and respect.

† These authors contributed equally.

* Corresponding author

Table of Contents

List of Tables

List of Figures

List of Schemes

CHAPTER 1

Introduction

1.1 Motivation for Research

Biomedical diagnostics and food quality control represent two of the major impacts on the quality of human life. Diagnostics depend on methods that can detect and quantify disease-related proteins and compounds, and food safety and quality depend on inspection and monitoring methods that can detect contaminants and nutrients. Until now, instruments involving gas chromatography with mass spectrometry (GC-MS) and liquid chromatography with mass spectrometry (LC-MS) are usually the methods of choice for detection and quantitation of analytes.[1-7] However, these analytical methods require expensive, bulky, and complicated instruments and need a separation step (GC, or LC) prior to detection. Therefore, the development and research of sensors are becoming one of the most popular scientific areas to increase efficiency and overall benefit for detecting and quantitation of analytes of interest.

Detection systems based on optical methods and electrochemical methods are most exploited in medical testing and food quality control.[8-15] However, the cost of optical sensors is impractically high for use in field, and measurements are sensitive to the environment, such as local light and weather conditions and certain contaminants presented in the sample. On the other hand, electrochemistry detection offers great signal stability, simple instrumentation, high sensitivity, and ease of calibration, as well as

excellent compatibility with miniaturization technologies.[10,11] Hence, electrochemical sensors are considered as the ideal candidate in developing portable devices with high sensitivity and selectivity at reasonable cost.

1.2 Background of Electrochemical Sensors

A typical electrochemical sensor[10,16,17] comprises of a) recognition elements that specifically bind to the analyte; b) a transducer where a specific reaction takes place on the interface with recognition elements and gives rise to a signal; c) an electronic system that converts an electronic signal to a meaningful parameter describing the process being investigated and presents final results through an interface to the human operator (Figure 1.1.).[10] A successful electrochemical sensor for the nonspecialist market should meet the following requirements:[10]

1. The recognition elements must be highly specific for the purpose of the analysis, stable under normal storage and show acceptable variation between assays.

2. The reaction should be independent of physical conditions such as convection, pH and temperature.

3. The response should be rapid, precise, reproducible, clear, and linear over the relevant concentration range. It should be capable of measuring unprocessed samples, such as human blood or urine.

4. The complete sensor should be low-cost, compact, small, portable, and easy to operate.

Designed for the purpose, one crucial aspect of building electrochemical sensors is the choice of electrochemical detection technique that provides simple, rapid, and

specific measurements of the reaction of interest.[18] Typically in electrochemical detection, the reaction under investigation would either generate a measurable current (amperometric), a measurable potential or charge accumulation (potentiometric), or measurably alter the conductive properties of a medium (conductometric) between electrodes.[10,19] Conductometric technique is based on the current flow established by migration of ions of opposite charge, when an electric field is applied between two electrodes immersed in the electrolyte solution.[20] This transduction is the least sensitive among three main electrochemical techniques. Since conductivity is additive, it is impossible to discriminate between two ions. Moreover, if the concentration of one ion is very high, it could foul others.[21,22] Potentiometry is based on potential difference created across a membrane placed between two solutions with charged species of different activity.[20] Potentiometric sensors are suited for measuring low concentration in small sample volume because they do not chemically influence a sample.[19,23-25] Amperometry continuously measures current generated from the oxidation or reduction of an electroactive species in a sample.[10] It is the most widely used technique since the oxidation or reduction potential of a particular analyte is its intrinsic property.[20] In general, if the current is measured at a constant potential, it is referred to as amperometry, and if the current is measured in a controlled range of potential, it is referred to as voltammetry.[19]

Sensitivity and selectivity are two other crucial aspects for the development of electrochemical sensors. Surface modification of electrodes by immobilizing recognition elements on the sensor substrates is a very efficient approach to reach enhanced current responses and obtain an interface with highly specific binding affinity to the desired

molecule.[26] The concept of surface modification of electrodes was introduced by Bard[27] and others[28-30] about 30 years ago for electrocatalysis purpose and has been highly developed over the years for applications in a wide range, such as energy storage,[31] bioelectronics,[32] and most importantly electrochemical sensors.[10,11,26] Typical recognition elements used in electrochemical sensors can be roughly divided into two categories: a) biomolecules, including enzymes, nucleic acids, antibodies and whole cells; b) synthetic materials such as cavitands[33] and molecularly imprinted polymers (MIPs). Of these, nucleic acids, antibodies, and MIPs are the focus of discussions here.

1.3 Antibodies and Aptamers as Recognition Elements

Biomolecules are most commonly used as recognition elements for sensors in detection and qualification of target molecules in clinical and biomedical speciments.[10,11,34] Antibodies have been mainly applied in immunoassays as bioreceptors for antigen binding.[35-37] Immunoassays typically employ dual antibodies as probes for target binding to increase specificity and sensitivity. Assay of this format is named the sandwich type immunoassays that currently play a central role in the analytical and regulatory communities. A famous example of this type is enzyme-linked immunosorbent assays (ELISA) (Figure 1.2.A). In ELISA, a layer of antibodies is pre-immobilized on a solid substrate. When a testing solution containing antigens flows across the surface, analytes can be captured by the antibodies absorbed on the surface and a secondary enzyme-linked antibody can bind the same antigen at another region. Color change or fluorescence will appear as a result of chemical reactions catalyzed by the linked enzyme. The utility of antibodies in molecular recognition offers excellent sensitivity, selectivity,

and stability.[36] In addition, with the success of sandwich immunoassays, there exists a large, commercially available library of antibody pairs against many targets.[38] Traditionally, the result of immunoassays is displayed as a color change that is only suitable in binary scenario indicating the presence or absence of analytes, such as a pregnancy test, but not for quantitative analysis. Precise analysis on the other hand, requires professional personnel and complicated testing procedures involving multiple washing steps. Even so, the dual-antibody recognition concept is highly valuable and has served as a guide to various alternative strategies in the past few years.[39-41] Proximity immunoassays such as proximity ligation assay (PLA)[42] can solve some of the major issues of traditional sandwich type immunoassays. PLA is one of the most simple-to-use and sensitive assay for protein detection and analysis of other biological targets (Figure 1.2.B).[43] It relies on simultaneous recognition of a target molecule by a pair of affinity probes in homogeneous solution and measurements are currently highly depended on fluorescence readout, which is not ideal for sensor development because of the high cost and drifting of experimental results.

Electrochemical techniques have attracted much attention because of their potential in building relatively compact device, capability of quantitation of analytes and ease of operation and result interpretation.[44,45] However, there are two major drawbacks when incorporate antibodies onto electrode surfaces to build electrochemical sensors: a) an electrochemically active label is necessary for generating electrical signal since most analytes cannot intrinsically act as redox partners in an electrochemical reaction. The labeling process for antibodies is inconvenient, expensive, and time-consuming;[35,36] b) the immobilization of antibodies on surfaces by conventional physical absorption can

cause random orientation and inefficient coverage, while other linking methods require difficult modifications to introduce functional groups for coupling reaction.[46]

The use of antibody-oligonucleotide conjugates[39,47] can overcome these two limitations. Antibody-oligonuleotide conjugates can be simply prepared by coupling antibodies with short nucleic acids using an All-In-One Conjugation Kit from Solulink.[38] Compared with antibodies, nucleic acids can be easily modified with a variety of molecules (methylene blue, ferrocene). That allows introduction of electrochemically active labels or functional groups (primary amine, thiol groups) that enable improved immobilization of conjugates on to electrodes at a reasonable cost.[48] Particularly, the introduction of thiol groups to the probes allows the use of well-developed self-assembled monolayers (SAMs) technique that has been proven to avoid random orientations of biomolecules on the surface, protect surface from nonspecific absorption, produce good surface coverage, and improve the overall quality of surface modification and sensor performance.[49] On the other hand, finding new molecules that mimic antibodies have also attracted increasing interests for bioanalytical applications.[48] Aptamers currently are one of the major alternatives.[50,51] Aptamers are short, single-stranded oligonucleotides that have been selected for high affinity against a target protein, small molecule, or even whole cells.[52] One of the main advantages of nucleic acid aptamers compared with antibodies is their in vitro selection procedure and chemical synthesis, while antibodies have to be produced in vivo, by immunizing animals.[48] These manufacturing procedures do not depend on a particular analyte and enable the use of nonphysiological conditions, such as relatively low or high temperature and pH, and do not require animals and cell lines.[48] Thus, aptamers are temperature stable, cost-efficient

and reusable. Furthermore, owning to the nature of nucleic acids, aptamers allow easy modification with various functional groups as mentioned previously. Finally, the size of aptamers is much smaller than that of antibodies, which helps to increase the binding efficiency on an electrode surface for fabrication of electrochemical sensors.[48]

1.4 Molecularly Imprinted Polymers (MIPs) as Recognition Elements

Although high sensitivity and selectivity can be achieved, the poor long-term chemical and physical stability of the antibodies or aptamers prevent their use in practical devices.[53] Therefore, a great effort has been made to replace biological receptors with synthetic counterparts as recognition elements in sensors. Of many approaches, the molecularly imprinting technique has become a powerful tool for the preparation of polymeric materials that have the ability to specifically bind a target molecule.[53-57] The concept of molecular imprinting was first introduced by Dickey[58] in 1949 as "purely synthetic materials with a memory for an imprint molecule", and the technique has been evolved intensively during the past 40 years. As the artificial recognition element, MIPs have several advantages over their biological counterparts, including their robustness, low cost, and ease of preparation. However, the development of MIPs-based sensors has suffered from low sensitivity and selectivity due to a lack of surface integration methods and swelling of pores inside the polymeric structures. Thus, MIPs have been widely used as recognition component for detection of small molecules in food safety management and environmental monitoring,[55,56] but rarely for biomedical applications.

The typical preparation of MIPs involves a) preassembly of template molecule and functional monomer; b) copolymerization with cross-linking monomers; c) removal of

template molecules from the polymer matrix and generation of the recognition sites complementary to the shape, size, and functionality of the template molecule (Figure 1.3.).[55] There are two distinct approaches for molecular imprinting because the prepolymerization complex between template molecule and functional monomers can be formed either through noncovalent interactions or covalent couplings. The covalent approach developed primarily by Wulff[59,60] utilizes template species with covalently attached polymerizable functionality. Owing to the greater stability of covalent bonds, covalent imprinting method should provide a higher yield in binding sites and a more homogeneous population of binding sites with reduced nonspecific adsorption[59,61] compared with noncovalent protocols. However, because removal and rebinding of target molecules require chemical cleavage of the supporting covalent bonds and reformation of the cleaved covalent bonds within the cavities, the kinetics of the process is rather slow. Moreover, successful covalent imprinting requires the bonds of the functional groups with the template to be cleavable under relatively mild conditions. This necessity of covalent coupling restricts the applicability of this approach just to templates with functional groups that can be converted to readily cleavable derivatives, such as boronic ester and ketals.[62] On the other hand, the noncovalent imprinting method established by Mosbach[63] employs weak intermolecular interactions for template directed prearrangement of complementary functional groups. The formation of noncovalent template-monomer complexes via mainly hydrogen bonding is achieved by equilibrating the template molecules with an excess of suitable functional monomers in solvents. Template removal from the imprinted sites can be accomplished conveniently by extraction with competing solvents owning to the reversible nature of the functional

monomer-template interactions. Noncovalent imprinting approach is more flexible in terms of the choice of functional monomers, possible target molecules, and the use of the imprinted materials. Moreover, it is more similar to natural processes in the sense that most biomolecular interactions are noncovalent in nature.[55,62] Therefore, it is currently the most commonly used approach for the preparation of MIPs. Nevertheless, because of the need of excess functional monomers to achieve appreciable levels of template-monomer complexes, nonspecific interactions within the polymeric matrix are a big concern due to random incorporation of interactive functional groups outside the imprinted cavities.

In the past few decades, a number of read-out methods for MIP-sensors, including piezoelectric,[64-66] optical,[67-69] and electrochemical[20,56,70] methods have been developed. Given the electrochemical sensors available in the market, electrochemical approaches are considered as the easiest and most economic way to fabricate a commercial MIP-sensor. The adaption of MIPs onto signal transducers is a key aspect in the development of electrochemical MIP-sensors since the efficiency of integration of MIPs onto electrode surfaces directly affects the sensitivity of the sensor.[55,71] The conventional approach requires the preparation of a MIP monolith that needs to be grounded and sieved to particles after solution polymerization. Then the polymeric particles are deposited on the electrode surface as close as possible and stabilized with an agarose gel.[72] However, for sensing layers using particulate MIPs, the sensor response time is closely related to the particle size, which generally led to slow kinetics due to the random particle sizes of a wide range up to 50 μm[73] obtained via crushing and intraparticle diffusion. Moreover, the stabilizing agent generates a high diffusion barrier that leads to slow binding

accessibility.[57] In addition, the grinding process yields a particle matrix with low density of recognition sites that severely sacrifices binding capacity and sensitivity.[73-75] New integration strategy most frequently used to date is direct preparation of the recognition element as a film on the electrode surface. The grafting of MIP films onto an electrode surface could offer improved communication between the binding events happening within the polymeric matrix and the electrical transducer, thus overcome some of the limitations associated with the conventional coating method and achieve good site accessibility and faster mass transfer.[57,76] One promising approach is to deposit MIP films via electropolymerization process in the presence of target molecules.[53,77] This method is an efficient way to fabricate a molecularly imprinted layer on the electrode surface, and the film thickness can be easily controlled by changing the charge capacity of deposition. In order to obtain an electrochemical response efficiently, conducting polymers were often used to construct the MIP film on electrodes. Although conducting polymers could increase the sensitivity of the sensor, they would also contribute a large current response even in the case of a non-MIP electrode prepared in the absence of target molecules, thus result in a high limit of detection.[54] The use of SAMs to immobilize monomers, cross-linkers, or initiators onto a transducer surface followed by surface polymerization is another attractive pathway for direct grafting of MIP films on electrodes. This type of approaches has attracted a lot of attentions because SAM systems are very well-developed, allow surface characterization, and are compatible with many surface patterning strategies.[78,79] Typically, surface modification with functionalized monolayers is accomplished by the chemical modification of the surfactant prior to the self-assembly step. This procedure could lead to low yields and limited applicability because of the

complicated organic synthesis involved.[57] Of many work searching for alternative and more versatile chemistry to modify surface, “click” chemistry has attracted great interest. The concept of “click” chemistry was introduced by Sharpless[80] in 2001 and is defined as a set of reactions that are modular, wide in scope, require simple conditions, give high yields, and generate only inoffensive byproducts that can be removed by nonchromatographic methods. The first use of “click” chemistry to modify a well-defined electrode surface using the classic azide alkyne Huisgen cycloadditions was reported by Chidsey[78] in 2004. In Huisgen 1,3-dipolar cycloadditions, azide and acetylenes are convenient to introduce, do not react among themselves, and show excellent tolerance of other functionalities. Triazole formation is irreversible and quantitative that allows easy surface characterization. Moreover, this reaction benefits from an extremely mild and regioselective copper (I)/sodium ascorbate catalyst system that is insensitive to solvent and pH. Thus, “click” reactions, especially the Huisgen cycloaddition reaction, provide a general and robust way of surface modification. To date, “click” chemistry has been widely adapted in surface fuctionalization[81] and polymer grafting[82] applications. Therefore, the combination of “click” chemistry and molecular imprinting technique would offer an extremely easy, yet efficient way to graft MIP films on electrode surface for fabrication of electrochemical MIP-sensors with improved sensitivity.

1.5 Sensors Based on Bipolar Electrochemistry

Typically, electrochemical sensors are constructed based on a three-electrode configuration, which consists of a working electrode, an auxiliary electrode, and a reference electrode. The potential of the working electrode is controlled using a

potentiostat with respect to that of a reference electrode, and the faradaic current measured in the circuit connecting the working electrode is a direct reporter of the rate of electrochemical reactions of interest.[83] Because of the requirement of direct electric contact and an electrochemical cell with three-electrode setup, traditional electrochemical detections usually make use of just a single working electrode for sensing of a single analyte, and are difficult to be adapted into miniaturized systems, such as microfluidic devices.[84,85] In the past few years, the emerging and developing of bipolar electrochemistry attract a lot of interests. The use of bipolar electrodes can overcome most of the limitations associated with the traditional electrochemical configuration. A bipolar electrode (BPE) is referred to an electronic conductor in contact with an ionically conductive phase.[83] When a sufficiently high electric field is applied across the ionic phase, different electrochemical behaviors can be observed at the surface of BPE, oxidation on one side, and a simultaneous reduction on the other side (Figure 1.4.).[86,87] In the experimental configuration of bipolar electrochemistry, a conductive material is located inside a channel with no external connection, and a simple power supply applies a potential difference, E_{tot},[87] between two driving electrodes situated in pools at both ends of the channel. The majority of E_{tot} is dropped within the channel because of the high electrolyte solution resistance, and the fraction of E_{tot} dropped across the length of BPE is defined as ΔE_{elec}.[87] A particular position (χ_0) along the BPE where the potential of the solution is equal to the potential of the bipolar electrode (E_{elec}) divides the BPE into two poles: a cathodic pole, where the solution potential is higher than E_{elec}, and an anodic pole, where the solution potential is lower than E_{elec}. The difference in potential between the electrode and the solution at each lateral position is the driving force leading to an

electrochemical reduction or oxidation respectively, and this value varies linearly across the BPE surface.[83,87] ΔE_{elec} represents the total driving force available to couple the two faradaic reactions at both poles of the BPE. It increases with the increase of the length of BPE according to the equation shown in Scheme 1.1.[83] The current density at the BPE mainly depends on: a) the overpotential available at each location at the electrode/solution interface, and b) the kinetics of the redox couples involved in the faradaic processes. Therefore, the value of E_{tot} required to induce faradaic reactions varies depending both on the species present in solution and on the length of the BPE. For most of the results reported in literature, E_{tot} is in the range of 20-30 V and never exceed 100 V.[83] Thus, inexpensive power supplies are sufficient to carry out many different kinds of interesting experiments with BPEs.

Although the phenomenon of bipolar electrochemistry has been known for over 40 years[86] and widely applied in battery technologies,[88] for electrosynthesis,[89,90] in solar cells,[91-93] and for surface modification with gradients of various materials[94-96] over the past decade, BPE is still a technique with a rather young history in the field of electroanalytical chemistry. The main advantage of BPEs for analytical purpose is the ease of controlling their potential: a simple power supply or even a battery, and no direct electrical contact. These features make it possible to integrate a large array of BPEs into a portable or a microfluidic device for simultaneous detection of multiple analytes at low cost.[83] However, the lack of direct connection is also a drawback due to the difficulty of measuring current flowing through the BPE. Three main approaches for current readout have been developed for detecting electroactive analytes in microfluidic environments using BPEs. One attractive method is to induce bipolar behavior between two electrodes

by taking advantage of a split electrode design[97] that makes it possible to directly measure current passing through the BPE. But the compromise of this design is complicating the detection system with an external electrical connection (Figure 1.5.A).[83,97] A second method relies on electrodissolution of the BPE itself.[98] Specifically, a layer of silver metal is deposited onto the anodic pole of the BPE prior to detection. When a cathodic sensing event occurs, the silver begins to dissolve by oxidation. Based on the charge neutrality in the bipolar system, the amount of oxidized silver corresponds to the number of electrons transferred at the cathodic pole of the BPE (Figure 1.5.B).[83,98] However, this topic is still being underinvestigated, and just one literature[98] was found till now. A powerful alternative strategy for detecting faradaic processes at BPEs is to use electrogenerated chemiluminescence (ECL) as an indirect reporter of the current (Figure 1.5.C).[99,100] ECL is a highly developed and sensitive detection protocol that has been used for a variety of analytical applications.[101,102] This approach eliminates the need of an external connection to the BPE, and the direct detection of ECL just requires a CCD camera, which is a very convenient way for collecting information continuously on the processes occurring at the BPE. Because ECL does not require an excitation light source, it is generally better than fluorescence for low-cost and simple sensor systems. Moreover, because the ECL reactions only occur close to the surface of an electrode, the interrogated volume can be limited to a small value that is ideal for making portable and micro devices. Therefore, the combination of ECL with BPE opens up the possibilities of using optical detection approach to quantify faradaic current for a much broader range of applications.

A well-known ECL system uses $Ru(bpy)_3^{2+}$ as the light-emitting species and a co-reactant, such as sodium oxalate ($Na_2C_2O_4$). $Ru(bpy)_3^{2+}$ based ECL has been widely used in analytical purpose due to its excellent stability, good water solubility, and high sensitivity.[102] The mechanism of $Ru(bpy)_3^{2+}$ based ECL have been intensively studies and most of the analytical applications are based on "oxidative-reductive" ECL.[103] Specifically, $Ru(bpy)_3^{2+}$ is first oxidized to $Ru(bpy)_3^{3+}$, which further reacts with the $CO_2\cdot^-$ radical anion to generate $Ru(bpy)_3^{2+*}$, as shown in Scheme 1.2. When $Ru(bpy)_3^{2+*}$ decays to the ground state, a red light will emit. The intensity of the emitted light is used as indicator for the sensing event. Specific DNA detection at the cathodic pole of BPE reported indirectly by the intensity of ECL generated at the anodic pole of BPE has been reported for several times.[83,85] On the other hand, detection of analytes based on ECL quenching is also a very useful sensing strategy.[101] Although detection of analytes, such as DNA detection through hybridization using photoluminescence quenching,[104] has been widely reported, the investigation of ECL quenching has been very limited. A variety of compounds, such as phenols,[105] hydroquinones,[105] $Fe(CN)_6^{3-}$,[106,107] $Fe(CN)_6^{4-}$,[106,107] and O_2,[108] have been reported for their excellent characteristics for photoluminescence quenching of $Ru(bpy)_3^{2+}$ via energy-transfer or charge-transfer mechanism. These well-established ECL quenchers can be incorporated into different designs and assays as reporters for target sensing, such as DNA labels for specific DNA detection.[101] As an alternative, they can also serve directly as the analyte for ECL quenching, such as the monitoring of dissolved O_2 concentration for food processing and waste water management. Because the quenching event happens at the same pole of BPE with ECL, this approach would provides a more direct measurement compared with those relies on

electroneutrality at the two poles of BPE. Moreover, the reactions at the anodic pole can be simple reactions such as oxygen reduction or hydrogen evolution. Therefore, the ECL quenching method coupled with BPE is believed to provide a flexible and simple platform for sensing applications ranging from medical diagnostics and food quality management.

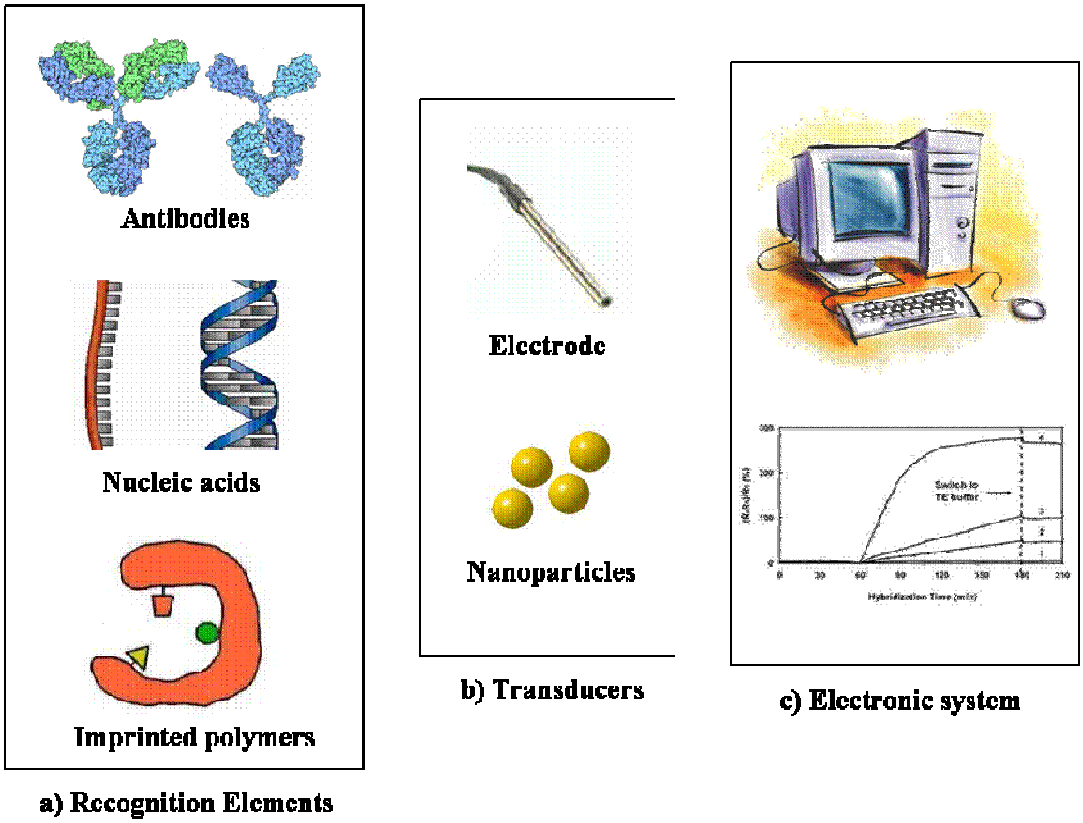

Figure 1.1. Components of a typical electrochemical sensor.[10,16,17] Adapted from ref. 10.

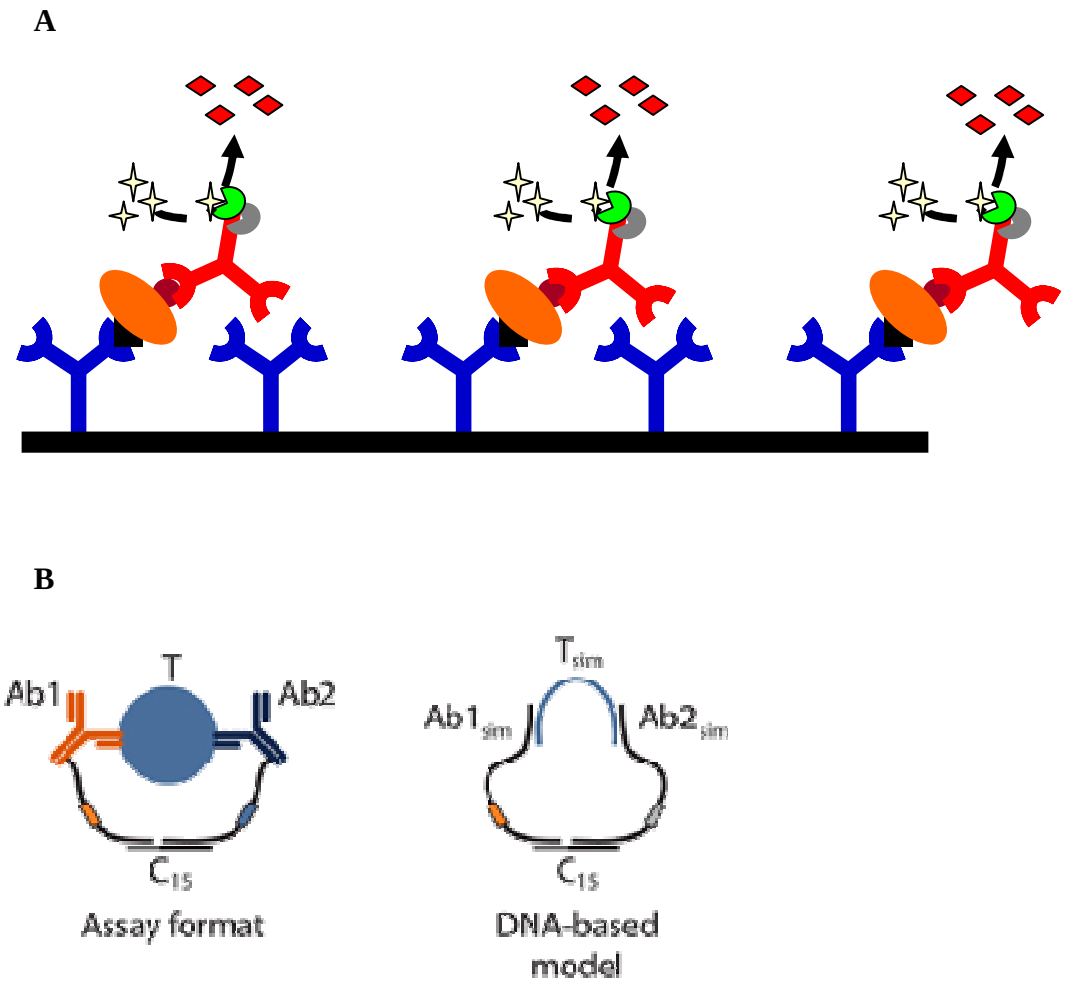

Figure 1.2. (**A**) Schematic representation of the sandwich type ELISA. (**B**) Schematic representation of PLA.[43] Reprinted with permission from ref. 43. Copyright © (2010) American Chemical Society.

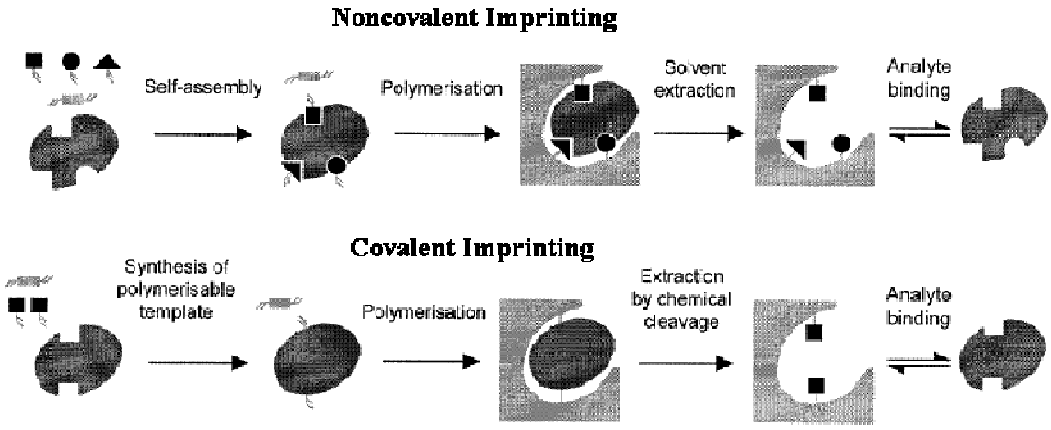

Figure 1.3. Schematic representation of covalent and noncovalent molecularly imprinting procedures.[55] Reprinted with permission from ref. 55. Copyright © (2000) American Chemical Society.

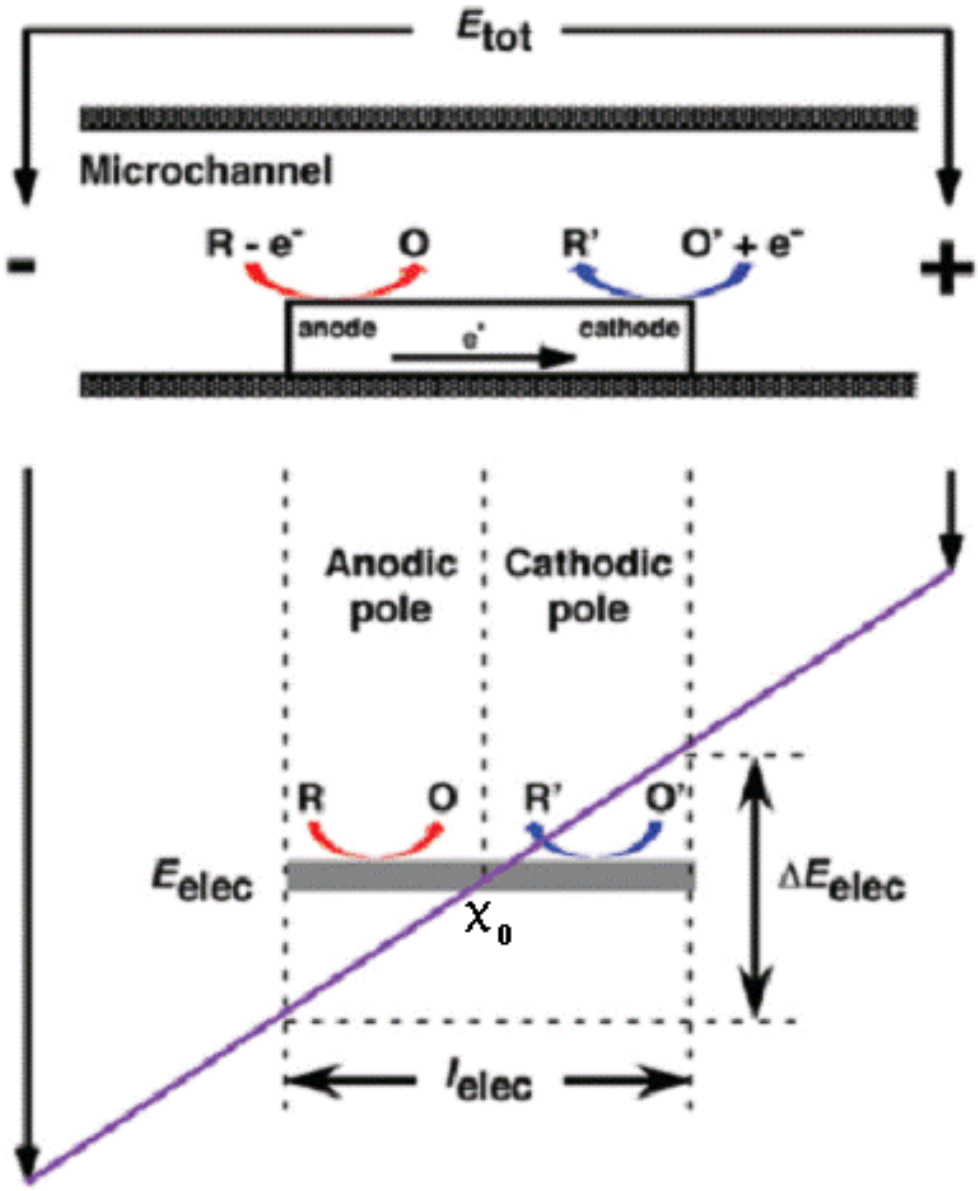

Figure 1.4. The experimental configuration of bipolar electrochemistry.[87] Reprinted with permission from ref. 87. Copyright © (2009) American Chemical Society.

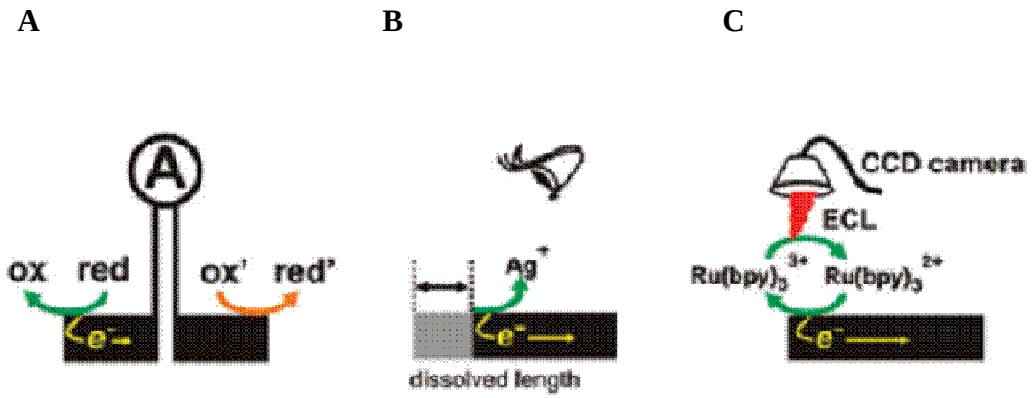

Figure 1.5.[83] Approaches used to measure faradaic current at bipolar eletrodes (BPEs): (**A**) direct measurement of current passing through BPEs with an external electrical connection based on a split electrode design;[97] (**B**) sensing method using Ag electrodissolution;[98] (**C**) sensing strategy using electrogenerated chemiluminescence (ECL) reporting.[99,100] Reprinted with permission from ref. 83. Copyright © (2010) American Chemical Society.

Scheme 1.1.[83]

$$\Delta E_{elec} = \frac{E_{tot}}{l_{channel}} l_{elec}$$

Scheme 1.2.

$$Ru(bpy)_3^{2+} - e^- \longrightarrow Ru(bpy)_3^{3+}$$

$$C_2O_4^{2-} - e^- \longrightarrow C_2O_4^{\cdot -}$$

$$C_2O_4^{\cdot -} \longrightarrow CO_2^{\cdot -} + CO_2$$

$$Ru(bpy)_3^{3+} + CO_2^{\cdot -} \longrightarrow Ru(bpy)_3^{2+*} + CO_2$$

$$Ru(bpy)_3^{2+*} \longrightarrow Ru(bpy)_3^{2+} + h\nu$$

Chapter 2

Quantitation of Protein at Femtomolar Levels via Direct Readout with the Electrochemical Proximity Assay

This project is the collaboration with the group of Dr. Christopher Easley. Jiaming Hu and I contributed equally in this work.

2.1 Introduction

Diagnostics is one of the most critical steps in health care and medical treatment.[109] Specific protein detection is of great importance in this realm, since it is currently one of the predominant methods to diagnose the onset or progression of disease states.[110,111] Unless specialized point-of-care assays are available for the protein of interest, quantitation is typically performed in a centralized laboratory by technicians.[112] This process is expensive and could waste time that is critical to patient care. Over the years, clinical approaches for point-of-care testing have addressed this challenge for select analytes,[113-117] yet these assay formats are highly specialized to the particular target molecule, thus inflexible to apply to other targets. To keep pace with expectations in future point-of-care testing, there is a need for more flexible, yet highly sensitive, quantitative, and easy-to-use methods.[112]

Although point-of-care devices are welcome in clinical and research laboratories, the existence of surrounding infrastructure places fewer constraints on methodology. Based on their inherent flexibility, sandwich enzyme-linked immunosorbent assays (ELISA) have emerged as the method of choice for protein quantitation in clinical and research laboratories.[111] Unfortunately, these heterogeneous assays require expert users with dedicated instrumentation, and they are time-consuming, laborious, and expensive. Quantitative, point-of-care protein analysis is thus not possible with standard sandwich ELISA formats. Nonetheless, the flexibility of the dual-antibody recognition concept is highly valuable and has served as a guide to various alternative strategies in recent years.[39-42,47,118,119]

Proximity immunoassays such as the proximity ligation assay (PLA)[42,47] or the molecular pincer assay[39] can overcome some of the limitations of ELISA. PLA, for example, is one of the most simple-to-use and sensitive protein assays developed to date.[43] The assay is homogeneous (no washing steps), and detection limits rival or outperform ELISAs, even with much smaller sample volumes. A key concept in PLA is the "proximity effect," which relies on simultaneous recognition of a target molecule by a pair of affinity probes. The bound probes can then be covalently linked by enzymatic ligation of their oligonucleotide tails, and qPCR is used as the readout, with products proportional to target protein concentration. PLA has been shown functional with aptamer pairs[42] and with a variety of antibody pairs.[47] Although nucleic acid aptamers have garnered significant attention in the analytical and biosensing communities based on their many potential advantages,[120-126] the use of aptamers as affinity probes in PLA is severely limited. PLA requires two aptamers binding at separate sites on the same protein

target, but aptamer pairs unfortunately do not yet exist against most targets. In PLA[47] or in the pincer assays,[39] this limitation was overcome by employing antibody-oligonucleotide conjugates as probes, since the popularity and success of sandwich methodology (ELISA, Western blots) has afforded a large, commercially available library of antibody pairs against many proteins. These assays thus provide simpler and less expensive alternatives to ELISA.

Nonetheless, limitations in current proximity assays impede their use in a point-of-care setting. Although the use of qPCR gives PLA its high sensitivity, this readout requires that each sample be added to a tube with ligation and PCR reagents, and then be inserted into a qPCR instrument followed by 1-2 hours of amplification and analysis. The molecular pincer assays are simpler and more rapid (<20 min), making them more amenable to point-of-care measurements by fluorescence readout; however, the limit of detection of these assays is several orders of magnitude higher than PLA. Thus, there is a need for a more sensitive yet simpler readout for proximity assays that is amenable to point-of-care testing.

Electrochemical detection is of particular interest in the development of biosensors because it offers great signal stability, simple instrumentation, high sensitivity, and ease of calibration compared to fluorescence, as well as excellent compatibility with miniaturization technologies.[44,45] Here, we present the marriage of the proximity assay concept with electrochemical detection to give a simple, highly sensitive, flexible strategy for specific protein quantitation, termed the electrochemical proximity assay (ECPA). ECPA uses the proximity effect to move an electrochemically active label, methylene blue (MB),[127] closer to a gold electrode upon binding of two probes to a

protein target, an approach akin to electrochemical DNA sensing[52,128] or specialized aptamer-based protein sensing[129-131] reported by others. In the presence of protein targets, the redox current in ECPA is quantified using square wave voltammetry (SWV) and is found to depend directly on the concentration of target. This detection strategy is based largely upon pioneering work by the Plaxco group,[132-136] in using MB-labeled DNA for biosensing. Building upon this work and on aptamer-based protein sensing by Zhang et al.,[131] we have added the antibody-based proximity assay concept. We used a DNA-based experimental model to optimize signal-to-background ratios, ultimately providing a direct insulin detection limit that is lower than most commercially available ELISAs, with a dynamic range >40-fold wider than these ELISAs. These results were achieved with direct electrochemical readout, i.e., without requiring washing steps, which bodes well for the future of ECPA in point-of-care settings. In contrast to other approaches for electrochemical protein sensing,[124,130] ECPA should be useful for any protein with available antibody pairs.

2.2 Experimental

2.2.1 Materials and Reagents

All solutions were prepared with deionized, ultra-filtered water (Fisher Scientific). The following reagents were used as received: insulin antibodies (clones 3A6 & 8E2; Fitzgerald Industries), 4-(2-hydroxyethyl)-1-piperazineethanesulfonic acid (HEPES) (99.5%), tris-(2-carboxyethyl) phosphine hydrochloride (TCEP), (Sigma-Aldrich, St. Louis, MO), bovine serum albumin (BSA, 98%; EMD Chemicals Inc), human thrombin, immunoglobulin E (IgE), and insulin (Sigma Aldrich). Methylene blue-conjugated DNA

(MB-DNA) was purchased from Biosearch Technologies (Novato, CA), purified by RP-HPLC. Oligonucleotides were obtained from Integrated DNA Technologies (IDT; Coralville, Iowa), with purity and yield confirmed by mass spectrometry and HPLC, respectively. Sequences (listed 5' to 3') for aptamer based ECPA were as follows. Thrombin aptamer A (THRaptA): AGTCCGTGGTAGGGCAGGTTGGGGTGACTT-TTTTTTTTTTTTTTTATATTTTT-TTTTCTCGCGGATTTGAACCCTAACG; Thrombin aptamer B (THRaptB): TAGGAAAAGGAGGAGGGTGGGATTGGTGTGT-GTTTTTTTTTTTTTTTTTTTTTTTTTTTTTTTTTGGTTGGTGTGGTTGG. Sequences (listed 5' to 3') for antibody- based ECPA were as follows. Insulin antibody arm 1 (AbArm1): /5AmMC6//iSp18/CCCACTTAAACCTCAATCCACGCGGATTTGAACC-CTAACG; Insulin antibody arm 2 (AbArm2): TAGGAAAAGGAGGAGGTGGCCCAC-TTAAACCTCAATCCA/iSp18//3AmMC6/. Sequences of ssDNA strands used in the experimental model are given in Table 2.1.

2.2.2 Preparation of the Electrode and DNA Monolayer Assembly

ECPA sensors for the model system, for thrombin detection, and for insulin detection were fabricated using a gold working electrode (Bioanalytical Systems Inc., r = 0.75 mm). The gold electrode was polished carefully to a mirror surface with an aqueous slurry of 0.05 μm diameter alumina particles and then successively washed in an ultrasonic cleaner with water. The electrode was then immersed into fresh piranha solution (H_2SO_4/H_2O_2, 3:1) for 5 minutes, rinsed with D. I. water, and dried under a stream of nitrogen gas. (*Caution: piranha solution is dangerous to human health and should be used with extreme caution and handled only in small quantities*). Finally, the

gold electrode was electrochemically polished by scanning the potential from -0.5 to 1.5 V in 0.1 M H_2SO_4 at a scan rate of 0.1 V s^{-1} for 50 cycles. The cleaned gold electrode was thoroughly washed with D. I. water and ethanol and dried under flowing nitrogen.

Prior to modification of the electrode, 1 μL of 200 μM thiolated-DNA and 1 μL of 200 μM MB-DNA were each separately mixed with 2 μL of 10 mM TCEP in two 200-μL PCR tubes. These tubes were incubated for 90 min at room temperature (21 °C) for reduction of disulfide bonds in the thiolated-DNA and to reduce the MB-moeity of the MB-DNA. Both of these solutions were then diluted to a total volume of 200 μL in HEPES/$NaClO_4$ buffer (10 mM HEPES and 0.5 M $NaClO_4$, pH 7.0)[52] to a final concentration of 1 μM. Unless otherwise noted, all solutions used in the experiments to follow were carried out at pH 7. For immobilization, the previously cleaned gold electrode was transferred directly to the diluted and reduced thiolated-DNA solution and incubated for 16 h at room temperature in the dark. Following the formation of a self-assembled monolayer (SAM), excess thiolated-DNA physically adsorbed on the electrode surface was removed via a room temperature-deionized water rinse (~ 20 s). For all assay strategies employing the competitor DNA strands (most formats listed below), this same process was followed, except after reduction by 10 mM TCEP, the reduced thiolated-DNA solution was diluted to a total volume of 200 μL in HEPES/$NaClO_4$ buffer and incubated with 2 μM competitor DNA sequence (C9) for 60 min at room temperature in the dark. For immobilization in competitor systems, the cleaned gold electrode was transferred directly to this equilibrated thiolated-DNA/competitor solution then incubated for 16 h at room temperature in the dark.

2.2.3 ECPA Probe Assembly and Electrochemical Measurements

Electrochemical measurements were performed using an Epsilon electrochemistry workstation (Bioanalytical Systems, Inc.) with a standard three-electrode configuration consisting of a Ag|AgCl(s)|KCl(sat) reference electrode (Bioanalytical Systems, Inc.), a homemade platinum gauze flag (0.77 cm^2) counter electrode, and a gold working electrode. All potentials are reported relative to the saturated Ag|AgCl reference electrode. Electrochemical measurements were performed in HEPES/$NaClO_4$ buffer using square wave voltammetry (SWV) with a 50 mV amplitude signal at a frequency of 60 Hz, over the range from -0.45 V to 0.00 V versus Ag|AgCl reference. The characteristic voltammetric peak of MB was detected by SWV at -210 mV (vs Ag/AgCl). MB was chosen as the redox tag due to its excellent shelf life and robust electrochemical response in serum compared to other redox tags, such as ferrocene.[52,129] The electrochemical response of each sensor was measured as follows: (1) reference and measurement SWV data sets were collected; (2) both raw data sets were smoothed using a 21-point boxcar function and baseline corrected (all data corrected with B-spline generated baseline in Origin 8 using two regions: -0.40 V to -0.35 V and -0.08 V to 0.00 V); and (3) difference traces were generated. Signal (with target) and Background (no target) voltammograms were treated in this manner and are presented as difference traces. To prepare calibration graphs and calculate standard deviations, traces were integrated from -0.330 to -0.100 V. In the case of the aptamer-based system, we report the average of three measurements, while in the case of the antibody-based system the average of two measurements is reported.

Model System Strategy 1 – Decreasing binding affinity by reducing the number of complementary bases. The electrode was modified as described above and was placed into a glass electrochemical cell with HEPES/$NaClO_4$ buffer. Three different thiolated DNA sequences, G5, G7, and G10 (Table 1), were used in Strategy 1 of the model system. In this way, the affinity of thiolated DNA and MB-DNA were adjusted through changes in the number of complementary bases between them. For modeling signal, the sensor was immersed in 10 nM ECPA-loop and 15 nM MB conjugated DNA sequences in 3 mL HEPES/$NaClO_4$ buffer. For modeling background, the sensor was immersed in 15 nM MB conjugated DNA in 3 ml HEPES/$NaClO_4$ buffer. Both signal and background currents were measured at the 15-min time point.

Model System Strategy 2 – Use of a short DNA competitor. The electrode was modified as described above and was placed into a glass electrochemical cell with HEPES/$NaClO_4$ buffer. Three different competitor DNA sequences, C7, C8, and C9, were used in Strategy 2 of the model system (Table 2.1). The sensor was allowed to equilibrate in 3 ml HEPES/$NaClO_4$ buffer with various concentrations of competitors for 6 h. For modeling background in the competitor systems, redox current was measured at each 10 min of the first hour, then at 90 and 120 min. Once C9 was chosen, 1:3, 1:7, 1:10, and 1:25 molar ratios of MB-DNA:C9 were tested at a fixed concentration of 15 nM MB-DNA.

Aptamer-based ECPA system. The sensor was allowed to equilibrate in 3 ml HEPES/$NaClO_4$ buffer with 100 nM C9 for 6 h. Thrombin aptamers (THRaptA and THRaptB) were first folded by heating to 95 °C and cooled rapidly by immersion in ice water to promote intramolecular interactions. Thrombin of various concentrations (from

50 pM to 50 nM) was incubated with folded 10 nM THRaptA and 15 nM THRaptB in HEPES buffer for 90 min prior to measurements. The thrombin/aptamer incubations were then added into the glass electrochemical cell. Before conducting voltammetric measurements, the sensor surface was allowed to react with analytes for 90 min. Selectivity tests with other proteins (IgE, insulin, or BSA), were made under the same conditions.

Antibody-based ECPA system. The sensor was equilibrated in 500 µl HEPES/$NaClO_4$ buffer with 300 nM C9 for 6 h. Prior to measurements, HEPES/$NaClO_4$ buffer was supplemented with 0.5% BSA (to minimize antibody adsorption), 10 nM Ab1, 10 nM Ab2, 10 nM MB (for background measurements), and various concentrations of insulin (from 128 fM to 2 nM). Before conducting voltammetric measurements, the sensor surface was allowed to react with analytes for 40 min. Selectivity tests were performed in the same manner by substituting 2 nM C-peptide or insulin-like growth factor 1 (IGF-1) for insulin.

2.2.4 Preparation of Antibody-Oligonucleotide Conjugates

The antibody-oligonucleotide conjugates used in the insulin ECPA, AbArm1-3A6 and AbArm2-8E2, were prepared by conjugating AbArm1 to insulin antibody 3A6 ($K_d \approx$ 1 nM) and AbArm2 to insulin antibody 8E2 ($K_d \approx 0.1$ nM), respectively (antibodies obtained from Fitzgerald Industries). Conjugation reactions and purification steps were accomplished using an Antibody-Oligonucleotide All-In-One Conjugation Kit (Solulink), according to the manufacturer's instructions. Briefly, the oligonucleotides were first activated with sulfo-S-4FB, and their quantities and qualities were confirmed using

absorbance, specifically $A_{260\ nm}$ of unmodified activated oligonucleotides and the $A_{260\ nm}$ to $A_{360\ nm}$ ratio after the modification of activated oligonucleotides. Antibodies were also activated with S-HyNic. Activated oligonucleotides and antibodies were then mixed and incubated at room temperature for 2 h. Once the conjugation reaction was stopped, conjugates were further purified from excess 4FB-oligonucleotides and unmodified antibodies using the supplied magnetic affinity matrix. The final concentrations of the conjugates were determined by the Bradford protein assay. AbArm1-3A6 and AbArm2-8E2 were synthesized with 45 % and 86% recovery from the initial amount of antibodies (100 µg).

2.3 Results and Discussion

2.3.1 Signal and Background in ECPA

The principle of the electrochemical proximity assay (ECPA) is shown in Figure 2.1. The sensor is prepared by self-assembly of thiolated DNA strands onto a gold electrode via the alkanethiol moiety at the 5' terminus. The quantitative capacity of ECPA stems from cooperative hybridization of the five-part complex shown in Figure 1: thiolated DNA – DNA conjugated antibody 1 – target protein – DNA conjugated antibody 2 – MB conjugated DNA. The five-part complex forms a circular structure on the sensor surface through proximity-dependent hybridization of the thiolated DNA and MB-DNA, which is the step that brings MB close enough to the gold electrode surface for electrochemical current enhancement. This process results in a quantity of electrons transferred from MB to the electrode that is proportional to the original amount of protein analyte ("signal"), albeit with some analyte-independent current generated by hybridization of thiolated

DNA and MB-DNA only ("background"). Although SWV does not differentiate signal and background currents, under optimized conditions, the signal will greatly exceed the background to allow highly sensitive, direct electrochemical quantitation of the protein analyte. Similar to what has been observed in PLA[42,43] or the molecular pincer assays,[39] signal enhancement over background in ECPA is based on the proximity effect; that is, the marked increase in the effective concentrations of the MB-DNA and thiolated DNA due to the simultaneous binding of the two probes to the same protein. This allows the MB-DNA/thiolated DNA interaction to be weak in the absence of protein ("background") yet strong in the presence of the protein ("signal"). Finally, it should be noted that the detection limits of proximity assays are often well below the K_d values of the individual probes, which can be attributed to the chelate-like effect of utilizing two probes in a cooperative fashion, often termed the "proximity effect."

Through binding equilibria, a fraction of thiolated DNA will always hybridize with the MB-DNA sequences, even in the absence of target analyte, resulting in target-independent hybridization, recruitment of MB to the gold surface, and an increase in current. A portion of this background current could also result from non-specific adsorption of MB-DNA to the surface, although our results suggest that specific binding is the major cause. The presence of this background current is obviously detrimental to the assay. We applied two strategies in attempt to lower the background using our model system, as discussed below.

2.3.2 DNA-Based Experimental Model of ECPA

As in the previous work of Easley's group with PLA,[43] here we utilized a DNA loop to model the probe-target complex in ECPA (Figure 2.2.A), making the assumption that probe affinity for the target protein is infinite. The 80-nucleotide DNA loop mimics formation of the ECPA complex, bringing MB near the gold surface and increasing redox current. Background was modeled using only the thiolated DNA and MB-DNA (Figure 2.2.A). This experimental model greatly simplified the optimization of experimental parameters. Since the surface-dependent ECPA involves a different type of cooperative complex formation compared to homogeneous PLA, we devised two new strategies for minimizing background in ECPA.

The first strategy was to decrease the binding affinity between thiolated DNA and MB-DNA by reducing the number of complementary bases in the thiolated DNA (Figure 2.2.B). The hypothesis was that the amount of background hybridization between thiolated DNA and MB-DNA would be greatly reduced, thereby reducing background current greatly without a large decrease in signal current. Figure 2.2.C compares the signal and background responses of the system with 5, 7, and 10 complimentary bases (G5, G7, and G10 strands). Comparing G10 to G7, as hypothesized, the background current was reduced by 2-fold while signal current was reduced by only 1.6-fold. Furthermore, compared to a background peak current of 54 nA with G10, it was indeed possible to reduce the background current to baseline using G5. However, the background reduction was accompanied by a large decrease in signal peak current from 104 nA down to 38 nA, since the weakened connection also weakened hybridization of the DNA Loop (model of signal).

In an attempt to reduce background without such a large signal reduction, our second strategy was to utilize a short DNA competitor with the G10 system. We hypothesized that when using a competitor sequence, background hybridization would occur more slowly than signal hybridization, since both signal and background complexes must displace the short competitor prior to current enhancement by the MB-DNA strand. Figure 2.3.A shows a representation of the delayed background formation over time, mediated by competition with competitor strands. This way, signal of similar magnitude to that in the N=10 case above should form rapidly, while background would be delayed kinetically by the competitor. Figure 2.3.B shows signal and background responses of the system with 7-, 8-, and 9-base competitors (C7, C8, and C9). As hypothesized, the hybridized competitor sequences blocked access of MB-DNA to the thiolated DNA, thereby slowing background formation. Figure 2.3.B shows that with C7 and C8, background currents of 47 and 24 nA were detected even 10 min after addition of MB-DNA, while no background was detected for as long as 40 min using C9. Since C9 allowed a 40-min time window for detection, we chose C9 as the competitor for further experiments. Upon addition of the Loop (model of signal), significant signal current of 81 nA was possible after 30 min, while C9 prevented background formation (Figure 2.3.C). Optimal conditions were determined to be 15 nM MB-DNA and 100 nM C9, and these were applied in the aptamer-based ECPA system, below.

2.3.3 Aptamer-Based ECPA

A schematic of aptamer-based ECPA is shown in Figure 2.4.A (upper right). Two thrombin aptamers (THRaptA, THRaptB) that bind thrombin at different sites were

applied as affinity probes, and competitor C9 was used to minimize background. Using conditions optimized by the model system, background levels were measured in the absence of target protein (human thrombin). Similar to the model system, background remained at baseline current for up to 90 min, after which an increasing peak current at -210 mV was detected, indicating that MB-DNA was beginning to displace the competitors. This 90-min detection window was actually wider than the 40-min window observed in the model system. This difference is attributed to the decreased diffusion coefficient[137] of the MB-DNA (40-bases; ~70 $\mu m^2\ s^{-1}$) when hybridized with THRaptB (120-bases; ~30 $\mu m^2\ s^{-1}$), which would slow the kinetics of the competitor displacement process by ~2.3-fold in comparison to the model system. This estimation agrees very well with the 2.25-fold increase in time required for background formation. The lower right plot in Figure 2.4.A shows the background with no thrombin (black trace) and a typical MB oxidation peak appearing at -210 mV (red trace) in the presence of 2.5 nM thrombin after the 90 min incubation. As expected, the saturated peak current at 10 nM thrombin (52 nA) was of lower magnitude than the model system (81 nA), which had assumed probes with infinite affinity. This aptamer-based ECPA system calibrated versus thrombin concentration (Figure 2.4.A, left plot), with sensor responses recorded in triplicate as integrated MB peak areas from -330 mV to -100 mV. ECPA was capable of detecting thrombin levels as low as 50 pM using a direct electrochemical readout, with a dynamic range up to 10 nM at these probe concentrations.

To demonstrate specificity, the aptamer-based ECPA was challenged with nonspecific proteins including human IgE, insulin, and BSA. Figure 2.4.B shows that essentially no response was observed in the presence of 10 nM insulin or IgE; even with

4-fold lower thrombin (2.5 nM), the signal was ~40-fold larger than that of IgE or insulin. In addition, baseline current was observed in the presence of 2% BSA, while the signal from 2.5 nM thrombin was recovered by 93% in 2% BSA. This result is encouraging for future application of ECPA to biological samples and point-of-care settings.

2.3.4 Antibody-Based ECPA

The flexibility of the aptamer-based approach is limited because of the requirement of two aptamers for the target protein, since aptamer pairs exist only for a few select proteins. As noted above, the use of antibody-oligonuceotide conjugates as probes can overcome this challenge.[39,47] With the success of sandwich immunoassays, there exists a large, commercially available library of antibody pairs against many proteins. As proof of concept that ECPA can be applied to a wide variety of protein targets, we show herein that insulin can be directly detected using two antibody-oligonucleotide conjugates as ECPA probes.

A schematic of antibody-based ECPA is shown in Figure 2.5.A (upper right), again employing the short DNA competitor strategy. With this new assay format, a different set of conditions were determined as optimal, including the addition of 0.5% BSA to reduce nonspecific antibody adsorption and a C9 concentration of 300 nM. Using 10 nM of each antibody-oligo and 10 nM MB-DNA, the assay showed a 40-min detection window before competitor began to be displaced by MB-DNA. Since the antibody-oligo conjugates will significantly alter the diffusion rates of most components, we did not expect the kinetics of signal and background formation to follow trends observed in the model system or aptamer-based ECPA; nonetheless, the detection time window was

similar to the other systems. The lower right plot in Figure 2.5.A shows the background with no insulin (black trace) and a typical MB oxidation peak appearing at -210 mV (red trace) in the presence of 2 nM insulin after 40 min. This antibody-based ECPA system was then calibrated versus insulin concentration (Figure 2.5.A, left plot), with sensor response recorded in triplicate as integrated MB peak areas from -330 mV to -100 mV. Remarkably, using a direct electrochemical readout, ECPA was capable of detecting insulin levels as low as 128 fM (7.43×10^{-4} ng mL^{-1}) with a dynamic range extending to 2 nM (11.6 ng mL^{-1}). The selectivity of antibody-based ECPA was tested against insulin-like growth factor 1 (IGF-1), which has similar structure to insulin, and against C-peptide, which is co-secreted with insulin into the bloodstream. As expected, the sensor did not respond to higher concentrations of either IGF-1 or C-peptide (Figure 2.5.B). The drastically improved performance of the antibody-based ECPA compared to the thrombin aptamer ECPA was expected, since the aptamer K_d values[138] are several orders of magnitude higher than the typical antibody K_d.

Finally, Table 2.2 shows a comparison of our antibody-based ECPA to commercially available sandwich ELISAs for insulin detection.[139-144] In order to facilitate equal comparison of the direct-readout ECPA with various heterogeneous ELISAs, the concentrations of insulin in the incubation solution of each ELISA is reported in Table 2.2. ECPA outperforms all of the kits in terms of assay dynamic range (from 43- to 312-fold wider range). The impresssive ECPA dynamic range of 15 600 (from 128 fM to 2 nM) should provide enhanced flexibility in sample preparation. Only one of the "ultrasensitive" versions of ELISA (25-µL sample volume) has an essentially equal detection limit (1.1-fold higher) compared to ECPA. Compared to "standard" ELISA kits,

ECPA shows between 15.6- and 60.9-fold lower limit of detection for insulin. In fact, using the noise level of the blank, the linearly extrapolated LOD for insulin was calculated to be 20 fM, lower than all ELISAs shown in Table 2.2. These performance improvements come with the additional benefit of a direct-readout format, making ECPA amenable to point-of-care analysis. To our knowledge, ECPA represents the highest performing direct-readout insulin assay reported to date. Looking toward future application in point-of-care insulin measurements in human serum, if we leverage the pioneering efforts of the Plaxco group using similar DNA-based electrochemical sensors,[52,128,132-136] it should be possible to detect a variety of proteins in undiluted serum. Of course, since the ECPA detection limit for insulin (128 fM) is over 400-fold lower than the normal human serum insulin levels (~60-80 pM), serum samples could be simply diluted to minimize interferences in this case.

2.4 Conclusions

In this paper, we describe the development of the electrochemical proximity assay (ECPA), which leverages two aptamer or antibody-oligonucleotide probes and proximity-dependent DNA hybridization to move a redox active molecule near a gold electrode. A DNA-based experimental model was used to optimize the assay format, and aptamer- and antibody-based ECPA were shown functional with high sensitivities and low detection limits, employing a short DNA competitor to limit background current. This background-reduced ECPA was shown to match or outperform currently used ELISA kits for insulin detection. Of particular importance is the proof-of-concept provided by antibody-based ECPA. Judging from the successes of other proximity immunoassays,[39,47] it is reasonable

to assume that ECPA should perform well in quantifying any other protein with an available antibody pair. Combining the assay's flexibility and high sensitivity with the simplicity of direct electrochemical readout, ECPA should be useful in a variety of settings in the future, including medical diagnostics, biological research, and point-of-care testing.

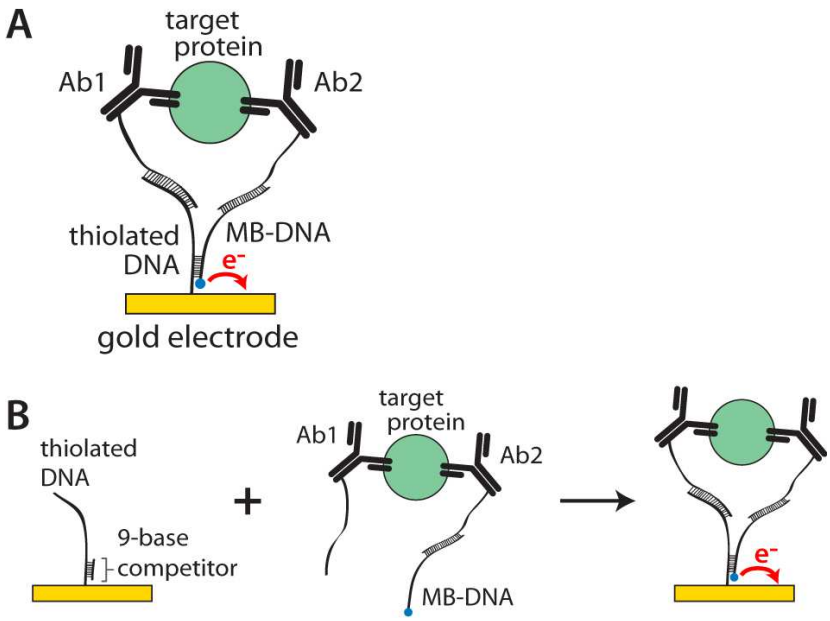

Figure 2.1. Principle of the electrochemical proximity assay (ECPA). In the presence of the target protein, this five-part complex moves the redox-active methylene blue (MB) near the gold surface, thus increasing current in proportion to the protein analyte. Depicted here are (**A**) the final, five-part cooperative complex and (**B**) the stepwise operation of the assay, in which the electrode with a pre-assembled DNA/competitor monolayer is immersed into a pre-mixed solution of EPCA probes (two Ab-oligos and MB-DNA) and target protein to generate current.

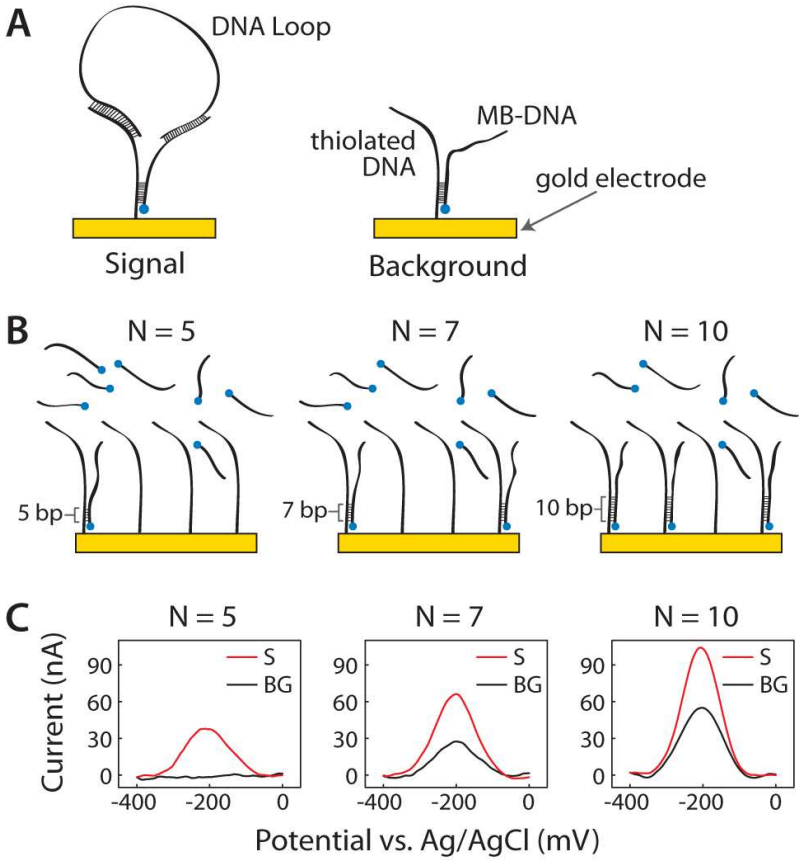

Figure 2.2. DNA-based model for ECPA. (**A**) A continuous DNA Loop is used to model the Signal complex shown in Figure 2.1. Background is modeled by simply adding MB-DNA without the Loop. (**B**) Depiction of Background reduction in Strategy 1. Fewer base pairs (weaker hybridization) between thiolated DNA and MB-DNA results in lower background current. (**C**) Experimental confirmation of Strategy 1, with both signal and background currents reduced in the voltammograms as the number of base pairs (N) is reduced. At N=5, background is minimized, but signal is reduced significantly.

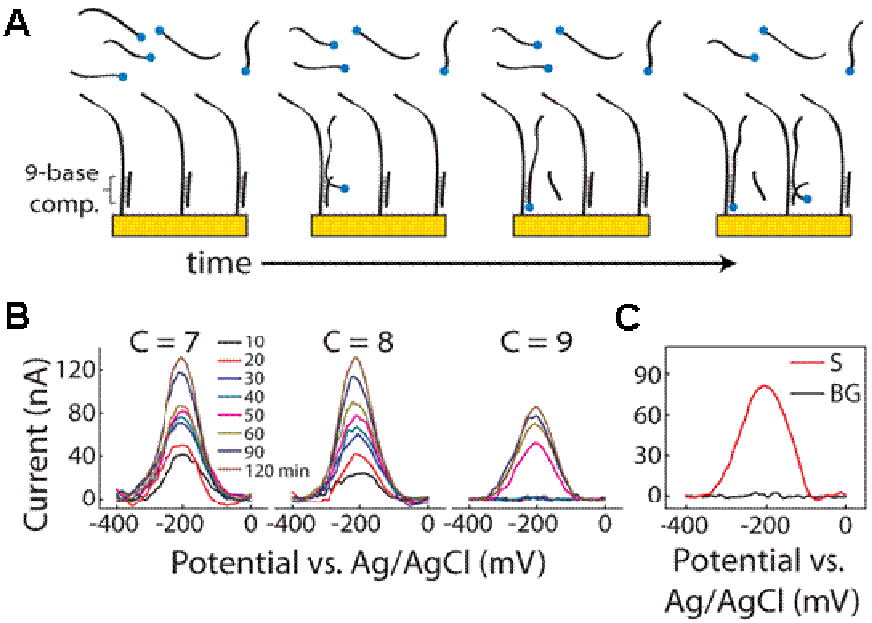

Figure 2.3. DNA-based model for ECPA. (**A**) Depiction of Background reduction in Strategy 2, where a competitor strand prevents or slows Background formation over a given time window. (**B**) Experimental confirmation of Strategy 2. The 9-base competitor (C9) was the only one to show baseline current for up to 40 min. (**C**) Signal and Background voltammograms are shown with C9 under optimal conditions, showing more than double the Signal current and equal Background current compared to N=5 from Strategy 1.

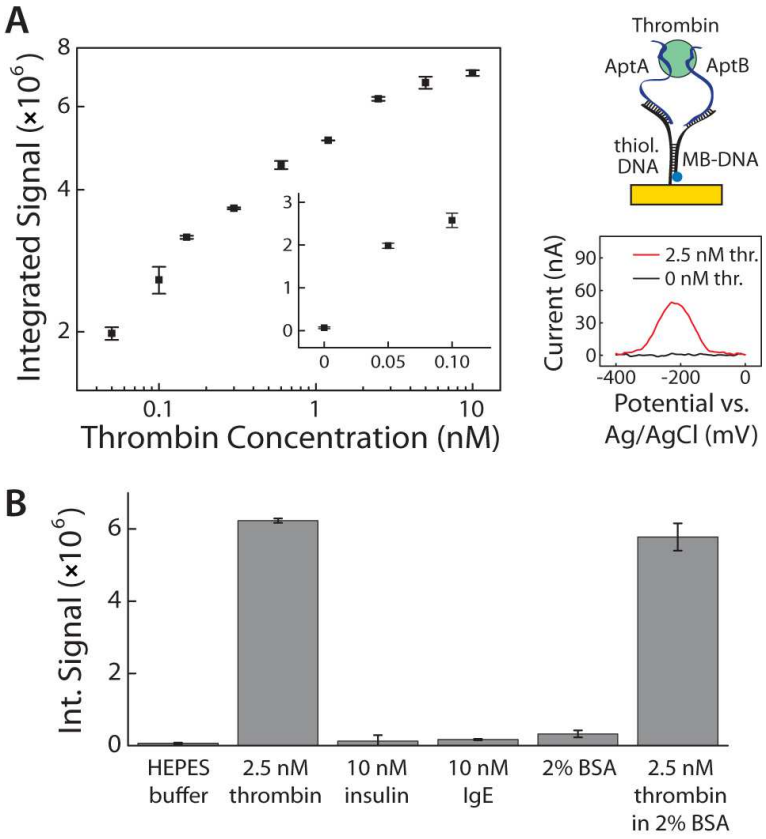

Figure 2.4. Aptamer-based ECPA. (**A**) With a direct readout, a human thrombin detection limit of 50 pM was achieved, with a dynamic range up to 10 nM. Upper right image shows the principle of the assay, with the lower right plot showing example voltammagrams for the blank (black) and in the presence of 2.5 nM thrombin (red). (**B**) The dual-probe assay shows high selectivity, as expected, with 93% recovery of signal in the presence of 2% BSA.

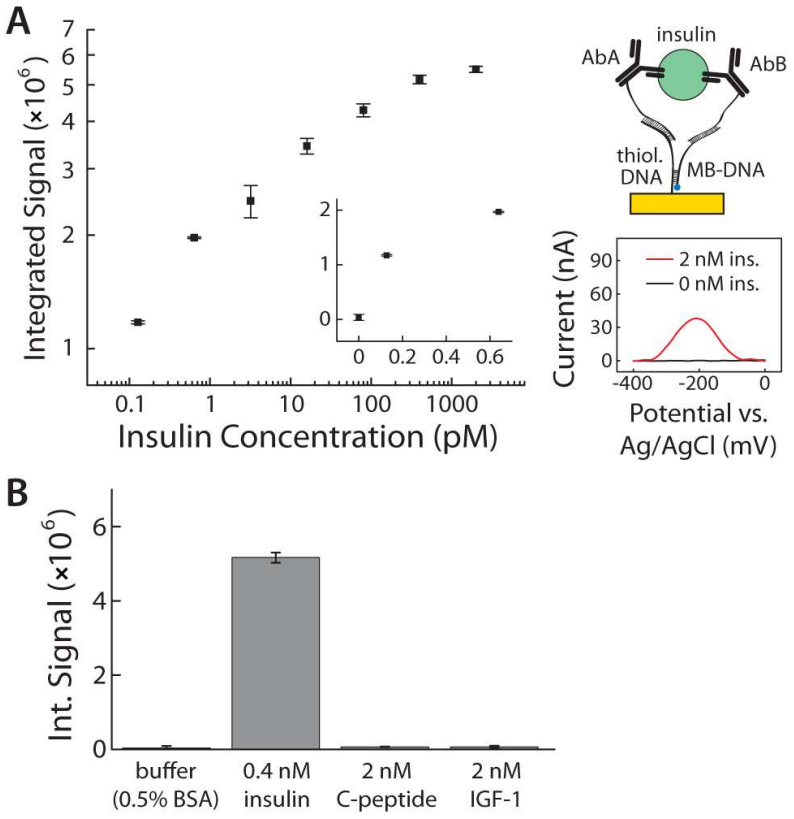

Figure 2.5. The success of antibody-based ECPA greatly improves the flexibility of the assay, since a large variety of protein targets could be quantified this way. (**A**) Insulin as low as 128 fM was detected with direct readout, with a dynamic range up to 2 nM. Upper right image shows the principle of the assay, with the lower right plot showing example voltammagrams for the blank (black) and in the presence of 2 nM insulin (red). (**B**) The dual-antibody assay also shows high selectivity, as expected.

Name (Abbreviation)	DNA Sequence, listed 5′ to 3′
ECPA-Loop (Loop)	TAG GAA AAG GAG GAG GGT GGC CCA CTT AAA CCT CAA TCC ACC CAC TTA AAC CTC AAT CCA CGC GGA TTT GAA CCC TAA CG
ECPA-MB-10 (MB-DNA)	CCA CCC TCC TCC TTT TCC TAT CTC TCC CTC GTC ACC ATG C /MB-C7/
ECPA-Gold-10 (G10)	/5ThioMC6-D/ GCA TGG TGA CAT TTT TCG TTC GTT AGG GTT CAA ATC CGC G
ECPA-Gold-7 (G7)	/5ThioMC6-D/ GCA TGG TAT TTT TCG TTC GTT AGG GTT CAA ATC CGC G
ECPA-Gold-5 (G5)	/5ThioMC6-D/ GCA TGA ATT TTC GTT CGT TAG GGT TCA AAT CCG CG
ECPA-Comp-9 (C9)	TCA CCA TGC
ECPA-Comp-8 (C8)	CAC CAT GC
ECPA-Comp-7 (C7)	ACC ATG C

Abbreviations: /MB-C7/ = methylene blue modification (Biosearch), /5ThioMC6-D/ = disulfide bond flanked by two six-carbon spacers (IDT)

Table 2.1. Single-stranded DNA sequences used in the ECPA model systems (strategies 1 and 2). MB-DNA, G10, and C9 were employed in the optimized detection system.

Assay	Analyte	LOD (fM)	Relative LOD (LOD_{ELISA} / LOD_{ECPA})	Dynamic Range	Relative Range ($Range_{ECPA}$ / $Range_{ELISA}$)	Citation
ECPA	human insulin	128	1	15 600	1	present work
ELISA*	human insulin					
	standard	5 200	40.6	100	156	139
		2 000	15.6	200	78	140
		7 800	60.9	75	208	141
	ultrasensitive	140	1.1	290	54	142
	mouse insulin					
	standard	3 100	24.2	50	312	143
	ultrasensitive	820	6.4	360	43	144

Abbreviations: ECPA = Electrochemical Proximity Assay, ELISA = Enzyme-Linked Immunosorbent Assay, LOD = Limit of Detection

* To provide valid method comparisons, LODs and Dynamic Ranges for ELISAs are defined by the concentrations in the incubation mixture, prior to the washing step and secondary antibody incubation.

Table 2.2. Performance comparisons between ECPA and various commercially available ELISA kits. ECPA has a lower detection limit than five of the six kits in the table (as much as 60-fold lower), with a comparable detection limit to one ‘ultrasensitive’ human insulin ELISA. The dynamic range of ECPA is >40-fold wider than all ELISAs shown in the table (as much as 300-fold wider). These improvements shown by ECPA come with the added benefit of a direct electrochemical readout, i.e. without requiring washing steps.

Chapter 3

Electrochemical MIP/GCE Sensor for Direct Detection of Chiral Catechin without Separation

3.1 Introduction

Catechin is an abundant natural product that has been known for its potential benefits to human health as an effective anticancer agent.[145,146] However its ecological functions have been under recognized. Catechin released to ground by a variety of plants, such as centaurea maculosa, can hinder the growth of their neighbors and has the potential to be safer alternatives to herbicides and pesticides.[147,148] Catechin is secreted into the soil as a mixture of two enantiomers, (+)-catechin and (-)-catechin that have been proven to possess different biological activities. Recent studies show that (+)-catechin is mainly responsible for antibacterial and antifungal activities with a low phytotoxic effect, while (-)-catechin is believed to own most of the phytotoxicity.[148-151] In order to better utilize this natural product and maximize their functions to serve human, a deeper understanding of the activities related with each enantiomer and their corresponding concentration ratio presented in raw sample is critical.

Until now, methods often used for chiral catechin monitoring involve gas chromatography with mass spectrometry (GC-MS) or liquid chromatography with mass spectrometry (LC-MS).[145,152-158] However, these analytical methods require expensive,

bulky, and complicated instruments and need a separation step (GC, or LC) prior to the detection. On the other hand, enzymes or antibodies based sensors have also been developed for the detection of chiral catechin in tea and wine samples.[145,159-161] However, the poor stability and high cost of these biological elements prevents their use in developing a rapid, inexpensive, yet robust assay for the detection of chiral catechin in nature.[162,163]

Numerous attempts have been made to replace biological receptors with synthetic compounds as recognition elements in biosensing to overcome the major limitations of enzymes and antibodies. Of many approaches, MIPs have become a powerful tool for the preparation of polymeric materials that have the ability to specifically bind a chemical specie due to their low cost, ease of preparation, and robustness.[57,59,164,165] The synthesis of MIPs involves the formation of template-monomer assembles through covalent and/or non-covalent interactions, followed by copolymerization with the aid of a cross-linking agent. Upon removal of the template, binding sites that are complimentary in shape, size, and functionality to the analyte are revealed.[162,57,166,167] A variety of readout methods for MIP-sensors, including piezoelectric[168,169], optical[170,171], and electrochemical methods[54,71,172,173] have been developed in the past decades. Among these detection methods, electrochemical approaches such as voltammetric response are often the easiest and most economic way to fabricate a commercial MIP-sensor.[54,172]

In this study, we report a rapid, simple and direct way to detect chiral catechin in a (±)-catechin solution without the need of additional separation steps. MIPs were synthesized in the presence of (+)- or (±)-catechin and integrated with a glassy carbon electrode using agarose gel.[57,167] The current responses of the (±)-catechin-MIP/GCE

sensor to catechin demonstrate a dynamic range from 10 µM up to 300 µM with great selectivity against nonspecific molecule, HQ. The voltammetric response of the chiral catechin imprinted MIP/GCE sensor to (+)-catechin shows its ability to detect chiral catechin from a mixture of both enantiomers simulating the natural product sample within 5 min. In addition, the method could be used to evaluate relative quantity of two enantiomers in mixture. The ratio of (+)-catechin to (-)-catechin was determined to be 1: (4.31±1.54), which agrees with the ratio evaluated by LC-MS that is 1: (3.95±1.58). Thus, the combination of molecular imprinting technique with electrochemical method offers an excellent sensor for rapid detection of not only chiral catechin, but a wide variety of chiral compounds at a very low cost.

3.2 Experimental

3.2.1 Materials and Reagents

(+)-catechin (98+%, Sigmal-Aldrich), (±)-catechin hydrate (98.5+%, Fluka), hydroquinone (HQ) (99+%, Sigmal-Aldrich), acrylamide (AA) (99+%, Sigmal-Aldrich), N,N-methylenebis(acrylamide) (MAAM) (99%, Sigmal-Aldrich), and azobisisobutyronitrile (AIBN) (98%, Fluka) were used as received. $NaH_2PO_4 \cdot H_2O$ (98–102%, Sigma–Adrich) and Na_2HPO_4 (99+%, Sigma–Adrich) were used to prepare 0.1 M phosphate buffer solution (PBS) at pH 7.4. Agarose (Sigma-Aldrich) was used to prepare 1 wt% agarose gel. Acetonitrile (ACN), methanol, acetic acid, formic acid and ethanol (all HPLC grade) were from commercial sources and used as received. Millipore-Q purified de-ionized (DI) water (18.2 M _ U cm^{-3}) was used to prepare all solutions and to rinse electrodes.

3.2.2 Fabrication of MIP/GCE Sensor

The synthesis of (+)-catechin molecularly imprinted polymers was adapted from the literature procedure.[57] 31.7 mg (+)-catechin and 46.6 mg acrylamide were dissolved in 10 mL ACN and the mixture was sonicated in ice-bath for 10 min. Then, 10 mL ACN, 404.7 mg MAAM and 10 mg AIBN were added to the solution while stirring. The mixture was purged with N_2 in ice-bath for another 20 min. The temperature was increased from room temperature to 60 °C and maintained at 60 °C for 24 h under N_2. After polymerization, the product was collected by centrifugation at 5000 rpm for 10 min. The collected polymer material was washed with methanol/acetic acid (9:1, v/v) to extract (+)-catechin. The extracted polymer was rinsed with ethanol 3 times to remove any remaining acetic acid and then dried in a vacuum desiccator overnight. The resulting bulk polymers then were crushed and ground to yield white particles. The (±)-catechin imprinted polymers was synthesized in the same way, but using (±)-catechin as template molecule. The non-imprinted polymer (NIP) used in control measurements was also prepared in the same way, but in the absence of the (+)-catechin. The GCE was polished to a mirror finish with 15, 3, 1 µm diamond suspension (Buehler), and 0.05 µm alumina (Buehler) on a smooth polishing cloth subsequently and then sonicated with DI water and ethanol prior to each polymer deposition. To fabricate the MIP/GCE and NIP/GCE sensors, 5.7 mg MIP was dispersed in 280 µL methanol with sonication for 20 min. Then 10 µL of the MIP suspension was coated on the clean GCE electrode surface and dried at room temperature. Then 10 µL of 1 wt% agarose aqueous solution was overlaid on the above electrode surface till the accomplishment of complete gelling.

3.2.3 Scanning Electron Microscopy (SEM)

Scanning electron microscopy image of the imprinted polymer particles was recorded on a Zeiss EVO 50 variable pressure scanning electron microscope on a gold sputtered sample.

3.2.4 Fourier-Transfer Infrared Spectroscopy (FTIR)

FTIR spectroscopic measurements were performed on model IRPrestige-21/FTIR-8400S FTIR spectrometer (Shimadzu corporation, Tokyo, Japan) with KBr pellet method. The wave numbers of FTIR measurement were ranging from 400 to 4000 cm^{-1}, and collected at one data point per 2 cm^{-1} with scanning for 16 times.

3.2.5 Electrochemical Measurements

All electrochemical measurements were carried out at room temperature using a three-electrode set-up in a home built glass cell (20 mL total volume). The supporting electrolyte was 0.1 M PBS (pH 7.4), the reference electrode was Ag/AgCl(sat) (Bioanalytical Systems, Inc.), and the counter electrode was Pt gauze (A = 0.77 cm^2). The working electrode was a glassy carbon disk (d = 0.3 cm, A = 0.071 cm^2). Before electrochemical measurements, the solution was purged with N_2 for 5 min. The electrochemical circuit was controlled using an Epsilon electrochemistry workstation (Bioanalytical Systems, Inc.). Amperometric measurements were carried out by stepping the potential to 0.4 V vs. Ag/AgCl(sat) to ensure complete oxidation of catechin. Aliquot of (±)-catechin was injected into stirred PBS at every 200 sec. The concentration of (±)-catechin in the bulk solution was varied from 0 to 300 µM. For specificity tests, aliquot

of (±)-catechin or HQ was injected into stirred PBS repeatedly at every 100 sec, making a final HQ concentration of 120 µM and a final (±)-catechin concentration of 70 µM at 1500 sec. For (+)-catechin detection, the MIP/GCE was dipped into 0.1 M PBS containing 72 µM (+)-catechin, 72 µM (±)-catechin, or a mixture of the two for 4 min, rinsed with DI water gently to remove physisorbed catechin, and then transferred to a catechin-free 0.1 M PBS at pH 7.4. Cyclic voltammograms were recorded between -0.2 V and 0.8 V using a scan rate of 50 mV/s. Data were collected from two different sensors and were measured at least twice from each individual sensor.

3.2.6 LC-MS

LC-MS analysis was performed on an Ultra Performance LC Systems (ACQUITY, Waters Corp., Milford, MA, USA) coupled with a quadrupole time-of-flight mass spectrometer (Q-TOF Premier, Waters) with electrospray ionization (ESI) in both ESI-MS and ESI-MS/MS modes operated by the Masslynx software (V4.1). 3 µL (±)-catechin in methanol was flowing through a Synergi 4 µm C18, 150 mm × 3 mm I.D. analytical column (Phenomenex, Aschaffenburg, Germany) kept at 35 ºC and injected into the ESI source. 0.1% Formic acid in ACN/purified water (v/v, 5/95) (mobile phase A) and 0.1% formic acid in ACN/purified water (v/v, 95/5) (mobile phase B) were applied at a flow rate of 0.35 mL/min, starting at 0% B with a linear gradient to 30% B after 60 min followed by washing with 100% B for 10 min and reequilibration with 100% A for another 10 min.[158] Separation was repeated for three times for accuracy.

3.3 Results and Discussion

3.3.1 Preparation and Characterization of MIP Particles

(±)-Catechin/(+)-catechin was dissolved in ACN and AA was selected as the functional monomer owning to the carbonyl group and amide groups that are favorable for hydrogen-bonding interaction with the five hydroxyl groups contained in catechin in the solvent.[174] The sonication process prior to polymerization facilitates the formation of stable donor-receptor complex between templates and functional monomer that leads to well-defined binding sites in the MIP matrix as shown in Scheme 3.1. The addition of the cross-linker, MAAM, was to ensure strong network and robustness of the polymers. Upon removal of the template molecule, specific imprinting sites were revealed and able to selectively rebind (±)-catechin/(+)-catechin. The bulk polymers were further crushed and grounded into small particles to ease the incorporation with GCE.

SEM is a suitable method to observe the morphology of MIPs and estimate the particle size after crushing.[175,176] Figure 3.1. shows the SEM image of (±)-catechin MIP particles, which presents a globular morphology with aggregated small globules. The particle size ranges from 124.5 nm up to 950.6 nm determined by ImageJ. No obvious difference was observed between MIPs and NIPs (data not shown). To further ensure that the MIPs had been made successfully, FTIR analysis was performed on AA, MAAM, MIPs after extraction, and NIPs. Figure 3.2.A shows the FTIR spectrum of AA. Broad asymmetric stretching bands of primary amine were found at 3367 cm^{-1} and 3205 cm^{-1}.[174] A stretching vibration band of carbonyl group was found at 1680 cm^{-1}, suggesting there are functional groups in AA to form hydrogen bonding with templates.[177,178] In addition, the stretching vibration band of alkene group was found at 1615 cm^{-1}.[174] The FTIR spectrum of MAAM is shown in Figure 3.2.B. A sharp, strong asymmetric stretching

vibration band of amine was found at 3310 cm^{-1}, while two other main vibration bands were found at 1666 cm^{-1} and 1628 cm^{-1}, which are assigned as carbonyl stretching and alkene stretching. For MIP particles, as shown in Figure 3.2.C, the broad peak situating at 3406 cm^{-1} was attributed to asymmetric stretching of N-H in amine. At 1668 cm^{-1}, the strong stretching vibration peak of carbonyl group suggests that there are functional groups left in the polymer network to interact with the hydroxyl groups of catechin, thus rebind targets. The disappearance of stretching vibration band of alkene groups at either 1615 cm^{-1} or 1628 cm^{-1} indicates completion of polymerization. The spectrum of NIP particles shown in Figure 3.2.D was identical with that of MIP particles, suggesting the complete removal of catechin after extraction. The FTIR results confirm that the polymerization reaction took place and was complete, and there were functional groups in the MIPs that would interact with targets via carbonyl groups and amine groups.

3.3.2 Optimization of Monomer to Template Ratio (M/T) for Detection of (±)-Catechin

In non-covalent MIP system, there are monomer-template complexes formed in the pre-polymerization solution. Because of the nature of non-covalent bonding, there is equilibrium between individual molecule and the complexes that determines assembly of complexes. Complexes formation is directly related to the number and quality of the MIP binding sites, thus M/T in the pre-polymerization mixture is found particularly important. Low M/T provides MIP particles with insufficient functional groups to bind targets, while a too high M/T, with the extreme case being a NIP, yields non-selective binding. (±)-catechin MIPs with varied M/T in the pre-polymerization solution were synthesized and their corresponding current responses to 300 μM (±)-catechin were tested

individually using chronoamperometry. The inset of Figure 3.3.A shows that a maximum current was obtained when the M/T is 6, which agrees with the results observed in previous literature.[174] Therefore, a ratio of 6 was proven to provide the highest sensitivity to target molecule.

3.3.3 Electrochemical Responses of MIP/GCE

Figure 3.3.A shows the chronoamperometric responses of (±)-catechin MIP/GCE to (±)-catechin by the comparison with NIP/GCE. Measurements were carried out with MIP/GCE (Figure 3.3.A black trace) and NIP/GCE (Figure 3.3.A red trace) by successive additions of (±)-catechin aliquots in PBS at pH 7.4. In each case, the potential was stepped from -0.10 V to a value of +0.40 V. At MIP/GCE, the oxidation currents achieved steady-state within 30 s after each aliquot was introduced and increase with the increase of (±)-catechin concentration in PBS. As expected, there was no current response at the NIP/GCE, which indicates a complete coverage of NIP on the surface that blocked electron transfer. The calibration curve shown in Figure 3.3.B (black trace) revealed a linear relationship with (±)-catechin concentration in the range from 10 to 70 µM and the currents tend to reach saturation at high concentration range, indicating that the imprinting sites were almost occupied by (±)-catechin molecules.

3.3.4 Selectivity Study

The selectivity of the (±)-catechin MIP/GCE sensor toward (±)-catechin was evaluated by testing its current response against interference molecule, HQ. The concentration dependent current response of single component solutions of (±)-catechin

(black trace) and HQ (blue trace) are shown in Figure 3.3.A. HQ only showed detectable current starting at 100 µM. When [(±)-catechin] = 300 µM, the current response of HQ (Figure 3.3.A blue trace and Figure 3.3.B blue trace) was only 11.7% of the (±)-catechin current response. The results indicate that the MIP/GCE sensor has binding preference to the template molecules. The low current responses at higher HQ concentrations were likely due to the hydroxide groups in HQ that can form hydrogen bonding with the functional groups in the MIP matrix and its smaller size than that of (±)-catechin. Thus small amount of this structurally similar compound was transported through the cavities of the MIP particles to reach at the GCE surface where it can be oxidized. To further ensure the selectivity of the cavities in MIP matrix, a second experiment was carried out using chronoamperometry by injecting aliquots of HQ and (±)-catechin solutions alternatively into the same PBS. The concentration of HQ in PBS was ranging from 0 to 120 µM while the concentration of (±)-catechin was from 0 to 70 µM. The results were shown in Figure 3.4. At the initial stage, only aliquots of HQ solution were injected into the stirred PBS solution and no current response was detected. A current was produced immediately when an aliquot of (±)-catechin solution was injected into the PBS and aliquots of HQ and (±)-catechin were injected alternatively after then. As expected, the oxidation current of (±)-catechin increases with the addition of (±)-catechin, while HQ only produces small current responses only after 90 µM in PBS that agrees with the result in the individual test. These two lines of investigation confirm the outstanding selectivity of MIP/GCE sensor for (±)-catechin over potentially interfering compound. In plant samples, HQ and other phenolic and polyphenolic compounds present at low

concentrations compared to catechin.[145] Thus the interference from HQ and similar compounds for catechin detection is not significant in real sample.[145]

3.3.5 Detection of Chiral Catechin

The (±)-catechin MIP/GCE sensor was demonstrated to work well for detecting template molecules and showed excellent selectivity toward targets against potential interferent, such as HQ. Because the chronoamperometric measurements were done under constant stirring, the noise of current is fairly large and not ideal for quantitative analysis. On the other hand, Cyclic voltammetry is potentially a good method of choice for precise analysis and would reveal the binding affinity of target molecules within the cavities of MIPs. To test the feasibility, Cyclic voltammetric measurements were performed right after the chronoamperometry measurements for (±)-catechin. MIP/GCE and NIP/GCE were taken out from the PBS and gently washed with DI water to remove unspecifically absorbed (±)-catechin molecules. Cyclic voltammograms (CV) at MIP/GCE (black trace) and NIP/GCE (red trace) shown in Figure 3.5. were recorded in a (±)-catechin free PBS at pH 7.4. For the MIP/GCE, a quasi-reversible redox peak with the peak potential difference of 134 mV vs Ag/AgCl was observed, while almost no electrochemical response could be seen for the NIP/GCE. These results confirm that selective binding sites were created in the MIP matrix for rebinding of (±)-catechin and the bindings of target molecules were fairly tight. The inset of Figure 3.5. demonstrates a linear relationship between the anodic peak current of (±)-catechin and scan rate, proving that the (±)-catechin molecules were situating in the cavities upon rebinding. Therefore, given the inspiration of tight binding of catechin molecules in the cavities, cyclic

voltammetry was the method of choice for chiral catechin detection to obtain more quantitative results.

To test the performance of the MIP/GCE sensor in more challenging settings, (+)-catechin MIPs were synthesized for detection of (+)-catechin in a (±)-catechin solution and determination of the relative amount of two enantiomers in the mixed sample. An accumulation step was introduced to obtain a better sensitivity of the MIP/GCE sensor.[53,179] The (+)-catechin MIP/GCE sensor was preconcentrated in a stirring PBS at pH 7.4 containing 144 µM (+)-catechin before measurement. After gently washing with DI water to remove physisorbed molecules, current was measured using cyclic voltammetry. A typical CV of the sensor's response to (+)-catechin is shown in the inset of Figure 3.6. A pair of quasi-reversible redox peaks indicates the rebinding of chiral catechin in cavities. Figure 3.6. shows the change of the anodic peak current with the preconcentration time. The anodic peak current increased significantly with the increase of preconcentration time at the initial stage, and a stable response was obtained after 4 min, suggesting that the adsorption equilibrium was reached. Therefore, the preconcentration time of 4 min before measurement was proven to give the strongest electrochemical response.

The ability of (+)-catechin MIP/GCE sensor for detection of (+)-catechin in a mixture of (±)-catechin with unknown enantiomers ratio was further tested using optimal conditions. The sensor was preconcentrated in PBS with 72 µM (+)-catechin, 72 µM (±)-catechin, and 72 µM (+)-catechin with 72 µM (±)-catechin, respectively and the CVs were recorded after gentle washing. 72 µM was the choice of testing concentration because it was reported as the useful limit of detection for naturally produced catechin

while studying its phytotoxicity effects.[149,180] Figure 3.7.A shows the representative CVs on (+)-catechin MIP/GCE. A pair of quasi-reversible redox peaks of catechin appeared after preconcentration with 72 µM (+)-catechin only (black trace). After preconcentration with a soluton of 72 µM (+)-catechin with 72 µM (±)-catechin, the anodic peak current increased slightly (red trace). The sensor incubated with just 72 µM (±)-catechin showed the smallest current response (blue trace). A summary of anodic peak currents corresponding to three testing solutions from multiple measurements was shown in Figure 3.7.B. The current response of the (+)-catechin MIP/GCE sensor to 72 µM (+)-catechin is about 4 times larger compared with the one to 72 µM (±)-catechin, and the anodic peak current to the mixture of 72 µM (+)-catechin with 72 µM (±)-catechin is only 1.20 times larger than the one to 72 µM (+)-catechin solely. This is possibly caused by the specificity of (+)-catechin imprinted binding sites since just (+)-catechin molecules were present during the polymerization. Therefore, after removal of templates, the polymer only holds cavities complimentary to (+)-catechin. Only a small portion of (+)-catechin presents in the mixed (±)-catechin sample of 72 µM, which results in a corresponding small amount of current response compared with pure (+)-catechin of 72 µM. (-)-Catechin molecules can not bind to the cavities because of the different stereos. Therefore, only (+)-catechin molecules could rebind and trapped in the cavities. Furthermore, the molar ratio of (+)-catechin to (-)-catechin in the unknown (±)-catechin sample was determined to be 1: (4.31±1.54) based on the CV results, which agrees very well with the number determined by LC-MS that is 1: (3.95±1.58)[158] showed in Figure 3.7.C. This result indicates that the (+)-catechin MIP/GCE sensor has stereoselectivity

and is capable of detection of chiral catechin quantitatively in a mixture of enantiomers without the need of separation.

3.4 Conclusions

In this work, we have successfully demonstrated a simple, direct, and fast MIP/GCE sensor for detection of chiral catechin in enantiomers mixture without separation. MIP particles were prepared and grafted onto a GCE using agrose gel. (±)-Catechin MIP/GCE was first fabricated to validate the sensitivity of the sensor to target and its great specificity toward template molecules against potential interferent, HQ. Moreover, (+)-catechin MIP/GCE was prepared to detect (+)-catechin in (±)-catechin solution and the ratio of (+)-catechin to (-)-catechin was determined based on CVs and confirmed by LC-MS. The sensor showed good stereoselectivity and it is promising in the use of fast determination of relative amount of two enantiomers in natural products. This is significant in studying distinct functions of enantiomer separately on site at a low cost. Finally, this sensing strategy is general in nature, and can be extended to the development of chiral sensors for other electroactive molecules.

Scheme 3.1

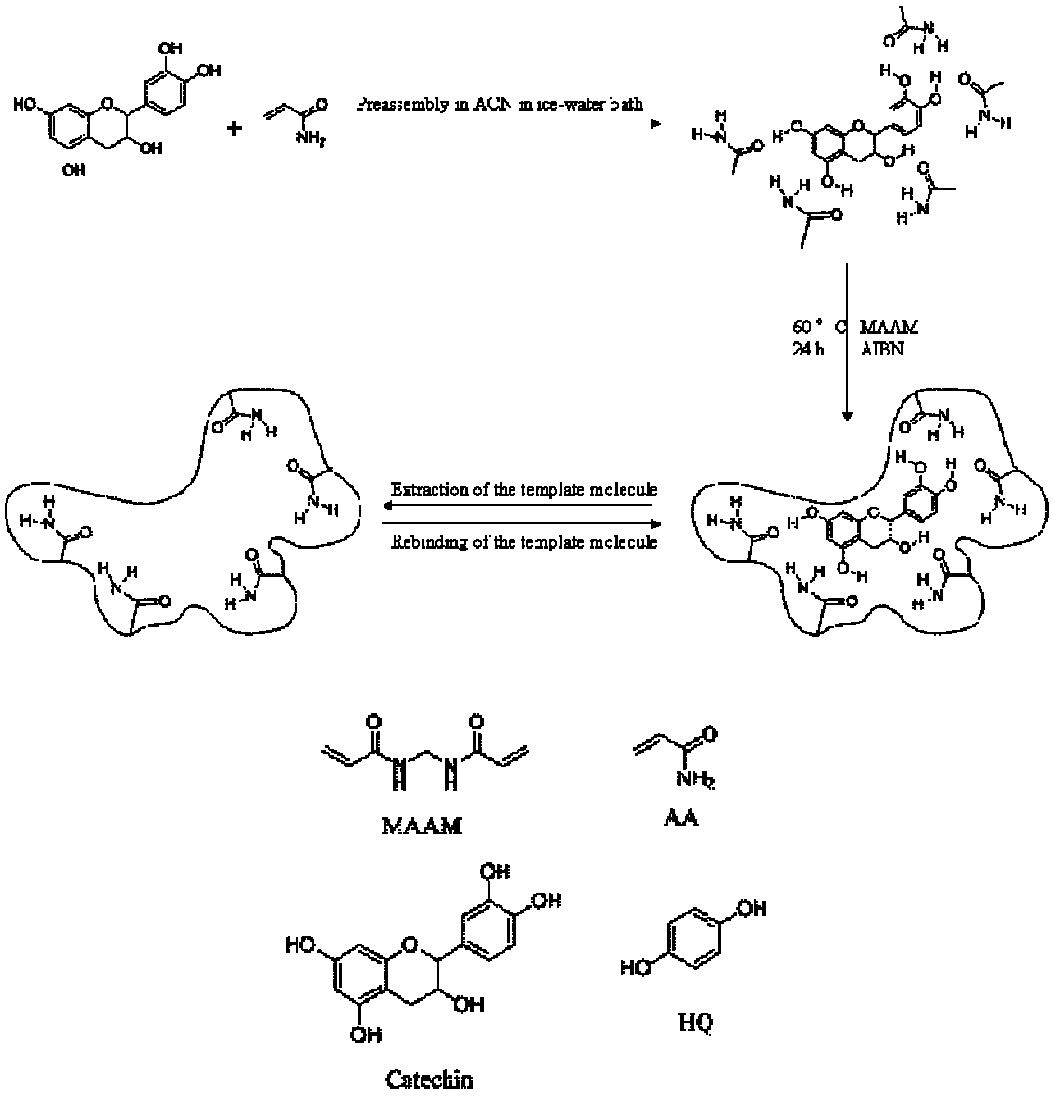
Preassembly in ACN ice-water bath
60 °C
24 h
MAAM
ATBN
Extraction of the template molecule
Rebinding of the template molecule
MAAM
AA
Catechin
HQ

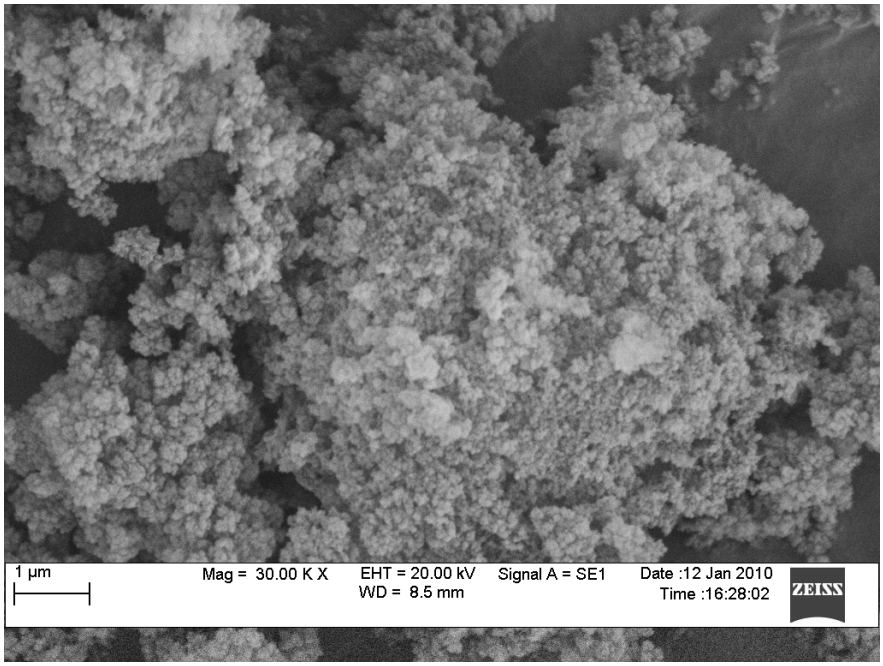

Figure 3.1. SEM image of the (±)-catechin imprinted polymer particles. particle size: 124.5nm to 950.6nm determined by ImageJ.

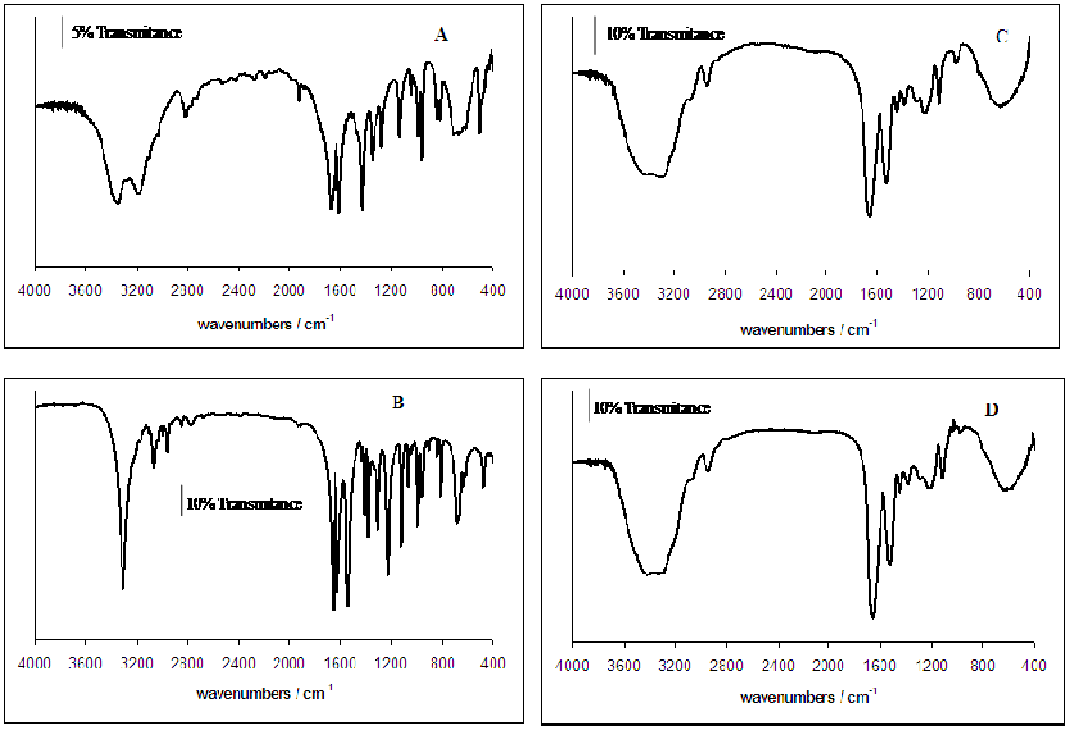

Figure 3.2. FTIR spectra of AA (**A**), MAAM (**B**), extracted MIP (**C**), and NIP (**D**).

A

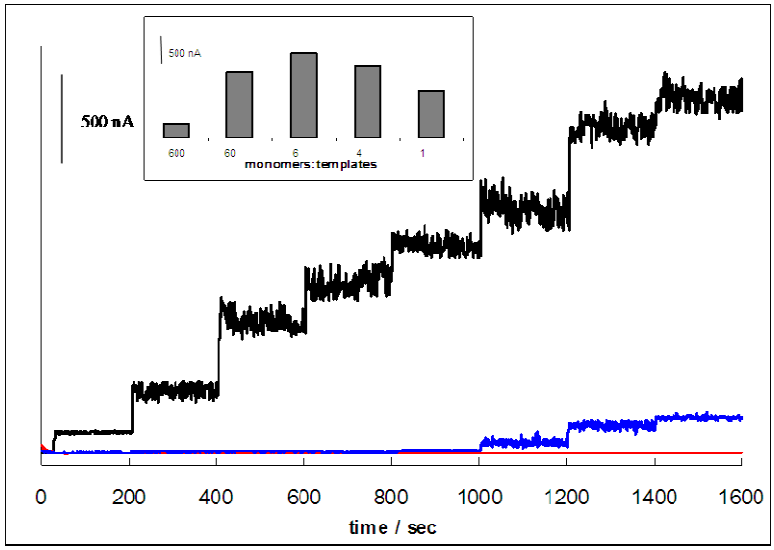

B

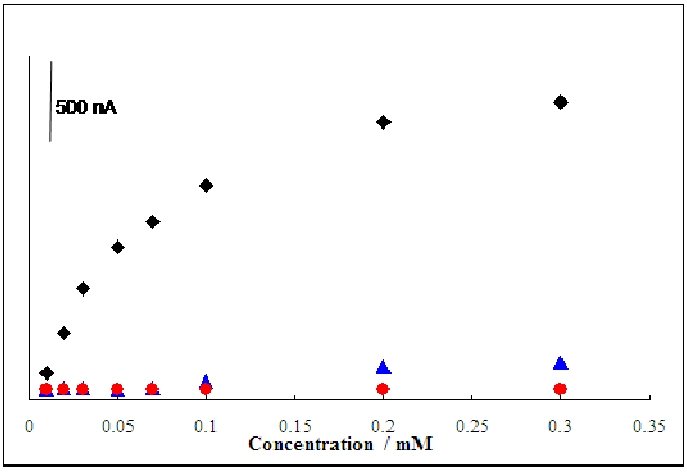

Figure 3.3. (**A**) Typical current response curves of (±)-catechin (black trace) and HQ (blue trace) with increasing concentrations at (±)-catechin MIP/GCE and response of (±)-catechin at NIP/GCE (red trace) in 0.1 M PBS with stirring at a constant potential of 0.4 V, pH at 7.4. The inset shows effect of M/T on the chronoamperometric response of the (±)-catechin MIP/GCE to 300 µM (±)-catechin in 0.1 M PBS, pH at 7.4. (**B**) Calibration curves for (±)-catechin (black trace) and HQ (blue trace) on (±)-catechin MIP/GCE and (±)-catechin on NIP/GCE (red trace) obtained by i-t curves in Fig. 3.3.A.

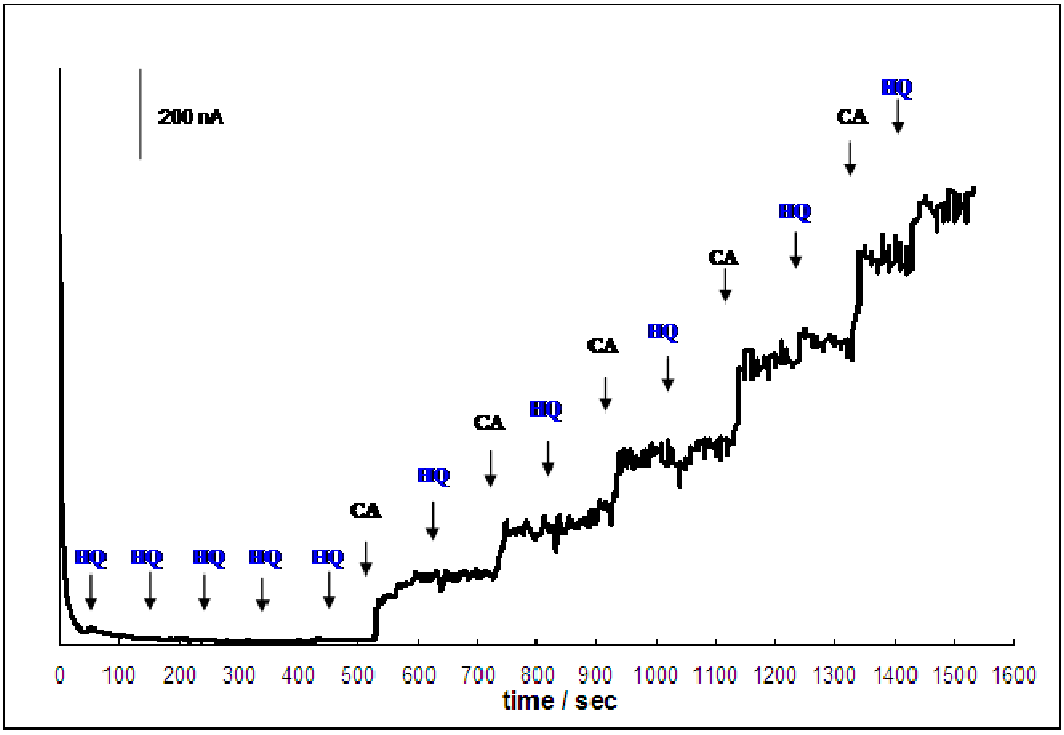

Figure 3.4. The chronoamperometric current responses of (±)-catechin against HQ on (±)-catechin MIP/GCE in 0.1 M PBS with stirring at a constant potential of 0.4 V, pH at 7.4.

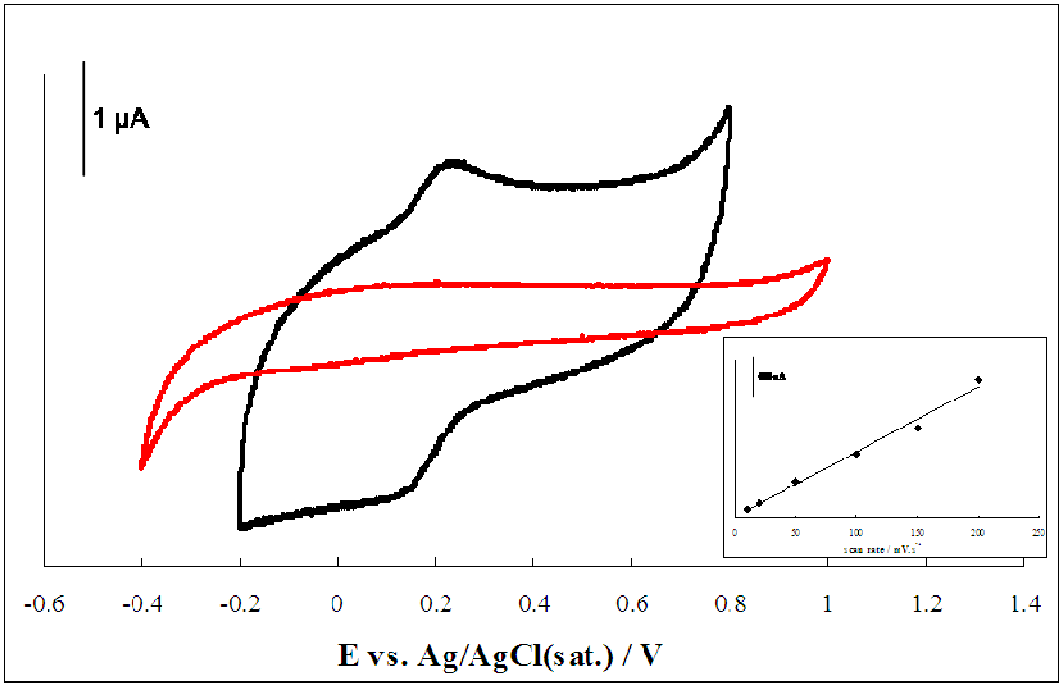

Figure 3.5. Cyclic voltammograms of (±)-catechin on MIP/GCE (black trace) and NIP/GCE (red trace) in 0.1 M catechin-free PBS, pH at 7.4 after gently washing following the chronoamperometric experiment. Scan rate: 50 mV/s. The inset shows the effect of the scan rate on the anodic current of (±)-catechin on MIP/GCE in 0.1 M PBS, pH at 7.4. Scan rate: 10, 20, 50, 100, 150, 200 mV/s.

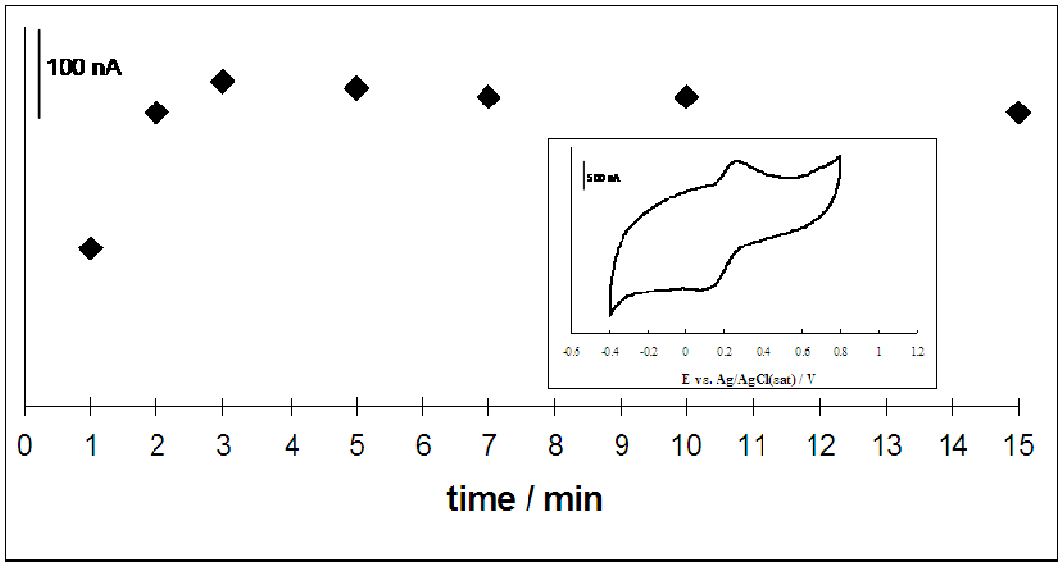

Figure 3.6. Effect of preconcentration time on the anodic current of the (+)-catechin MIP/GCE to 144 µM (+)-catechin in 0.1 M PBS, pH at 7.4. Scan rate: 50 mV/s. The inset shows a typical cyclic voltammogram of 144 µM (+)-catechin on (+)-catechin MIP/GCE in 0.1 M PBS after preconcentration step, pH at 7.4. Scan rate: 50 mV/s.

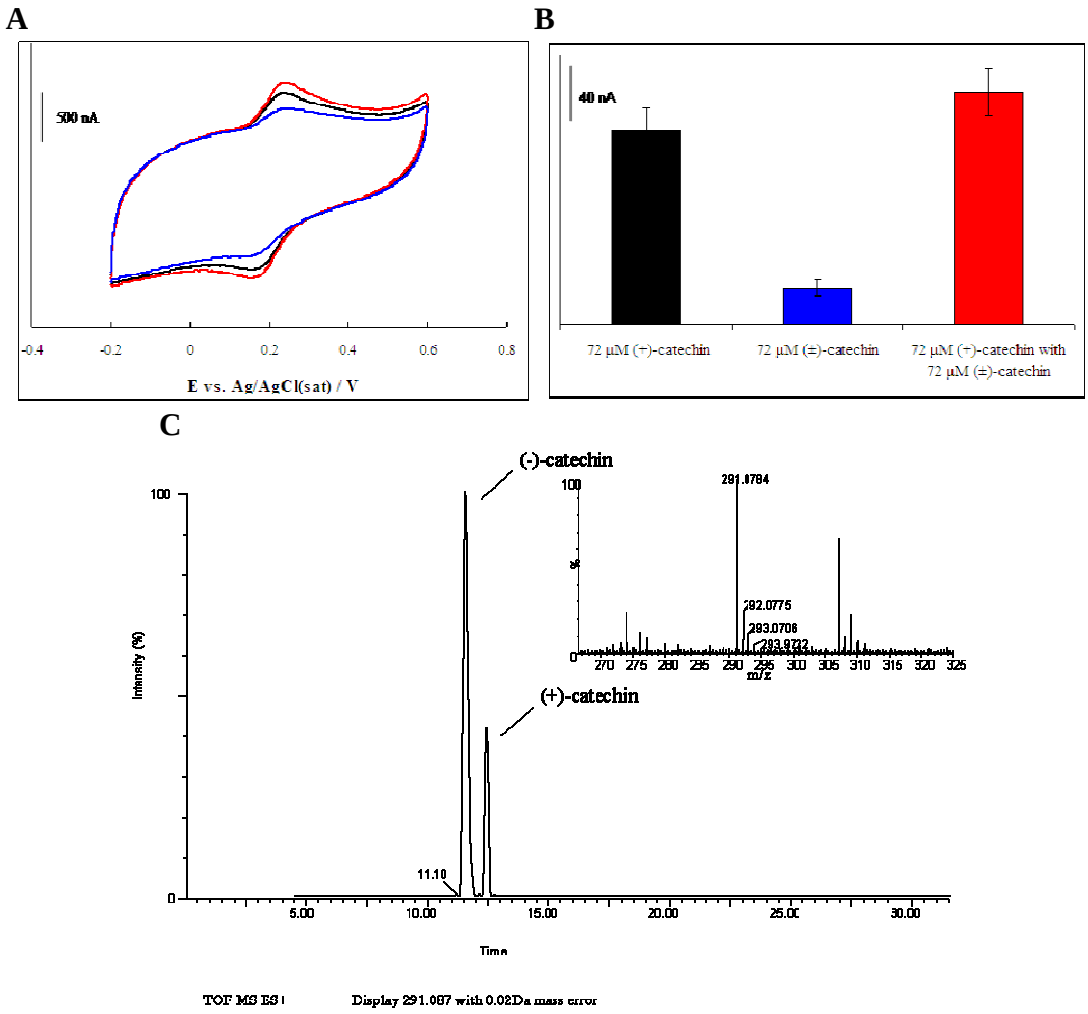

Figure 3.7. (**A**) Representative cyclic voltammograms of 72 µM (+)-catechin, 72 µM (±)-catechin, and 72 µM (+)-catechin together with 72 µM (±)-catechin on (+)-catechin MIP/GCE in 0.1 M PBS after 4 min of preconcentration, pH at 7.4. Scan rate: 50 mV/s. (**B**) Average anodic peak currents of the (+)-catechin MIP/GCE to 72 µM (+)-catechin, 72 µM (±)-catechin, and 72 µM (+)-catechin together with 72 µM (±)-catechin based on three different measurements. Preconcentation time is 4 min before each measurement. (**C**) Representative liquid chromatogram showing the enantioselective separation of (±)-catechin. The inset confirms the mass of (±)-catechin.

Chapter 4

Electrochemical Sensors Based on Molecularly Imprinted Polymers Grafted onto Gold Electrodes Using Click Chemistry

4.1 Introduction

The development of sensors for the detection of toxic compounds in the environment and in foodstuffs has received increasing attention in recent years.[181-185] In addition, numerous electrochemical metabolic and immunoassays are based on the detection of small molecules such as hydrogen peroxide and electron transfer mediators such as hydroquinone.[186] Biological molecules, ranging from enzymes to antibodies, are frequently used as the molecular recognition element in these devices, owing to their high sensitivity and selectivity. The challenge of employing biomolecules in practical devices, however, lies in the high cost, complicated preparation and handling, and poor long-term chemical stability of many of these molecules.[162,163] Molecularly imprinted polymers (MIP) are synthetic materials, which are widely used as biomimetic molecular recognition elements due to their low cost, ease of preparation, and robustness.[59,164,165,187-191] The synthesis of MIPs involves the formation of template–monomer assemblies through covalent and/or non-covalent interactions, followed by copolymerization with the aid of a cross-linking agent. Upon removal of the template, binding sites that are complementary in shape, size, and functionality to the analyte are revealed.[162, 166,167,177] A large number of read-out methods for MIP-sensors, including piezoelectric,[168,169

optical,[170,171] and electrochemical methods[54,71,173] have been developed in the past decades. Among these detection methods, electrochemical approaches, especially amperometric methods, are often the easiest and most economic way to fabricate a commercial MIP-sensor.[54,172]

A key aspect in the design of a MIP-sensor is the efficient integration of the polymer with the signal transducer.[55,71] In the case of amperometric sensors, the conventional approach is to deposit ready-made MIP particles onto the electrode, and stabilize them with an agarose gel.[72] However, there are many drawbacks in using this approach, such as a low density of recognition sites inside matrix particles obtained via crushing and grinding, and a high diffusion barrier for the analytes through the agarose binder. These factors lead to slow binding site accessibility and low binding capacity.[167,73-75] A surface chemistry approach, such as the direct grafting of thin MIP films onto an electrode surface, could in principle overcome some of the limitations associated with conventional methods and achieve good site accessibility and faster mass transfer characteristics.[168,169,76,192-195] Direct electropolymerization of MIPs is another promising approach to better integration of MIPs to electrode surfaces.[77]

The use of self-assembled monolayers (SAMs) to immobilize monomers or initiators onto a sensor surface is attractive because these systems are very well-characterized, and are compatible with many miniaturization and surface patterning strategies.[78,79] Surface modification with functionalized monolayers has typically been accomplished by the chemical modification of the surfactant prior to the self-assembly step, which can result in low yields and limited applicability. On the other hand, the surface “click” chemistry (i.e., the Cu(I)-catalyzed azide-alkyne cycloaddition reaction),

introduced by Sharpless and co-workers[196] and Chidsey and coworkers,[78,79,196] offers a powerful surface modification strategy because of its fast kinetics, high reaction yields, and ease of monitoring by routine surface characterization techniques.[80,196-198] In addition, core–shell MIP particles and water soluble MIPs have been prepared using a 'click chemistry' approach.[199,200]

In this study, we report a simple and straightforward three step synthetic strategy for grafting thin MIP films directly onto the surface of Au electrodes that employs a novel 'clickable' selfassembled monolayer/monomer system. In the first step, a two component SAM containing an azo-terminated thiol is formed. In the second step, propargyl acrylate is 'clicked' onto the SAM. In the third step, the desired MIP is polymerized directly on the Au surface using conventional UV initiated radical polymerization. In this study, hydroquinone was chosen as a model analyte for the purpose of demonstrating the suitability of these grafted imprinted polymers for sensing applications.

4.2 Experimental

4.2.1 Materials and Reagents

Hydroquinone (HQ) (99+%, Sigma–Aldrich), acrylamide (99+%, Sigma–Aldrich), N,N'-methylenebis(acrylamide) (MAAM) (99%, Sigma–Aldrich), NaN_3 (99.5+%, Sigma–Aldrich), methanesulfonyl chloride (99.7+%, Sigma–Adrich), (+)-sodium l-ascorbate (99+%, Sigma), $CuSO_4 \cdot 5H_2O$ (99+%, Sigma–Aldrich), propargyl acrylate (98%, Aldrich), potassium ferricyanide (KFCN) (99%, Sigma–Aldrich), (L)-ascorbic acid (99+%, Sigma), 1-decanethiol (99%, Aldrich), 11-bromo-1-undecanol (99+%, Fluka),

azobisisobutyronitrile (AIBN) (98+%, Fluka), catechin (98.5+%, Fluka), triethylamine (99.7%, Acros Organics), potassium thioacetate (98%, Acros Organics), and serotonin (99%, Acros Organics) were used as received. Azidoundecanethiol (ADT, $N_3(CH_2)_{11}SH$) was synthesized according to the literature procedures.[78] $NaH_2PO_4 \cdot H_2O$ (98–102%, Sigma–Adrich) and Na_2HPO_4 (99+%, Sigma–Adrich) were used to prepare 0.1 M phosphate buffer solution (PBS) at pH 7.4. Acetonitrile (ACN), methanol, acetic acid, and ethanol (all HPLC grade) were from commercial sources and used as received. Millipore-Q purified de-ionized (DI) water (18.2 $M\Omega Ucm^{-3}$) was used to prepare all solutions and to rinse electrodes.

4.2.2 Fabrication of Coated-On MIP Sensors

The synthesis of hydroquinone (HQ) molecularly imprinted polymers was adapted from the literature procedure.[173] 22 mg HQ and 56.9 mg acrylamide were dissolved in 20 mL acetonitrile and the mixture was sonicated for 10 min. Then, 493.3 mg MAAM and 10 mg AIBN were added to the solution while stirring. The temperature was increased from room temperature to 70 $^{\circ}C$ and maintained at 70 $^{\circ}C$ for 24 h under N_2. After polymerization, the product was collected by centrifugation at 5000 rpm for 10 min. The collected polymer material was washed with methanol/acetic acid (9:1, v/v) to extract HQ until it could no longer be detected in the eluent by UV–vis spectrophotometry. The extracted polymer was rinsed with ethanol 3 times to remove any remaining acetic acid and then dried in a vacuum desiccator overnight. The resulting bulk polymers then were crushed and ground to yield white particles. The non-imprinted polymer (NIP) used in control measurements was prepared in the same way, but in the absence of the HQ. To

fabricate the coated-on MIP and NIP sensors, 1 mg MIP was dispersed in 0.5 mL methanol with sonication for 20 min. Then 10 μL of the MIP suspension was spin-coated on the clean Au electrode surface and dried at room temperature. Then 10 μL of 1 wt% agarose aqueous solution was overlaid on the above electrode surface till the accomplishment of complete gelling.

4.2.3 Fabrication of the Click-On MIP Sensors

Au substrates were polished to a mirror finish using an aqueous slurry of 0.05 μm alumina particles and then washed with water and ethanol in an ultrasonic cleaner. The Au electrode was then immersed in fresh piranha solution (H_2SO_4/H_2O_2, 3:1) for about 5 min, rinsed with DI water, and dried under nitrogen gas. *Caution: Piranha solution is dangerous to human health and should be used with extreme caution and handled only in small quantities.* The Au electrode was then subjected to 100 oxidation–reduction cycles, scanning between −0.5 and 1.5 V in 0.1 M $HClO_4$ at 0.1 Vs^{-1}. Self-assembled monolayers were formed by immersing the clean Au electrode in 200 μL of an ethanolic solution that was 1 mM decanethiol and 2 mM 1-azidoundecan-11-thiol for 24 h.[201] The SAM/Au electrode was rinsed in ethanol and water and dried in a stream of flowing N_2 prior to being transferred for 18 h to a 2 mM propargyl acrylate (PA) solution (solvent, 3:1 ethanol:water) that also contained 10 mol% sodium ascorbate and 5 mol% $CuSO_4 \cdot 5H_2O$. The reaction chamber was covered with aluminum foil and stored inside a darkened drawer for the duration of the reaction in order to prevent photo-oxidation of the monolayer. After reaction, the monomer/SAM/Au electrode was rinsed with ethanol and water repeatedly to remove any physisorbed PA. Next, 10 μL of MIP reagent

solution (1.1 mg HQ, 24.7 mg MAAM, and 3.3 mg AIBN in 1 mL ACN) was applied to the electrode by spin coating. Polymerization was carried out by applying UV light (365 nm) to the electrode surface for 1 h.[54] Finally, HQ was removed by exposing the electrode to a DI water and methanol flux. Scheme 4.1 summarizes the procedure used to prepare the MIP/SAM/Au electrodes. Non-imprinted polymer films were prepared under identical conditions to those used for the MIPs in the absence of HQ.

4.2.4 Raman Spectroscopy

Raman spectroscopy was performed using the 514 nm line (20 mW) from an air-cooled argon ion laser (model 163-C42, Spectra-Physics Lasers, Inc.) as the excitation source. Raman spectra were collected and analyzed using a Renishaw in via Raman microscope system.[202]

4.2.5 Electrochemical Measurements

All electrochemical measurements were carried out at room temperature using a three-electrode set-up in a home built glass cell (20 mL total volume). The supporting electrolyte was 0.1 M PBS (pH 7.4), the reference electrode was Ag/AgCl(sat) (Bioanalytical Systems, Inc.), and the counter electrode was Pt gauze (A = 0.77 cm^2). The working electrode was an Au disk (d = 0.15 cm, A = 0.018 cm^2). Before electrochemical measurements, the solution was purged with N_2 for 5 min. The electrochemical circuit was controlled using an Epsilon electrochemistry workstation (Bioanalytical Systems, Inc.). Cyclic voltammograms were recorded between −0.1 V and 0.6 V using a scan rate of 100 mVs^{-1}. Amperometric measurements were carried out by stepping the potential to

0.4 V to ensure complete oxidation of HQ. The concentration of HQ in the bulk solution was varied from 0 to 200 μM. The solution was stirred after each addition of HQ and then held without disturbance for 200 s to make chronoamperometric measurements. Selectivity among structurally related analogs was also studied by using chronoamperometry. The current response of MIP/SAM/Au electrodes to catechin, (L)-ascorbic acid, and serotonin at various concentrations were tested both individually and in the presence of 30 μM HQ. In all cases, data were collected from three or more different sensors and were measured at least twice from each individual sensor.

4.2.6 Profilometry

Profilometry measurements were performed using a Tencor Instruments Alpha Step 200 instrument.

4.3 Results and Discussion

4.3.1 Preparation and Characterization of Clicked-On MIP Sensors

The three-step synthesis based on the Sharpless 'click' reaction used in this study to covalently attach thin molecularly imprinted polymer (MIP) films to Au electrodes is illustrated in Scheme 4.1. Raman spectroscopy was employed to monitor the outcome of the click reaction on the SAM surface as well as the formation of the grafted MIP thin films on the monomer modified Au electrodes. Figure 4.1. shows the Raman spectra of the SAM-modified Au electrode before and after clicking propargyl acrylate to the surface. The asymmetric azide stretching mode at 1251 cm^{-1} is distinctly observed in the spectrum of the mixed SAM. After carrying out the click reaction, a new band appears at

1507 cm^{-1} which we assign as the triazole ring stretching mode. Comparison of the two Raman spectra clearly shows the decrease of the azide stretching band and the increase of the triazole ring stretching band, and indicates that the monomer molecules were successfully clicked onto the azidoundecanethiol modified Au surface.

To evaluate damage to the SAM caused by the 'click' reaction step, we used Au oxide stripping voltammetry to measure the surface area of Au exposed to solution after completion of the 'click' procedure. The integrated area of the Au oxide stripping peak is 2.1 μCcm^{-2}. Using Faraday's law and the known packing density of Au, we calculate that this corresponds to about 0.05 monolayer.[202] That is, ~5% of the SAM was lost during the click reaction and ~95% of the SAM remains intact. Representative voltammetric data are included as an inset to Figure 4.1. The Raman spectrum of the MIP membrane grafted onto an Au surface is compared with the spectrum of MIP particles prepared by solution polymerization that were drop coated onto an Au surface in Figure 4.2. For the MIP particles drop coated onto Au, the spectrum shows bands at 1584 cm^{-1}, 1452 cm^{-1}, and 1345 cm^{-1}, which are assigned to the following vibrations: carbonyl stretching, C–H inplane bending, and C–O bending.[203-205] The Raman spectrum of the MIP membrane grafted on the surface showed similar bands at 1598 cm^{-1}, 1456 cm^{-1}, and 1350 cm^{-1}, with an additional band at 1500 cm^{-1} that is assigned to the triazole ring stretching mode as noted previously.[206-208] The observation of the triazole ring stretch in this spectrum indicates that the monomers clicked on the surface were not displaced by the subsequent polymerization step. These results confirm the formation of MIP on the surface through our synthetic strategy.

4.3.2 Amperometric Detection of Hydroquinone

Comparison of the cyclic voltammetric response of the clicked-on MIP sensors before and after washing confirms that HQ molecules were indeed embedded in the MIP thin film during the polymerization step (Figure 4.3.). More specifically, the cyclic voltammogram of the as-prepared clicked-on MIP sensor displays a pair of quasi-reversible redox waves centered at ca. +0.20 V with a peak potential difference (ΔEp) of 117 mV (solid line). In addition, the ratio of the anodic and cathodic peak currents is approximately 1:1. After the extraction of HQ, the voltammetric signal disappears (dotted line) and is similar to the response of the clicked-on NIP electrode (dashed line). It should be noted that these electrochemical measurements were carried out in a HQ-free solution. These results indicate that the HQ molecules embedded in the MIP membranes could be efficiently removed from the imprinted polymer membranes by washing with a water and methanol flux.

Figure 4.4. shows the results of chronoamperometric experiments performed using both a clicked-on MIP sensor and the corresponding clicked-on NIP electrode (inset). The concentration of HQ was increased stepwise from 0 to 200 μM. In these measurements, the potential was stepped from −0.1 V to 0.4 V. The amperometric *I*–t curves showed large current responses in the case of the clicked-on MIP sensor, and the current increases linearly with the increase of the HQ concentration. This suggests that cavities complementary to HQ were produced inside the MIP membrane after the removal of template HQ molecules. The porosity of the MIP membranes allows the rebinding of HQ molecules and promotes the redox reaction of HQ on the electrode surface. As expected, almost no current response was observed with the clicked-on NIP

electrode, which demonstrates the excellent coverage of the non-conducting acrylic polymer membrane on the surface that completely blocks electron transfer processes in the absence of imprinted pores. Moreover, the current responses were found to be very reproducible, which suggests the MIP membranes are quite stable.

We also tested the current responses of sensors prepared by the conventional coat-on method. For these experiments, MIP and NIP particles were synthesized by solution polymerization, keeping the concentration ratio of template, monomer, and cross-linker the same as what was used in the fabrication of the click-on polymer films. In addition, in an effort to keep the total amount of polymer approximately the same, the volume of polymer suspension drop-coated onto the Au electrode was kept as close as possible to the volume of the MIP reaction solution used for the surface polymerization reaction (see Section 4.2 for details).

Figure 4.5. shows the calibration curves constructed using the amperometric data just discussed. From the slope of the calibration curves, the sensitivity for each electrode was obtained. For the clicked-on MIP sensor, the sensitivity was found to be 113±5 $mAcm^{-2}M^{-1}$, while the sensitivity of the coated-on MIP sensor was 40±2 $mAcm^{-2}M^{-1}$, a difference of a factor of three. It should be noted that the slope of the calibration curve for the clicked-on MIP sensor appears to decrease slightly above [HQ]~15 μM. The origin of this behavior is not fully understood at this time, but is consistent with the existence of a finite density of pores inside the MIP. This would be expected to lead to mass transfer limitations at higher HQ concentrations, with a corresponding drop in sensitivity, consistent with our observations. The sensitivity reported above is the average value of the two slopes. Finally, the detection limit of the clicked-on MIP sensor was calculated to

be 1.21±0.56 μM based on 3σ of the blank signals, while the detection limit of the coated-on MIP sensor was 4.43±0.40 μM; that is, 3.7 times higher than that of the clicked-on MIP sensor.

The diffusion coefficient (D_0) is a useful parameter for studying mass transfer phenomena at a surface modified electrode. When the current reaches a steady-state value, D_0 can be calculated using the Cottrell equation.[209] D_0 for HQ measured using the clicked-on MIP sensor was found to be $(2.19\pm0.83)\times10^{-5}$ cm^2s^{-1}, in good agreement with the diffusion coefficient in aqueous electrolyte (2.26×10^{-5} cm^2s^{-1}) measured previously.[210] In contrast, the HQ D_0 measured at the coated-on MIP sensor was found to be $(6.75\pm1.63)\times10^{-6}$ cm^2s^{-1}, a factor of 3.2 times smaller than what was measured using the clicked-on MIP sensor. These comparisons suggest that the higher sensitivity, lower detection limit and faster diffusion observed at the clicked-on MIP sensor should be mainly attributed to two factors: (i) the surface imprinting technique provides a large population of binding sites which improves the binding capacity of the sensor; (ii) the 'click-on' imprinting strategy does not require the use of a supporting agarose gel layer, lowering the mass transfer resistance. The gel layer impedes the diffusion of HQ into the recognition sites contained within the MIP, and slows down the apparent electron transfer rate.[20] To test the importance of hypothesis (ii), film thicknesses were measured using profilometry, were found to be 1.1±0.3 μm, 1.4±0.3 μm, and 5.0±0.3 μm, respectively, for the 'click-on', 'coat-on' and 'coaton'+ agarose samples. In all cases, we measured thickness values from multiple spots on multiple samples and averages are reported. From this data, the thickness of the agarose layer is estimated to be ca. 3.6 μm. Finally,

the detection limit achieved using the 'clicked-on' system is sufficiently low for many practical applications, as the suggested exposure level of for HQ in water is 1.82 μM.[211]

4.3.3 Selectivity Study

The selectivity of the clicked-on MIP sensor toward HQ was evaluated by testing its current response against three model interfering compounds (Scheme 4.2), including catechin, (L)-ascorbic acid (AA), and serotonin, as a function of concentration. The concentration dependent current response of single component solutions of hydroquinone and the three model interferents are shown in Fig. 4.6. In each case, the potential was stepped from −0.10 V to a value of +0.4 V as in previous experiments. Serotonin and AA show detectable current responses at concentrations near 10 μM, while for catechin, measurable currents were observed only at 100 μM. When [HQ] = 150 μM, the current response of catechin, AA, and serotonin were 1.28%, 11.6%, and 9.82%, respectively, of the HQ current response. This behavior is likely due to the transport of small amounts of these structurally similar compounds through the cavities of the imprinted membrane to reach at the Au electrode surface where they can be oxidized. This hypothesis is supported by the observation that AA, which is the molecule that is most similar to HQ with respect to both its functional groups and size, gave the highest interfering current. On the other hand, while serotonin is smaller size than HQ, but its functional groups are quite dissimilar, leading to a lower interfering current. The functional groups of catechin are similar to HQ, but its large size limits its ability penetrate into the cavities. The selectivity of the 'clicked-on' MIP sensor represents a significant improvement compared

to the ‘coat-on’ strategy, for which the response of interferents was found to be greater than 40% of the target analyte signal.[173]

In a second series of experiments, the selectivity of the ‘clicked-on’ MIP sensor in a solution containing 30 μM HQ was tested in the presence of different concentrations of catechin, AA, and serotonin. The selectivity was evaluated by calculating the current ratio (I_{HQ+i}/I_{HQ}), where I_{HQ+i} and I_i are the amperommetric currents in the presence and absence of interfering compounds, respectively. As shown in Fig. 4.7., a 2-fold excess of catechin, AA, and serotonin over HQ results in only minor changes of the current ratio, which varied from 1.09 to 1.19. On the other hand, a 5-fold excess of interfering species over HQ resulted in current ratios that ranged from 1.22 to 1.34. In the case of all three interferents, the magnitude of interfering current was greater in the presence of HQ than in its absence (i.e., when compared to the results in Fig. 4.6.). This may be due to the fact that the HQ molecules in the test solution facilitate the mass transfer of interfering molecules through the sensing membrane, but this phenomenon needs to be investigated further.

These two lines of investigation indicate that the ‘clicked-on’ MIP sensor showed outstanding selectivity for HQ over other potentially interfering compounds. Low concentrations of HQ corresponding to EPA-specified exposure levels in the environment could be detected in a complex matrix without the need of an additional separation step.

4.4 Conclusions

In this work, we have successfully demonstrated a simple, three-step synthetic method to graft thin MIP films onto Au surfaces, and the use of these modified electrodes

as amperometric sensors. The key idea is to covalently attach monomer molecules to a SAM using click chemistry. From there, direct polymerization of the MIP membrane on the electrode surface is straightforward. This approach allows us to achieve a sufficiently high density of molecularly imprinted sites for sensitive measurements without significant loss of specificity. In addition, our method eliminates the need for an agarose adhesion layer, which leads to improved mass transfer of the analyte to the electrode. This is borne out by the fact that the sensitivity of the clicked-on MIP sensor is about 3-fold higher than the conventional coated-on MIP sensor, and the detection limit for HQ is 3.7 times lower than that by the coated-on MIP sensor. Finally, this synthetic strategy is general in nature, and can be extended to the development of sensors for other electroactive small molecules.

Scheme 4.1

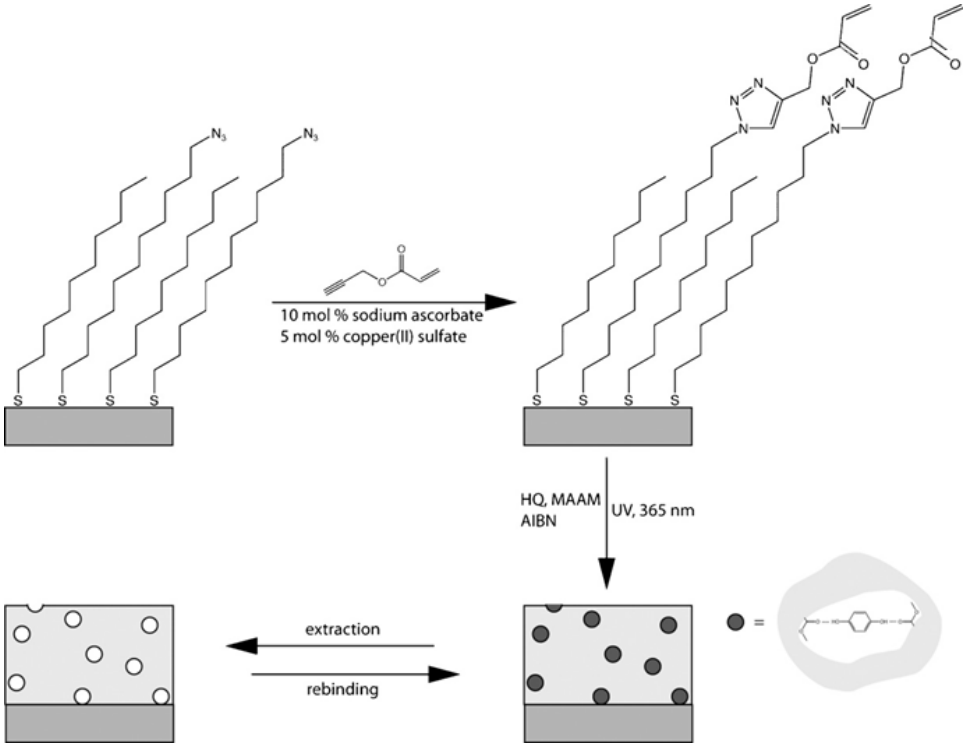
10 mol % sodium ascorbate
5 mol % copper(II) sulfate
HQ, MAAM
AIBN
UV, 365 nm
extraction
rebinding

Scheme 4.2

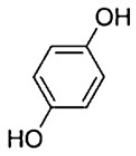

Hydroquinone (HQ)

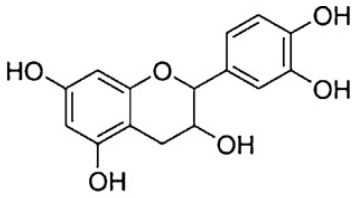

Catechin

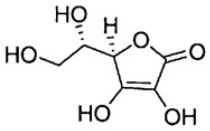

(L)-ascorbic Acid

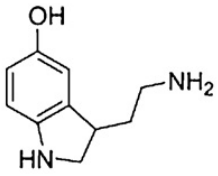

Serotonin

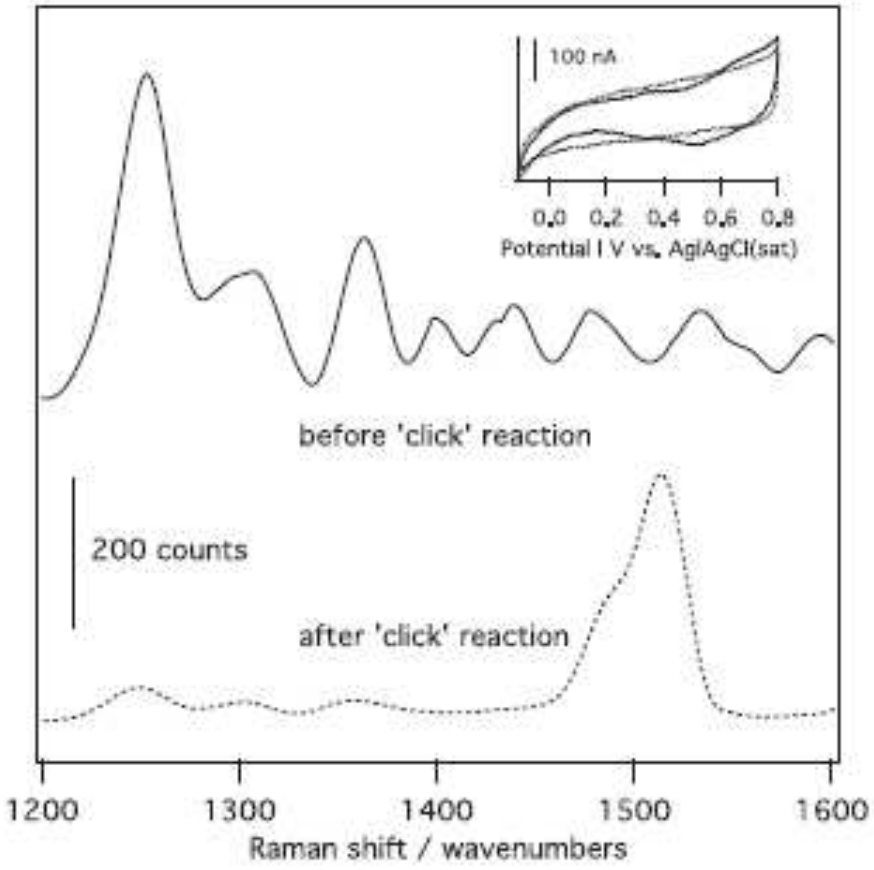

Figure 4.1. Raman spectra of the 1-azidoundecan-11-thiol/decanethiol mixed monolayer on Au before (upper trace, solid line) and after (lower trace, dashed line) clicking on propargyl acrylate. Excitation wavelength: 514 nm. Inset: gold oxide stripping voltammetry reveals that SAM is ~95% intact after click reaction. See text for details.

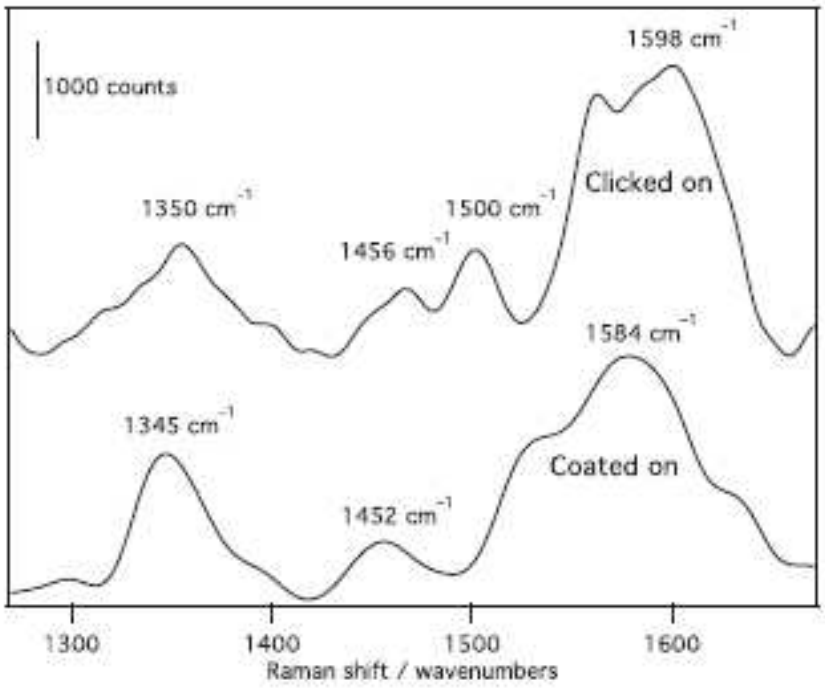

Figure 4.2. Raman spectra of a MIP membrane clicked onto the Au electrode surface (upper trace) and a MIP prepared by solution polymerization drop coated onto the Au electrode surface (lower trace). Excitation wavelength: 514 nm. The triazole ring stretching mode can clearly be seen at ca. 1500 cm^{-1} in the spectrum of the 'clicked' on polymer (upper trace).

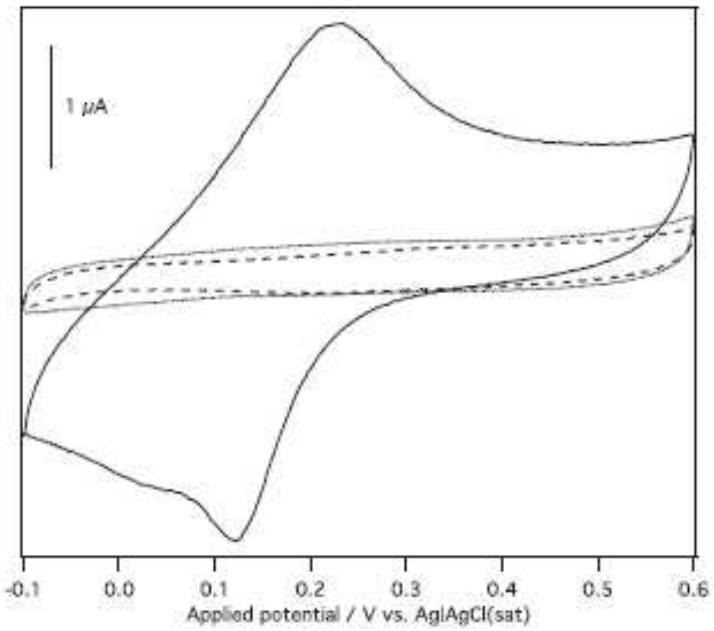

Figure 4.3. Cyclic voltammetric response of the clicked-on MIP sensor before (solid line) and after extraction (dotted line) of HQ. Also shown is the response of a clicked-on NIP electrode (dashed line). All data were measured in N_2-saturated PBS (0.1 M, pH 7.4) electrolyte using a scan rate of 100 mV s^{-1}.

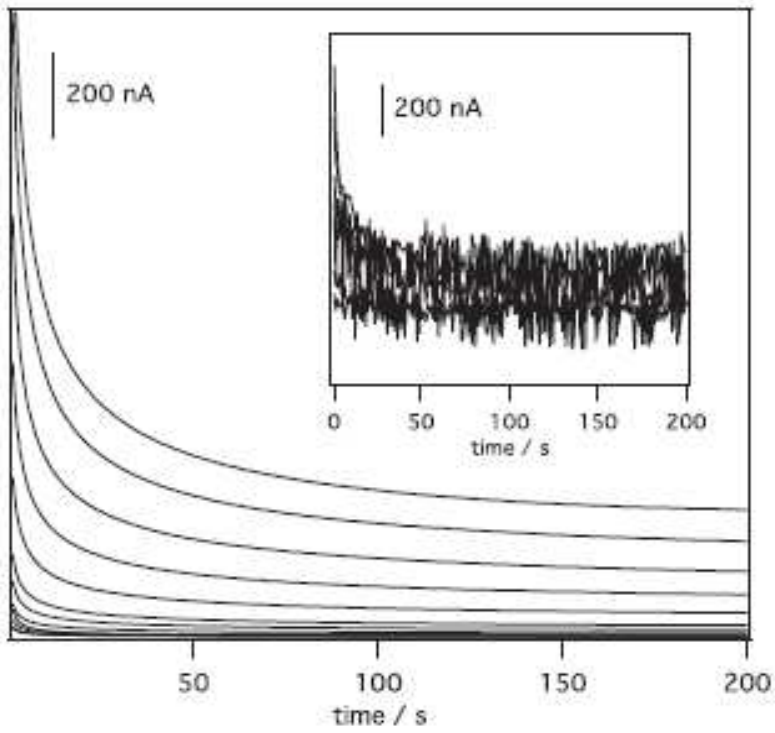

Figure 4.4. Chronoamperometric (i vs. t) response of a clicked-on MIP sensor as a function of HQ concentration. The potential was stepped from −0.10 V to a value of +0.40 V to oxidize HQ; the supporting electrolyte was 0.1 M PBS (pH 7.4). The inset shows the response of the corresponding NIP/SAM/Au electrode under identical conditions. The HQ concentration was varied from 0 to 200 μM.

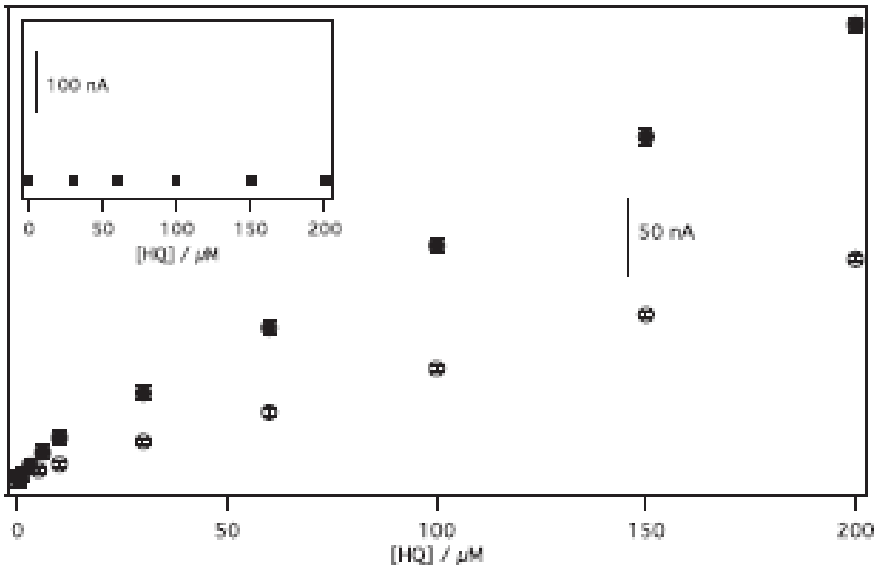

Figure 4.5. Calibration curves constructed for the clicked-on MIP sensor (filled circles) and clicked-on NIP sensor (inset, filled squares) electrodes using the data shown in Fig. 4.4. The behavior of the coated-on MIP/Au (open circles) and NIP/Au (inset, open squares) electrodes are also shown. Average standard deviation values are 5 nA, 2 nA, 0.5 nA, and 0.2 nA, respectively, for the 'clicked-on' MIP, 'coated on" MIP, 'clicked-on' NIP, 'coated on" NIP sensors.

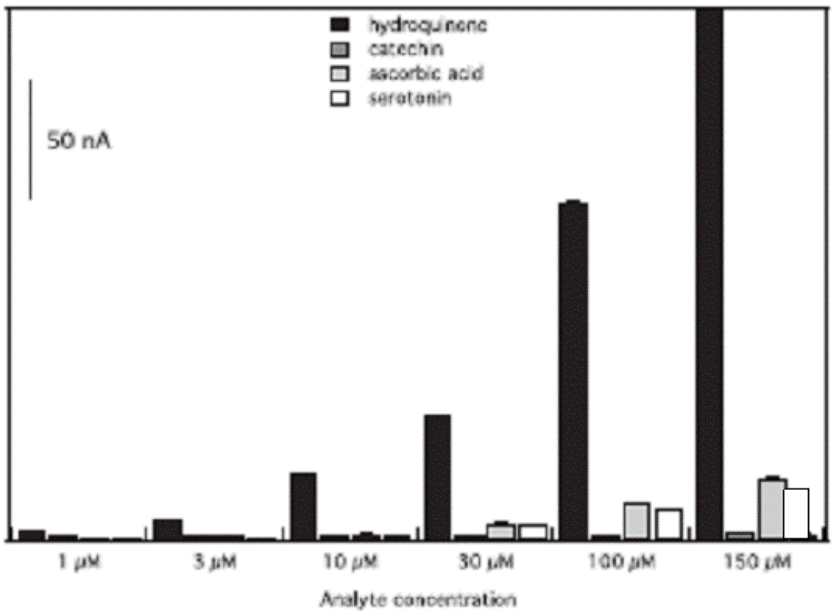

Figure 4.6. Current response of the clicked-on MIP sensor to HQ, catechin, AA, and serotonin measured individually. Average standard deviation values are 7, 0.4, 1, and 0.4 nA for these analytes, respectively.

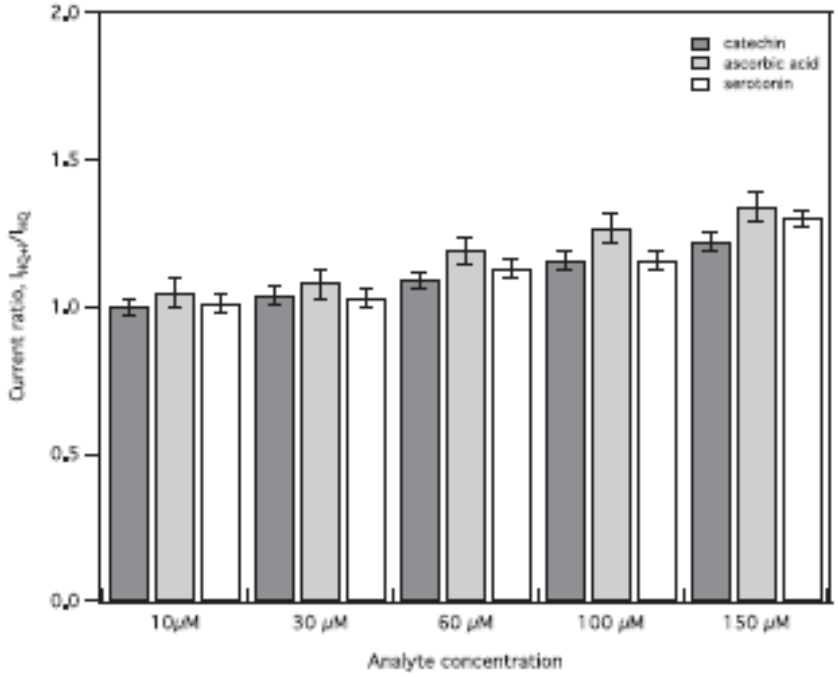

Figure 4.7. Current ratio (I_{HQ+i}/I_{HQ}) of the clicked-on MIP sensor measured in a 30 μM HQ solution in the presence of varying concentrations of catechin, AA, and serotonin. Average standard deviation values are 0.03, 0.05, and 0.03 for these interferents, respectively.

Chapter 5

Bipolar Electrochemical Oxygen Sensor using Quenching of the Electrogenerated Chemiluminescence (ECL) as a Photonic Reporter

5.1 Introduction

Electrochemical detection is predominant in sensor development and applications in market. Traditionally, the electrochemical measurement is based on a three-electrode configuration. One working electrode is employed in the system which just allows for detection of single analyte.[84,85] In addition, the current readout requires a direct electrical connection with the working electrode that makes the integration with miniaturized systems difficult. Over the past decade, a wireless technology, bipolar electrochemistry, has emerged to provide a promising approach for integration of electrochemistry with lab-on-a-chip systems and it has potential for simultaneous detection of multiple analytes by employing an array of microelectrodes.[83] In the bipolar configuration, an electronic conductor placed in contact with an conductive phase can act as a bipolar electrode (BPE).[83] When a sufficiently high external electric field is applied across the BPE, faradaic reactions occur at both ends of the electrode.[86] A simple power supply or even a battery is sufficient to perform the experiment, and no direct electrical connection between the BPE and the power supply is needed. Thus, the simplicity and the fact that it is a wireless technique make bipolar electrochemistry very attractive.

Although bipolar electrochemistry has been used in the field of material science,[94] battery technologies,[88] and electrosynthesis,[89,90] the application of BPE for electroanalytical field is very limited. This is mainly due to a lack of readout methods because of the difficulty of measuring current flowing through the BPE without a direct electrical connection. Several unique approaches for current readout have been reported over the past few years. Nyholm[97] and coworkers used BPEs to detect electrochemical active compounds by applying electrical field to induce bipolar behavior between two Au bands. The split design employed realizes direct measurement of the current passing through the BPE, but at the cost of complicating the detection system with an external electrical connection, which thus limited its applicability in miniaturized systems. A report by the group of Crooks[98] utilized the electrodissolution of the BPE itself by dissolving Ag at the anodic pole once a cathodic sensing event occurs. The amount of Ag dissolution provides a permanent record of the state of the BPE sensor. However, this method is not compatible with reusable sensors, and requires Ag metal deposition onto each BPE prior to detection which potentially decreases the reproducibility of experiment. Another popular alternative strategy for detecting faradaic processes at BPEs is to use ECL, especially the $Ru(bpy)_3^{2+}$/co-reactant system,[85,99,100] as an indirect reporter of the current. ECL does not require an excitation light source and the reaction can be performed with a very small sample volume,[102] making it ideal for integration with simple, yet portable devices at low cost. Moreover, direct detection of ECL just requires a CCD camera which allows for real-time monitoring of the detection event. Therefore, the marriage of ECL and BPEs has great potential in simultaneously detection of analytes with an array of BPEs for a wide range of applications using optical technique.[83]

The ECL-based detection using BPEs has been intensively explored by the group of Crooks.[83-85,87,100] They proposed that the presence of any electroactive analyte could be detected by taking advantage of both poles where the analyte of interest is reduced at the cathodic pole, and this reaction triggers light emission at the anodic pole by the corresponding oxidation of $Ru(bpy)_3^{2+}$ and the co-reactant.[83] On the other hand, competition assay that utilizes the quenching effect by an ECL quencher[101,105,212,213] is a powerful tool for detection of electrochemically inactive targets ranging from biomedical applications to food management. In assays using ECL quenching, the faradic reactions at cathodic pole can be simple reductions such as oxygen reduction or hydrogen evolution. In addition, the analyte is evolved in the ECL reactions which allows for straightforward measurements. One example applying ECL quenching for sensing in traditional electrochemical cell was reported by Landers[101] and coworkers, in which a quencher is attached to a complementary DNA strand and an intramolecular ECL quenching in hybridized oligonucleotide strands can be realized for sequence-specific DNA detection. Furthermore, effective ECL quenchers can also be the analyte of interest for direct detection, such as the measurement of dissolved O_2 concentration in aqueous solution. However, the investigation of electrochemical sensing using the quenching of ECL in bipolar platform is very limited.

In this work, we report a bipolar electrochemical sensor based on ECL quenching for the first time for detection of dissolved O_2. Ferrocene methanol (FcMeOH) was first employed as an ECL quencher to test the feasibility of using the quenching effect to determine the concentration of analytes. The $(I_0\text{-}I)/I$ values fit the Stern-Volmer equation and the quencher rate coefficient k_q was determined to be 1.56×10^9 $M^{-1}s^{-1}$ that is

comparable to the value of 3.1×10^9 $M^{-1}s^{-1}$ reported in previous literature.[101,214] Using this ECL quenching effect, the amount of O_2 that dissolved in an initially oxygen-free testing solution was evaluated. The intensity of ECL was continuously decreasing with the increase of time that allows O_2 in air to dissolve in the testing solution. Chronoamperometry was then performed to directly monitor the amount of O_2 dissolved in the testing solution with time and the current from oxygen reduction reaction (ORR) increases, indicating an elevated amount of O_2. The results confirmed that the reduced intensity of ECL was due to quenching by dissolved O_2, promising the potential application of this method for real-time O_2 monitoring in portable devices. More importantly, with a big selection of effective ECL quenchers currently available,[105-107,213,215,216] this work opens up the possibilities of applying ECL quenching based on a bipolar platform for detection of any analyte with an attached quencher or as the quencher itself.

5.2 Experimental

5.2.1 Materials and Reagents

Tris(2,2'-bipyridyl)dichlororuthenium(II) hexahydrate (Sigma-Aldrich), sodium oxalate ($Na_2C_2O_4$) (99.5+%, Sigma-Aldrich), ferrocene methanol (FcMeOH) (99%, Sigma-Aldrich) were used as received. $HClO_4$ (70%, Fisher Scientific) was diluted by DI water to prepare 1 mM stock solution at pH 3.4. Ethanol, H_2O_2, and sulfuric acid (all HPLC grade) were from commercial sources and used as received. Millipore-Q purified de-ionized (DI) water (18.2 $M\Omega Ucm^{-3}$) was used to prepare all solutions and to rinse electrodes.

5.2.2 Assembly of Bipolar Device

A platinum (Pt) rod (l_{elec} = 1.4 cm) was employed as the bipolar electrode (BPE) and two pieces of stainless steel foils were used as driving electrodes. Prior to assembly, stainless steel foils were polished using an aqueous slurry of 0.05 μm alumina particles and then washed with water and ethanol in an ultrasonic cleaner. The Pt-BPE was immersed in fresh piranha solution (H_2SO_4/H_2O_2, 3:1) for about 5 min, then rinsed with DI water, and dried under nitrogen gas. *Caution: Piranha solution is dangerous to human health and should be used with extreme caution and handled only in small quantities.* The Pt-BPE was then placed in the center of a glass dish (d = 5 cm) using a double sided tape. A glass cover for the glass dish was specially made to maintain an oxygen-free environment in the bipolar cell as shown in Scheme 5.1A. Two slips situated on opposite sides of the cover were cut to hold the driving electrodes. A small hole was drilled close to the anodic side of the BPE, allowing diffusion of O_2 into the cell, which was initially kept sealed by a piece of black tape to isolate the device from O_2 in air.

5.2.3 ECL Measurements

A testing solution of 5 mM $Ru(bpy)_3^{2+}$ with 25 mM $Na_2C_2O_4$ was prepared in $HClO_4$ at pH 3.4 and poured into the bipolar cell. The solution was then purged with N_2 for 20 min to exclude O_2 and then kept under N_2 environment. A FcMeOH solution of 5 mM was prepared and purged with N_2 for 20 min. After applying a potential of 15 V to the driving electrodes connected with a power supply, aliquots of FcMeOH was added into the testing solution. The concentration of FcMeOH in the testing solution was varied from 0 to 2 mM. The ECL signal was measured with a Nikon D3100 SLR digital camera

in a dark room and the image was processed using ImageJ downloaded from NSF website to obtain the gray value of light. The O_2 quenching experiments were performed following the same procedure but without the addition of FcMeOH. Instead, the small hole was exposed to air and allowed O_2 to dissolve in the testing solution after the black sealing tape was peeled off.

5.2.4 Electrochemical Measurements

Cyclic voltammetry (CV) and chronoamperometry were carried out at room temperature using a three-electrode set-up in the same bipolar cell. The supporting electrolyte was 1 mM $HClO_4$ (pH 3.4), the reference electrode was Ag/AgCl(sat) (Bioanalytical System, Inc.), and the counter electrode was a home-made Pt gauze. The working electrode is the Pt rod used in bipolar electrochemistry. Before electrochemical measurements, the solution was purged with N_2 for at least 20 min. The electrochemical circuit was controlled using an Epsilon electrochemistry workstation (Bioanalytical Systems, Inc.). Cyclic voltammograms were recorded between -0.2 V and 0.7 V using a scan rate of 20 mVs^{-1}. Amperometric measurements were carried out by stepping the potential to 0 mV to ensure complete reduction of O_2 and held at 0 mV for 1 sec.

5.3 Results and Discussion

5.3.1 Principle of Operation

Electrochemical sensing is carried out based on a bipolar platform. The physical layout and operation principle of the bipolar configuration used in our approach are illustrated in Scheme 5.1. Briefly, an external potential, E_{tot}, is applied to the two driving

electrodes situated at both ends of a cell, and the resistance of the electrolyte solution results in a linear potential gradient along the cell. The difference in potential between the two ends of the BPE, ΔE_{elec}, is the fraction of E_{tot} dropped across the length of the BPE. When ΔE_{elec} is sufficiently large, electrochemical reactions will occur at both ends of the BPE simultaneously. In the configuration designed for our experimental purpose, ECL reaction is the most energetically favorable process at the anodic pole of the BPE while hydrogen evolution is the most favorable reaction at the cathodic pole of the BPE. The intensity of ECL reports the amount of analyte in solution since the analyte, O_2 in here, is an effective ECL quencher.

5.3.2 $Ru(bpy)_3^{2+}$ ECL Quenched by FcMeOH

To test the feasibility of detecting analyte by ECL quenching, a model compound, FcMeOH was first employed as the quencher. We chose FcMeOH because it has been proven to be an efficient and stable ECL quencher by reacting with excited-state $Ru(bpy)_3^{2+}$ to quench ECL light emission[101,217] (Scheme 5.2). Prior to a measurement, the testing solution containing 5 mM $Ru(bpy)_3^{2+}$ and 25 mM $Na_2C_2O_4$ dissolved in 10 mL pH 3.4 perchloric acid was deoxygenated with nitrogen gas for 20 min to eliminate the possibility of oxygen evolved quenching.[218] E_{tot} of 15 V was applied to the driving electrodes and ΔE_{elec} value of 4.2 V was calculated for the BPE 1.4 cm in length using the equation $\Delta E_{elec} = E_{tot}/d_{cell} \times l_{elec}$.[83] Under these conditions, a stable and easily detectable luminescent signal was recorded by a camera. When aliquots of FcMeOH were injected into the testing solution, the intensity of the emitted light was decreasing with the increased concentration of FcMeOH as shown in Figure 5.1.A (from top to bottom).

Figure 5.1.B shows the gray values of light obtained by ImageJ plotted as a function of FcMeOH concentrations. The ECL intensity decreases significantly with the increased FcMeOH concentration at the beginning stage and tends to level off at high concentration range. When 2 mM FcMeOH was present in the ECL solution, the ECL intensity was decreased by more than 67%.

The results of the concentration-dependent experiments are further presented as Stern-Volmer plots for FcMeOH. Sern-Volmer equation is a useful tool for evaluating the performance of a quenching phenomenon.[215,219,220] The simple expression of the equation is $I_0/I = 1 + k_q\tau_0[Q] = 1 + K_{sv}[Q]$ ($(I_0-I)/I = K_{sv}[Q]$ upon rearrangement), where I_0/I is the observed ratio of luminescence intensity in an unquenched sample to that in a quenched one, k_q is the quencher rate coefficient, K_{sv} is the Stern-Volmer constant, τ_0 is the photoluminescence lifetime of $Ru(bpy)_3^{2+}$ in the absence of quencher, and [Q] is the concentration of the quencher. As illustrated in Figure 5.2., $(I_0-I)/I$ is linearly proportional to the concentration of FcMeOH indicating a diffusion-limited quenching process. Using the $(I_0-I)/I$ values from the Stern-Volmer plot for FcMeOH and the photoluminescence lifetime of $Ru(bpy)_3^{2+}$ in the absence of quencher of 589 ns,[101] a value for K_{sv} of 920.6 M^{-1}, corresponding to a k_q of 1.56×10^9 $M^{-1}s^{-1}$, was determined for FeMeOH. This value is about half of the value of 3.1×10^9 $M^{-1}s^{-1}$ reported by others.[101,214] This is possibly due to the fact that the quenching experiment is performed using a bipolar configuration rather than a traditional three-electrode set-up, and the quencher was added into the ECL solution by aliquots but not premixed in the testing solution. The results demonstrate the use of ECL quenching in a bipolar cell for detection of any analyte that can act as a quencher.

5.3.3 $Ru(bpy)_3^{2+}$ ECL Quenched by O_2

We evaluated the use of ECL quenching and the bipolar platform to monitor the concentration of dissolved oxygen. To ensure an oxygen-free environment prior to measurements, the testing solution containing 5 mM $Ru(bpy)_3^{2+}$ and 25 mM $Na_2C_2O_4$ was degassed with N_2 for at least 20 min and the cell was filled with N_2 and isolated from air by sealing the inlet on the glass cover with black tape. The ECL generated under N_2 was recorded with a camera and the image was evaluated as the light intensity at 0 sec. A stopwatch started running to record time as soon as the black tape was taken off and O_2 was allowed to diffuse into the bipolar cell. The emitted light at different time was recorded with the camera. Figure 5.3.A shows that the intensity of ECL was decreasing dramatically with time as the dissolved oxygen in the testing solution increases (from top to bottom). This is possibly due to the quenching effect of O_2 since O_2 is believed to be an effective quencher for ECL via an energy transfer mechanism[221] (Scheme 5.3). The intensity of each image was evaluated using ImageJ (Figure 5.3.B) and the gray value of the emitted light was plotted as a function of time as shown in Figure 5.3.C. The gray value of ECL decreases drastically with time at the initial stage and reaches plateau after around 400 sec. At 500 sec, the ECL intensity was decreased by 92% from the initial value. The quenching effect observed is believed as the result of increased dissolved oxygen level in the testing solution and agrees well with the behavior observed in the case of FcMeOH quenching with an improved quenching efficiency.

To demonstrate a direct correlation between the quenching phenomenon and the increased concentration of dissolved O_2, chronoamperometry was performed to directly measure the amount of O_2 in the testing solution with time using ORR in the same bipolar

cell employing a three-electrode configuration. The potential required for ORR was determined by cyclic voltammetry carried out in a $HClO_4$ solution at pH 3.4 under oxygen-free atmosphere and that saturated with oxygen (Figure 5.4.). In oxygen-free electrolyte solution, no peak was observed in the cyclic voltammogram (CV), while a characteristic reduction peak can be seen at 300 mV in the CV recorded under oxygen, indicative of ORR.[222] Therefore, a potential of 0 mV was held in chronoamperometry for complete ORR and the current was recorded at varied time starting with an oxygen-free solution. Figure 5.5.A shows representative chronoamperometric curves obtained at different time. For each curve, it starts with a large capacitive current and decays rapidly to reach a steady-state current that is proportional to the concentration of analyte. The calibration curve shown in Figure 5.5.B indicates a nearly linear increase of current with time, indicating the linear increase of dissolved O_2 in the testing solution by diffusing through the small inlet on the glass cover. The standard deviation (STD) was calculated with currents from three measurements and was varied from 3% to 15%. This large STD was likely due to the variations of the manual timing, and to the variations of the delay in time for each measurement. The reproducibility of experiment should be improved by using an automatic system that can carry out measurements at the exact programmed point of time.

To validate a direct relationship between the concentration of O_2 in the testing solution and the intensity of ECL, the gray values of ECL were presented as Stern-Volmer quenching data, $(I_0\text{-}I)/I$, and plotted as a function of time in the same graph with ORR currents measured by chronoamperometry for comparison purpose (Figure 5.6.). As expected, the quenching results of ECL show a similar behavior with the currents

measured by chronoamperometry for ORR, and the two sets of data demonstrate a very good fit. Based on the Stern-Volmer equation: $I_0/I = 1 + k_q\tau_0[Q] = 1 + K_{sv}[Q]$, a linear relationship could be revealed between the intensity of ECL and the concentration of dissolved O_2. However, because of the great difficulty of recording ECL at the exact time point at which the current of ORR was measured, a $(I_0-I)/I$ curve plotted as the function of O_2 concentration could not be generated at this stage of research. Nevertheless, we have demonstrated the quenching of ECL by dissolved O_2, indicating the feasibility of using ECL quenching as a photonic reporter for O_2 concentration based on a simple bipolar platform.

5.4 Conclusions

In this work, we presented the use of ECL quenching as a direct reporter for O_2 detection employing the unique bipolar electrochemistry. FcMeOH was first applied as the quencher to test the feasibility of applying ECL quenching to measure the concentration of analyte, and a linear relationship was obtained between I_0/I and FcMeOH concentration based on Stern-Volmer equation. Then, the use of ECL quenching by O_2 to directly monitor the amount of O_2 in the testing solution was demonstrated. Although a calibration curve between $(I_0-I)/I$ and O_2 concentration could not be plotted at this stage, a direct relationship between the two has been successfully proven. The current version of bipolar O_2 sensor is promising in real-time monitoring of O_2 level in scuba diving and vehicles. Further experiment of recording ECL and ORR current simultaneously could realize more precise and quantitative analysis. This bipolar electrochemical O_2 sensor allows easy integration with a portable device at low cost, such

as a commercial glucometer. It has great potential for field use in food processing, waste management, and medical testing. Furthermore, the flexibility of the sensing mechanism allows detection of not only O_2, but a variety of compounds that can serve as an ECL quencher.

Scheme 5.1

A

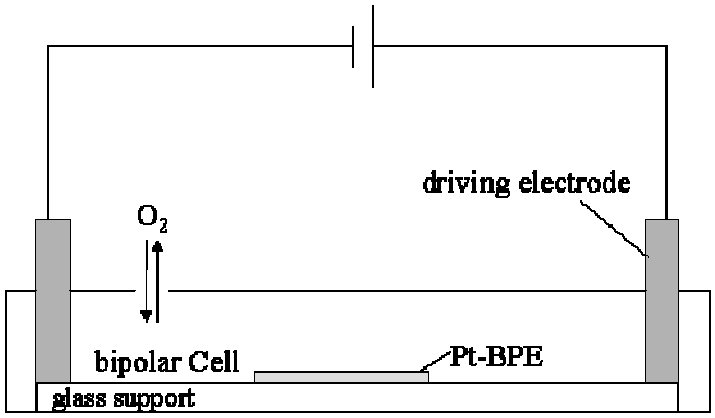

B

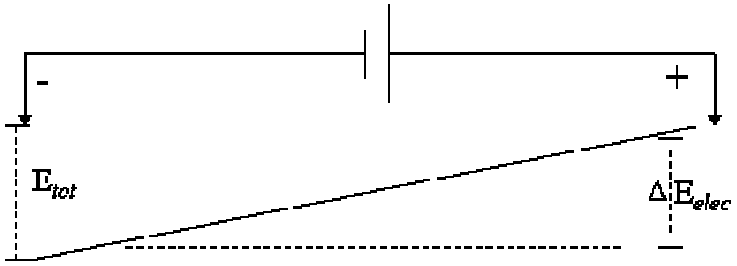

C

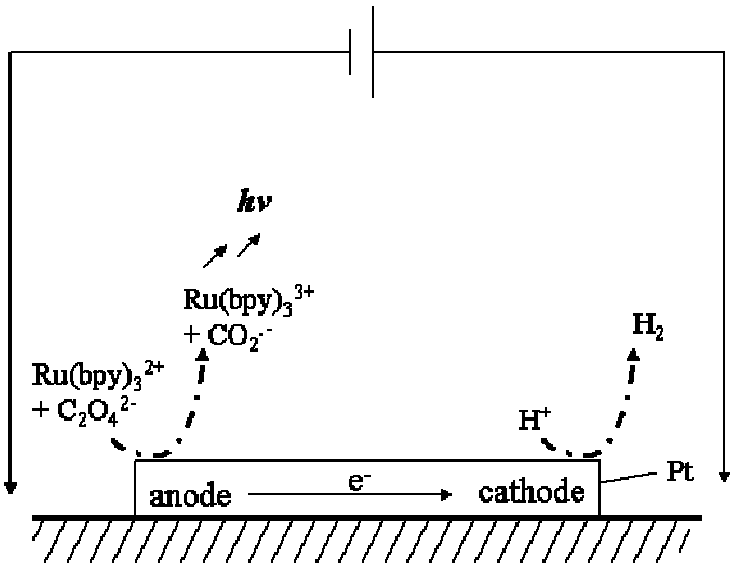

Scheme 5.2

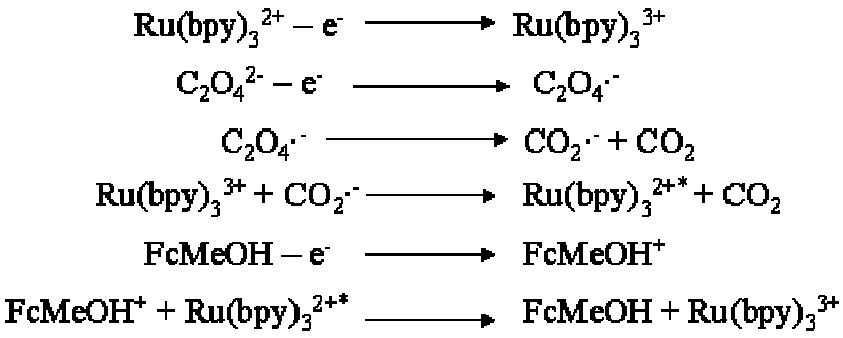
Ru(bpy)3 2+ – e- → Ru(bpy)3 3+
C2O4 2- – e- → C2O4·-
C2O4·- → CO2·- + CO2
Ru(bpy)3 3+ + CO2·- → Ru(bpy)3 2+* + CO2
FcMeOH – e- → FcMeOH+
FcMeOH+ + Ru(bpy)3 2+* → FcMeOH + Ru(bpy)3 3+

Scheme 5.3

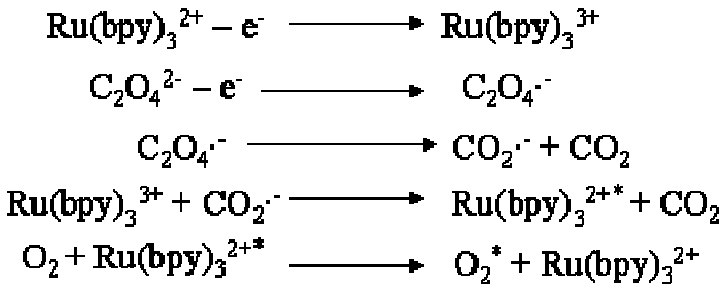
Ru(bpy)3 2+ – e- → Ru(bpy)3 3+
C2O4 2- – e- → C2O4·-
C2O4·- → CO2·- + CO2
Ru(bpy)3 3+ + CO2·- → Ru(bpy)3 2+* + CO2
O2 + Ru(bpy)3 2+* → O2* + Ru(bpy)3 2+

A

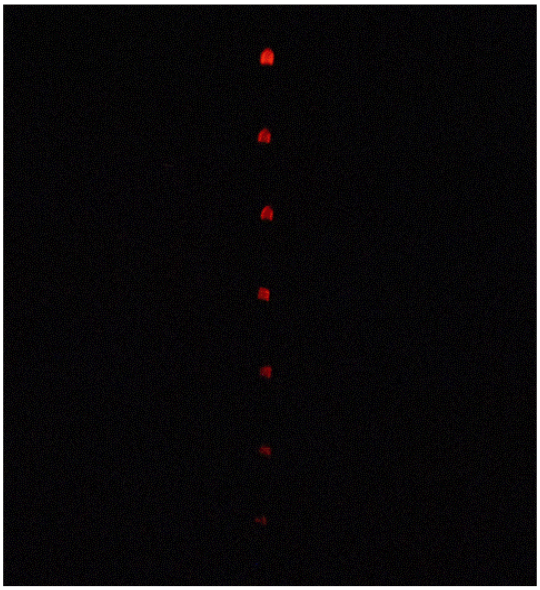

B

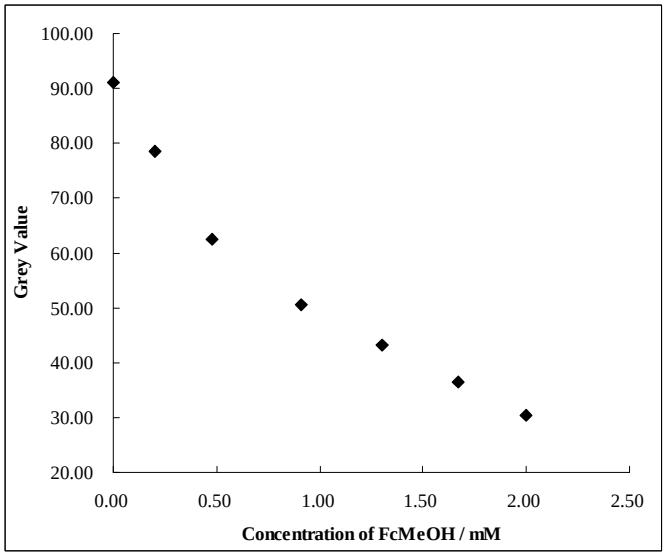

Figure 5.1. (**A**) The ECL emitted in the anodic pole of the BPE at E_{tot} = 15.0 V. From the top to bottom, the luminescence micrographs showing the magnitude of ECL as a function of the FcMeOH concentration from 0 to 2.0 mM in the testing solution containing 5 mM $Ru(bpy)_3^{2+}$ and 25 mM $Na_2C_2O_4$ in 1 mM $HClO_4$ at pH 3.4 in the absence of oxygen. (**B**) ECL intensity displayed as gray value calculated using ImageJ versus FcMeOH concentration.

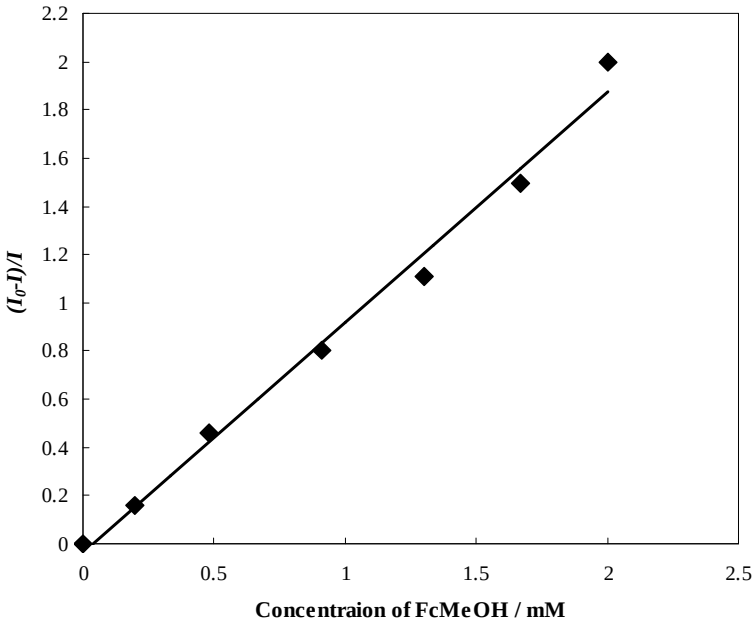

Figure 5.2. Intensity Stern-Volmer luminescence quenching plot for 5 mM $Ru(bpy)_3^{2+}$ by FcMeOH in 1 mM $HClO_4$ at pH 3.4 in the absence of oxygen.

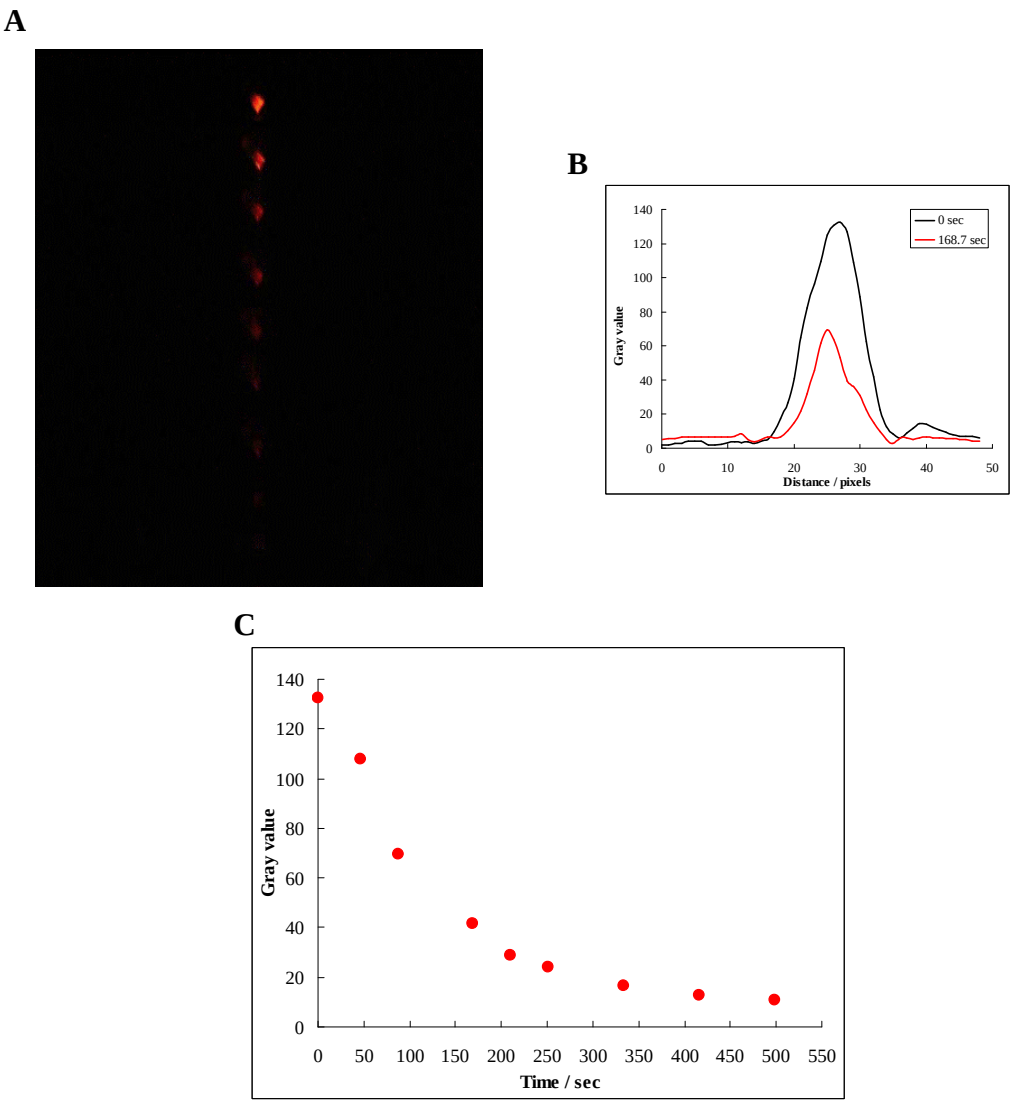

Figure 5.3. (**A**) The ECL emitted in the anodic pole of the BPE at E_{tot} = 15.0 V. From the top to bottom, the luminescence micrographs showing the magnitude of ECL as a function of time. The testing solution contained 5 mM $Ru(bpy)_3^{2+}$ and 25 mM $Na_2C_2O_4$ in 1 mM $HClO_4$ at pH 3.4 initially in the absence of oxygen and O_2 was then allowed to diffuse into the bipolar cell starting at 0 sec. (**B**) Representative gray value plot for ECL intensity analysis. (**C**) ECL intensity displayed as gray value (peak number) calculated using ImageJ versus time.

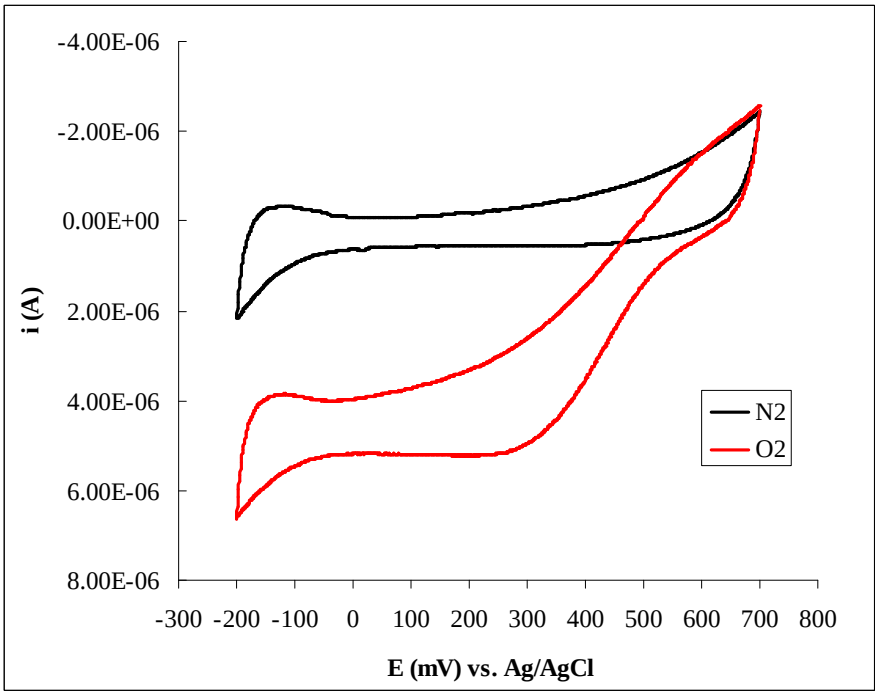

Figure 5.4. CVs of Pt electrode in 1 mM $HClO_4$ at pH 3.4 under N_2 (—) and O_2 (—). Voltammetry was carried out at room temperature at a scan rate of 20 mVs^{-1}.

A

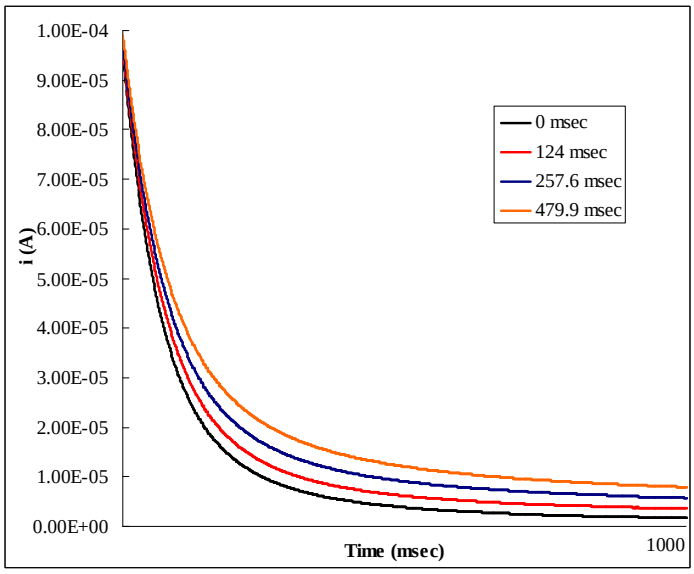

B

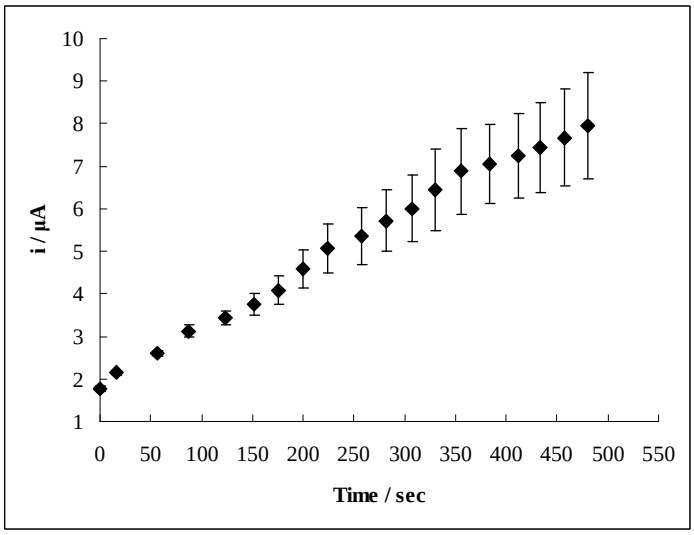

Figure 5.5. (**A**) Representative chronoamperomeric responses for ORR at varied times obtained using a three-electrode set-up in 1 mM $HClO_4$ at pH 3.4 in the same cell for bipolar experiment. The solution was first degassed with N_2 and then O_2 started to diffuse through the inlet on the glass cover and dissolved in the testing solution after 0 sec. (**B**) Calibration plot of current as a function of time. A 0 mV (vs. Ag/AgCl) step potential was used to generate ORR.

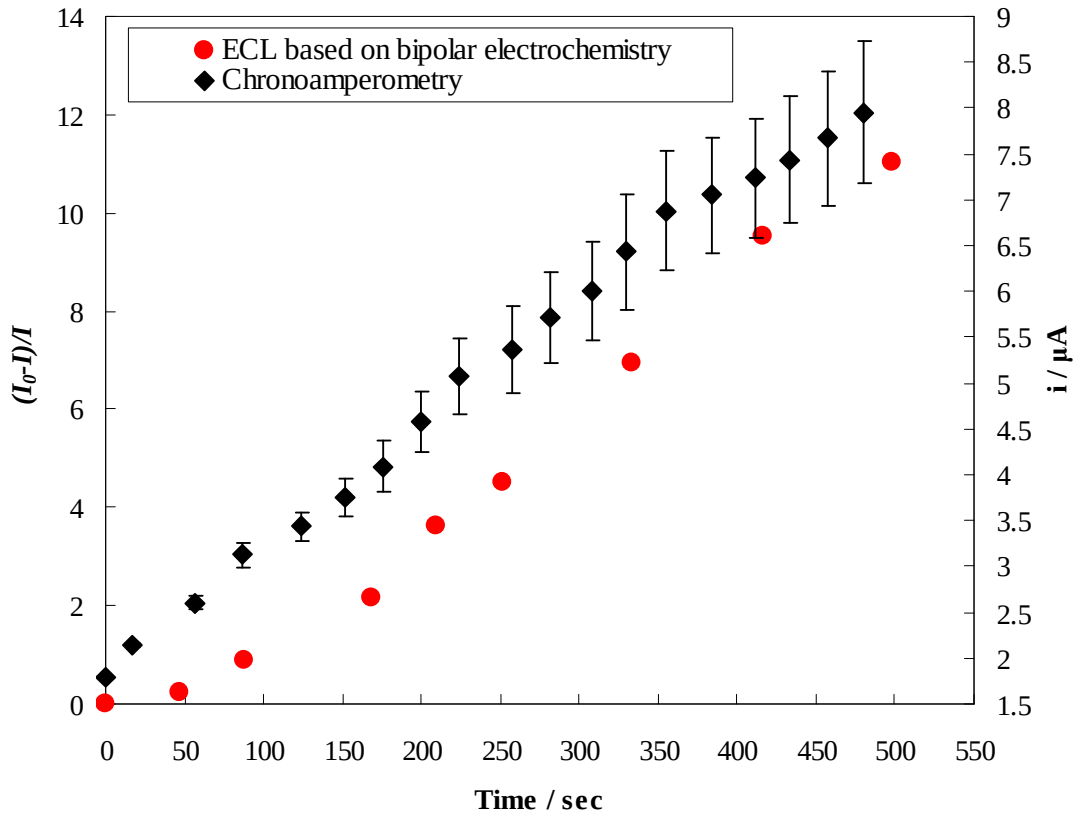

Figure 5.6. Calibration plots for the analysis of intensity Stern-Volmer luminescence quenching data (●), and the analysis of current ratio generated by ORR (◆), plotted as a function of time. The two curves represent a similar trend, indicating the possibility of using ECL quenching as a direct reporter for O_2 measurement.

CHAPTER 6

Conclusions and Recommendations for Future Work

The primary objective of this research work is to develop new platforms by applying versatile recognition elements for electrochemical sensors. We have successfully demonstrated the incorporation of biomolecules (aptamers and antibodies), MIP particles, and MIP thin films with transducer surface to construct electrochemical sensors for different applications including protein quantitation, chiral molecule detection, and environmental toxin measurement. In addition, a novel O_2 sensor using ECL quenching based on a bipolar platform was presented.

In terms of protein quantitation, an electrochemical proximity assay (ECPA) has been proven to detect insulin as low as 128 fM with base-line level background by introducing a short DNA competitor. This method relies on two affinity probes and proximity effect to move a redox active molecule, MB, close to a gold surface in the presence of target. Because of its intrinsic flexibility, ECPA should be useful in quantifying any protein with a pair of antibody. This assay is the first report of combining electrochemistry and proximity assay employing antibody-oligonucleotide conjugates, and is extremely sensitive and selective at an achievable cost for point of care applications. The ECPA sensor needs to be tested directly with unprocessed samples in the next step, such as human blood or urine. Meanwhile, minor modifications of the ECPA strategy have the potential to realize reusable sensors that would lower the

cost significantly. By further engineering and miniaturizing, ECPA could be easily integrated with portable electronic devices and applied in point-of-care settings.

In the development of MIP-based electrochemical sensors, MIP particles and thin films were synthesized and characterized successfully. By using conventional integration method, MIP particles were deposited on a glassy carbon electrode (GCE) and stabilized with a layer of agarose gel. This MIP/GCE sensor is capable of detecting (+)-catechin from a mixture of (±)-catechin and determining relative amount of the two isomers. To further improve the efficiency of integration of MIPs with transducers, a surface imprinting method was proposed. Monomers were attached onto a gold surface using unique “click” chemistry, and UV photopolymerization was then performed directly on the surface in the presence of target molecule. The MIP-sensor was demonstrated to specifically bind analyte of interest and showed enhanced sensitivity compared with the sensor fabricated by conventional coating method. The improved performance of the clicked-on MIP sensor is mainly attributed to the absence of a diffusion barrier and the homogeneous binding sites formed within the polymeric matrix. However, although MIPs are good alternative to biomolecules in terms of stability and cost, the lack of sensitivity and selectivity prevent their use in most medical settings. These drawbacks are attributed to the nature of the artificial polymeric binding sites. Nevertheless, the robustness and stability of MIP-sensors make them ideal for sensing applications in extreme environment, such as battlefield and space exploration. Further explorations on the properties of cavities and polymeric structures could be helpful to improve the overall performance of MIP-based electrochemical sensors.

Finally, a bipolar electrochemical sensor for detection of dissolved O_2 based on ECL quenching was reported for the first time. ECL intensity was recorded by camera and analyzed using ImageJ, while the change of O_2 concentration during the course of ECL experiment was measured by chronoamperometry. The quenching results and amperometric results suggested an excellent agreement between the decrease of ECL intensity and increase of dissolved O_2 concentration, suggesting a successful sensor that is promising in applications for any target that shows quenching effect. However, the reproducibility of experiment needs to be improved by using more mature technique and standardized procedure. Moreover, to achieve quantitation of analyte, further investigation of ECL quenching as a function of O_2 concentration is required in order to fit the Stern-Volmer equation. Once a precise analysis is accomplished, this simple, wireless, and energy-efficient electrochemical sensor can be combined with miniaturized systems at low cost, and allows continuous visual monitoring of sensing events.

References

(1) Pugliese, P.; Molto, J. C.; Damiani, P.; Marin, R.; Cossignani, L.; Manes, J. *J. Chromatogr.* **2004**, *1050*, 185.

(2) Salm, P.; Taylor, P. J.; Roberts, D.; Silva, J. D. *J. Chromatogr.* **2009**, *877*, 568.

(3) Silva, C. J.; Onisko, B. C.; Dynin, I.; Erickson, M. L.; Requena, J. R.; Carter, J. M. *Anal. Chem.* **2011**, *83*, 1609-1615.

(4) Silva, C. L.; Passos, M.; Camara, J. S. *Talanta* **2012**, *89*, 360-368.

(5) Sinha, S. N.; Pal, R.; Dewan, A.; Mansuri, M. M.; Saiyed, H. N. *Int. J. Mass Spectrom.* **2006**, *253*, 48.

(6) Williamson, L. N.; Terry, A. V.; Bartlett, M. G. *Rapid Commun. Mass Spectrom* **2006**, *20*, 2689.

(7) Zhou, Q.; Liu, N.; Qie, Z.; Wang, Y.; Ning, B.; Gao, Z. *J. Agric. Food. Chem.* **2011**, *59*, 12006-12011.

(8) Bau, L.; Tecilla, P.; Mancin, F. *Nanoscale* **2011**, *3*, 121-133.

(9) Dey, D.; Goswami, T. *J. Biomed Biotechnol.* **2011**, *348218*, 7.

(10) Grieshaber, D.; MacKenzie, R.; Voros, J.; Reimhult, E. *Sensors* **2008**, *8*, 1400-1458.

(11) Kimmel, D. W.; LeBlanc, G.; Meschievitz, M. E.; Cliffel, D. E. *Anal. Chem.* **2012**, *84*, 685-707.

(12) Lu, L.-M.; Zhang, X.-B.; Kong, R.-M.; Yang, B.; Tan, W. *J. Am. Chem. Soc.* **2011**, *133* 11686-11691.

(13) Reches, M.; Mirica, K. A.; Dasgupta, R.; Dickey, M. D.; Butte, M. J.; Whitesides, G. M. *ACS Appl. Mater. Inter.* **2010**, *2*, 1722-1728.

(14) Shang, J.; Cheng, F.; Dubey, M.; Kaplan, J. M.; Rawal, M.; Jiang, X.; Newburg, D. S.; Sullivan, P. A.; Andrade, R. B.; Ratner, D. M. *Langmuir* **2012**, *28*, 3338-3344.

(15) Yang, Y.-C.; Lu, H.-H.; Wang, W.-T.; Liau, I. *Anal. Chem.* **2011**, *83*, 8267-8272.

(16) Lowe, C. R. *Trends Biotechnol.* **1984**, *2*, 59-65.

(17) Thevenot, D. R.; Toth, K.; Durst, R. A.; Wilson, G. S. *Biosens. Bioelectron.* **2001**, *16*, 121-131.

(18) Mehrvar, M.; Abdi, M. *Anal. Sci.* **2004**, *20*, 1113-1126.

(19) Chaubey, A.; Malhotra, B. D. *Biosens. Bioelectron.* **2002**, *17*, 441-456.

(20) Blanco-Lopez, M. C.; Lobo-Catanon, M. J.; Miranda-Ordieres, A. J.; Tunon-Blanco, P. *Trends Anal. Chem.* **2004**, *23*, 36-48.

(21) Piletsky, S. A.; Piletskaya, E. V.; Elgersma, A. V.; Yano, K.; Karube, I.; Parhometz, Y. P.; Elskaya, A. V. *Biosens. Bioelectron.* **1995**, *10*, 959.

(22) Piletsky, S. A.; Piletskaya, E. V.; Panasyuk, T. L.; Elskaya, A. V.; Levi, R.; Karube, I.; Wulff, G. *Macromolecules* **1998**, *31*, 2137.

(23) Bakker, E.; Pretsch, E. *TrAC Trends Anal. Chem.* **2005**, *24*, 199-207.

(24) D'Orazio, P. *Clin. Chim. Acta* **2003**, *334*, 41-69.

(25) Hutchins, R. S.; Bachas, L. G. *Anal. Chem.* **1995**, *67*, 1654.

(26) Goyal, R. N.; Bishnoi, S. *Indian J. Chem.* **2012**, *51*, 205-225.

(27) Itaya, K.; Bard, A. J. *Anal. Chem.* **1978**, *50*, 1487-1489.

(28) Lennox, J. C.; Murray, R. W. *J. Electroanal. Chem.* **1977**, *78*, 395.

(29) Moses, P. R.; Wier, L.; Murray, R. W. *Anal. Chem.* **1975**, *47*, 1882.

(30) Watkins, B. F.; Behling, J. R.; Karlv, E.; Miller, L. L. *J. Am. Chem. Soc.* **1975**, *97*, 3549.

(31) Liu, C.; Li, F.; Ma, L.-P.; Cheng, H.-M. *Adv. Mater.* **2010**, *22*, 28-62.

(32) Tel-Vered, R.; Willner, I. *Isr. J. Chem.* **2010**, *50*, 321-332.

(33) Potyrailo, R. A.; Surman, C.; Nagraj, N.; Burns, A. *Chem. Rev.* **2011**, *111*, 7315-7354.

(34) Ispas, C. R.; crivat, g.; Andreescu, S. *Anal. Lett.* **2012**, *45*, 168-186.

(35) Chen, S.; Yuan, R.; Chai, Y.; Xu, Y.; Min, L.; Li, N. *Sens. Actuators* **2008**, *135*, 236-244.

(36) Corry, B.; Uilk, J.; Crawley, C. *Anal. Chim. Acta* **2003**, *496*, 103-116.

(37) Pampalakis, G.; Kelley, S. O. *Analyst* **2009**, *134*, 447-449.

(38) Wang, T.; Hu, J.; Kim, J.; Shannon, C.; Easley, C. J. *J. Am. Chem. Soc.* **2012**, *134*, 7066-7072.

(39) Heyduk, E.; Dummit, B.; Chang, Y. H.; Heyduk, T. *Anal. Chem.* **2008**, *80*, 5152-5159.

(40) Kim, D.; Daniel, W. L.; Mirkin, C. A. *Anal. Chem.* **2009**, *81*, 9183-9187.

(41) Konry, T.; Hayman, R. B.; Walt, D. R. *Anal. Chem.* **2009**, *81*, 5777-5782.

(42) Fredriksson, S.; Gullberg, M.; Jarvius, J.; Olsson, C.; Pietras, K.; M.Gustafsdottir, S.; Ostman, A.; Landegren, U. *Nat. Biotechnol.* **2002**, *20*, 473-477.

(43) Kim, J.; Hu, J.; Sollie, R. S.; Easley, C. *Anal. Chem.* **2010**, *82*, 6976-6982.

(44) Hianik, T.; Wang, J. *Electroanalysis* **2009**, *21*, 1223-1235.

(45) Sassolas, A.; Blum, L. J.; Leca_Bouvier, B. D. *Electroanalysis* **2009**, *21*, 1237-1250.

(46) Siqueira, J. R.; Caseli, L.; Crespilho, F. N.; Zucolotto, V. *Biosens. Bioelectron.* **2010**, *25*, 1254-1263.

(47) Gullberg, M.; Gustafsdottir, S. M.; Schallmeiner, E.; Jarvius, J.; Bjarnegard, M.; Betsholtz, C.; Landegren, U.; Fredriksson, S. *Proc. Natl. Acad. Sci. U.S.A* **2004**, *101*, 8420-8424.

(48) Palchetti, I.; Mascini, M. *Anal. Bioanal. Chem.* **2012**, *402*, 3103-3114.

(49) Dulay, S.; Lozano-Sanchez, P.; Iwuoha, E.; Katakis, I.; O'Sullivan, C. K. *Biosens. Bioelectron.* **2011**, *26*, 3852-3856.

(50) Skerra, A. *Curr. Opin. Biotechnol.* **2007**, *18*, 295.

(51) Zhou, J.; Battig, M. R.; Wang, Y. *Anal. Bioanal. Chem.* **2010**, *398*, 24-71.

(52) Kang, D.; Zuo, X.; Yang, R.; Xia, F.; Plaxco, K. W.; White, R. J. *Anal. Chem.* **2009**, *81*, 9109-9113.

(53) Xie, C.; Li, H.; Li, S.; Wu, J.; Zhang, Z. *Anal. Chem.* **2010**, *82*, 241-249.

(54) Chen, P.-Y.; Nien, P.-C.; Wu, C.-T.; Wu, T.-H.; Lin, C.-W.; Ho, K.-C. *Anal. Chim. Acta* **2009**, *643*, 38-44.

(55) Haupt, K.; Mosbach, K. *Chem. Rev.* **2000**, *100*, 2495-2504.

(56) Piletsky, S. A.; Turner, A. P. F. *Electroanalysis* **2002**, *14*, 317-323.

(57) Wang, T.; Shannon, C. *Anal. Chim. Acta* **2011**, *708*, 37-43.

(58) Dickey, F. H. *Proc. Natl. Acad. Sci. U.S.A* **1949**, *35*, 227-229.

(59) Wulff, G. *Angew Chem. Int. Ed.* **1995**, *34*, 1812.

(60) Wulff, G.; Sarhan, A. *Angew Chem. Int. Ed.* **1972**, *11*, 341.

(61) Wulff, G. *Chem. Rev.* **2002**, *102*, 12002.

(62) Maier, N. M.; Lindner, W. *Anal. Bioanal. Chem.* **2007**, *389*, 377-397.

(63) Andersson, L.; Sellergren, B.; Mosbach, K. *Tetrahedron Lett.* **1984**, *25*, 5211.

(64) Avila, M.; Zougagh, M.; Rios, A. *TrAC Trends Anal. Chem.* **2008**, *27*, 54-65.

(65) Ebarvia, B. S.; Binaq, C. A.; Sevilla, F. *Anal. Bioanal. Chem.* **2004**, *378*, 1331-1337.

(66) Ebarvia, B. S.; Cabanilla, S.; Sevilla, F. *Talanta* **2005**, *66*, 145-152.

(67) Kriz, D.; Ramstrom, O.; Svensson, A.; Mosbach, K. *Anal. Chem.* **1995**, *67*, 2142.

(68) Turkewitsch, P.; Wandelt, B.; Darling, G. D.; Powell, W. S. *Anal. Chem.* **1998**, *70*, 2025.

(69) Wu, N.; Feng, L.; Tan, Y.; Hu, J. *Anal. Chim. Acta* **2009**, *653*, 103-108.

(70) Suryanarayanan, V.; Wu, C.-T.; Ho, K.-C. *Electroanalysis* **2010**, *22*, 1795-1811.

(71) Lakshmi, D.; Bossi, A.; Whitcombe, M.; Chianella, I.; Fowler, S. A.; Subrahmanyam, S.; Piletska, E. V.; Piletsky, S. A. *Anal. Chem.* **2009**, *81*, 3576-3584.

(72) Kroger, S.; Turner, A. P. F.; Mosbach, K.; Haupt, K. *Anal. Chem.* **1999**, *71*, 3698-3702.

(73) Kirsh, N.; Hart, J. P.; Bird, D. J.; Luxton, R. W.; McCalley, D. V. *Analyst* **2001**, *126*, 1936.

(74) Gao, B.; Lu, J.; Chen, Z.; Guo, J. *Polymer* **2009**, *50*, 3275-3284.

(75) Yamazaki, T.; Meng, Z.; Mosbach, K.; Sode, K. *Electrochemistry* **2001**, *69*, 969-972.

(76) Syu, M. J.; Chiu, T. C.; Lai, C. Y.; Chang, Y. S. *Biosens. Bioelectron.* **2006**, *22*, 550-557.

(77) Pernites, R.; Ponnapati, R.; Felipe, M. J.; Advincula, R. *Biosens. Bioelectron.* **2011**, *26*, 2766-2771.

(78) Collman, J. P.; Devaraj, N. K.; Chidsey, C. E. D. *Langmuir* **2004**, *20*, 1051-1053.

(79) Collman, J. P.; Devaraj, N. K.; Eberspacher, T. P. A.; Chidsey, C. E. D. *Langmuir* **2006**, *22*, 2457-2464.

(80) Kolb, H. C.; Finn, M. G.; Sharpless, K. B. *Angew Chem. Int. Ed.* **2002**, *40*, 2596-2599.

(81) Im, S. G.; Kim, B.; Lee, L. H.; Tenhaeff, W. E.; Hammond, P. T.; Gleason, K. K. *Macromol. Rapid Commun.* **2008**, *29*, 1648-1654.

(82) Such, G. K.; Quinn, J. F.; Quinn, A.; Tjipto, E.; Caruso, F. *J. Am. Chem. Soc.* **2006**, *128*, 9318-9319.

(83) Mavre, F.; Anand, R. K.; Laws, D. R.; Chow, K.-F.; Chang, B.-Y.; Crooks, J. A.; Crooks, R. M. *Anal. Chem.* **2010**, *82*, 8766-8774.

(84) Chow, K.-F.; Mavre, F.; Crooks, J. A.; Chang, B.-Y.; Crooks, R. M. *J. Am. Chem. Soc.* **2009**, *131*, 8364-8365.

(85) Chow, K.-F.; Mavre, F.; Crooks, R. M. *J. Am. Chem. Soc.* **2008**, *130*, 7544-7545.

(86) Loget, G.; Kuhn, A. *Anal. Bioanal. Chem.* **2011**, *400*, 1691-1704.

(87) Mavre, F.; Chow, K.-F.; Sheridan, E.; Chang, B.-Y.; Crooks, J. A.; Crooks, R. M. *Anal. Chem.* **2009**, *81*, 6218-6225.

(88) Hagg, C. M.; Skyllas-Kazacos, M. *J. Appl. Electrochem.* **2002**, *32*, 1063-1069.

(89) Fleischmann, M.; Ghoroghchian, J.; Rolison, D.; Pons, S. J. *J. Phys. Chem.* **1986**, *90*, 6392-6400.

(90) Ghoroghchian, J.; Pons, S.; Fleischmann, M. *J. Electroanal. Chem.* **1991**, *317*, 101-108.

(91) Cerveramarch, S.; Smotkin, E.; Bard, A. J.; Campion, A.; Fox, M. A.; Mallouk, T.; Webber, S. E.; White, J. M. *J. Electrochem. Soc.* **1988**, *135*, 567-573.

(92) Smotkin, E.; Bard, A. J.; Campion, A.; Fox, M. A.; Mallouk, T.; Webber, S. E. *J. Phys. Chem.* **1986**, *90*, 4604-4607.

(93) Smotkin, E.; Cerveramarch, S.; Bard, A. J.; Campion, A.; Fox, M. A.; Mallouk, T.; Webber, S. E.; White, J. M. *J. Phys. Chem.* **1988**, *91*, 6-8.

(94) Ramakrishnan, S.; Shannon, C. *Langmuir* **2010**, *26*, 4602-4606.

(95) Ulrich, C.; Andersson, O.; Nyholm, L.; Bjorefors, F. *Angew Chem. Int. Ed.* **2008**, *47*, 3034-3036.

(96) Ulrich, C.; Andersson, O.; Nyholm, L.; Bjorefors, F. *Anal. Chem.* **2009**, *81*, 453-459.

(97) Klett, O.; Nyholm, L. *Anal. Chem.* **2003**, *75*, 1245-1250.

(98) Chow, K.-F.; Chang, B.-Y.; Zaccheo, B.; Mavre, F.; Crooks, R. M. *J. Am. Chem. Soc.* **2010**, *132*, 9228-9229.

(99) Arora, A.; Eijkel, J. C. T.; Morf, W. E. *Anal. Chem.* **2001**, *73*, 3282-3288.

(100) Zhan, W.; Alvarez, J.; Crooks, R. M. *J. Am. Chem. Soc.* **2002**, *124*, 13265-13270.

(101) Cao, W.; Ferrance, J. P.; Demas, J.; Landers, J. P. *J. Am. Chem. Soc.* **2006**, *128*, 7572-7578.

(102) Wei, H.; Wang, E. *Luminescence* **2011**, *26*, 77-85.

(103) Miao, W. J.; Choi, J. P.; Bard, A. J. *J. Am. Chem. Soc.* **2002**, *124*, 14478-14485.

(104) Miao, W.; Bard, A. J. *Anal. Chem.* **2003**, *75*, 5825-5834.

(105) McCall, J.; Alexander, C.; Richter, M. M. *Anal. Chem.* **1999**, *71*, 2523-2527.

(106) Geisser, B.; Alsfasser, R. *Inorg. Chim. Acta* **2003**, *344*, 102-108.

(107) Liu, D. K.; Brunschwig, B. S.; Creutz, C.; Sutin, N. *J. Am. Chem. Soc.* **1986**, *108*, 1749-1755.

(108) Ramamoorthy, R.; Dutta, P. K.; Akbar, S. A. *J. Mater. Sci.* **2003**, *38*, 4271-4282.

(109) Martinez, A.; Phillips, S. T.; Whitesides, G. M.; Carrilho, E. *Anal. Chem.* **2012**, *82*, 3-10.

(110) Burtis, C. A.; Ashwood, E. R. *Tietz Textbook of Clinical Chemistry*; Saunders: Philadelphia, PA, 1999.

(111) Rusling, J. F.; Kumar, C. V.; Gutkind, J. S.; Patel, V. *Analyst* **2010**, *135*, 2496-2511.

(112) von-Lode, P. *Clin. Biochem.* **2005**, *38*, 591-606.

(113) Davies, S.; Byrn, F.; Cole, L. A. *Clin. Lab Med.* **2003**, *23*.

(114) Jung, K.; Zachow, J.; Lein, M.; Brux, B.; Sinha, P.; Lenk, S.; Schnorr, D.; Loening, S. A. *Urology* **1999**, *53*, 155-160.

(115) Seamark, D. A.; Backhouse, S. N.; Powell, R. *Ann. Clin. Biochem.* **2003**, *40*, 178-180.

(116) Sorell-Gomez, L.; Rojas, G. *Clin. Chim. Acta* **1997**, *260*, 65-71.

(117) Stivers, C. R.; Baddam, S. R.; Clark, A. L.; Ammirati, E. B.; Irvin, B. R.; Blatt, J. M. *Diabetes Technol. Ther* **2000**, *2*, 517-526.

(118) Luminex Corporation, Technologies and Science, http://www.luminexcorp.com/TechnologiesScience/index.htm December 2011.

(119) Haab, B. B.; Dunham, M. J.; Brown, P. O. *Genome Biol.* **2001**, *2*, 1-5.

(120) Drummond, T. G.; Hill, M. G.; Brton, J. K. *Nature Biotech.* **2003**, *21*, 1192-1199.

(121) Famulok, M. *Curr. Opin. Struct. Biol.* **1999**, *9*, 324-329.

(122) Herr, J. K.; Smith, J. E.; Medley, C. D.; Shangguan, D.; Tan, W. *Anal. Chem.* **2006**, *78*, 2918-2924.

(123) Klussmann, S. *The Aptamer Handbook. Functional Oligonucleotides and Their Applications*; WILEY-VCH Verlag GmbH & Co. KGaA: Weinheim, 2006.

(124) Liu, Y.; Tuleouva, N.; Ramanculov, E.; Revzin, A. *Anal. Chem.* **2010**, *82*, 8131-8136.

(125) Osborne, S. E.; Ellington, A. D. *Chem. Rev.* **1997**, *97*, 349-370.

(126) Shangguan, D.; Li, Y.; Tang, Z.; Cao, Z. C.; Chen, H. W.; Mallikaratchy, P.; Sefah, K.; Yang, C. J.; Tan, W. *Proc. Natl. Acad. Sci. U.S.A* **2006**, *103*, 11838-11843.

(127) Kelley, S. O.; Barton, J. K.; Jackson, N. M.; Hill, M. G. *Bioconjug. Chem.* **1997**, *8*, 31-37.

(128) Fan, C.; Plaxco, K. W.; Heeger, A. *Proc. Natl. Acad. Sci. U.S.A* **2003**, *100*, 9134-9137.

(129) Ferapontova, E. E.; Olsen, E. M.; Gothelf, K. V. *J. Am. Chem. Soc.* **2008**, *130*, 4256-4258.

(130) Zhang, Y. L.; Huang, Y.; Jiang, J. H.; Shen, G. L.; Yu, R. Q. *J. Am. Chem. Soc.* **2007**, *129*, 15448-15449.

(131) Zhang, Y. L.; Pang, P. F.; Jiang, J. H.; Shen, G. L.; Yu, R. Q. *Electroanalysis* **2009**, *21*, 1327-1333.

(132) Bonham, A. J.; Hsieh, K.; Ferguson, B. S.; Vallee-Belisle, A.; Ricci, F.; Soh, H. T.; Plaxco, K. W. *J. Am. Chem. Soc.* **2012**, *134*, 3346-3348.

(133) Lubin, A. A.; Plaxco, K. W. *Acc. Chem. Res.* **2010**, *43*, 496-505.

(134) Rowe, A. A.; Chuh, K. N.; Lubin, A. A.; Miller, E. A.; Cook, B.; Hollis, D.; Plaxco, K. W. *Anal. Chem.* **2011**, *83*, 9462-9466.

(135) Vallee-Belisle, A.; Ricci, F.; Plaxco, K. W. *J. Am. Chem. Soc.* **2012**, *134*, 2876-2879.

(136) Xia, F.; Zuo, X.; Yang, R.; White, R. J.; Xiao, Y.; Kang, D.; Gong, X.; Lubin, A. A.; Vallee-Belisle, A.; Yuen, J. D.; Hsu, B. Y.; Plaxco, K. W. *J. Am. Chem. Soc.* **2010**, *132*, 8557-8559.

(137) Nkodo, A. E.; Garnier, J. M.; Tinland, B.; Ren, H.; Desruisseaux, C.; McCormick, L. C.; Drouin, G.; Slater, G. W. *Electrophoresis* **2001**, *22*, 2424-2432.

(138) Hu, J.; Easley, C. J. *Analyst* **2011**, *136*, 3461-3468.

(139) Millipore Corporation, Human Insulin ELISA, http://www.millipore.com/catalogue/item/ezhi-14k: December 2011.

(140) Mercodia AB, Insulin ELISA, http://www.mercodia.se/index.php?page=productview2&prodId=9: December 2011.

(141) AbCam plc., Insulin Human ELISA Kit - 1×96 Well Plate (ab100578), http://www.abcam.com/Insulin-Human-ELISA-Kit-1-×-96-Well-Plate-ab100578.html: December 2011.

(142) Mercodia AB, Insulin, Ultrasensitive ELISA, http://www.mercodia.se/index.php?page=productview2&prodId=11: December 2011.

(143) Millipore Corporation, Rat/Mouse Insulin ELISA, http://www.millipore.com/catalogue/item/ezrmi-13k: December 2011.

(144) ALPCO Diagnostics, Mouse Ultrasensitive Insulin ELISA, 80-INSMSU-E01, http://www.alpco.com/products/Insulin-Ultrasensitive-Mouse-ELISA.aspx: December 2011.

(145) Rahman, M.; Noh, H.; Shim, Y. *Anal. Chem.* **2008**, *80*, 8020-8027.

(146) El-Hady, D. *Anal. Chim. Acta* **2007**, *593*, 178-187.

(147) Kalinove, J.; Vrchotova, N. *J. Agric. Food. Chem.* **2009**, *57*, 2719-2725.

(148) Veluri, R.; Weir, T.; Bais, H.; Stermitz, F.; Vivanco, J. *J. Agric. Food. Chem.* **2004**, *52*, 1077-1082.

(149) Kaur, R.; Kaur, S.; Callaway, R. *Commun. Integr. Biol.* **2009**, *2*, 127-129.

(150) Bais, H.; Vepachedu, R.; Gilroy, S.; Callaway, R.; Vivanco, J. *Science* **2003**, *301*, 1377-1380.

(151) Pollock, J.; Callaway, R.; Holben, W. *PLos One* **2008**, *3*, 1-11.

(152) Goldberg, D. M.; Tsang, E.; Karumanchiri, A.; Diamandis, E. P.; Soleas, G.; Ng, E. *Anal. Chem.* **1996**, *68*, 1688-1694.

(153) Zeeb, D. J.; Nelson, B. C.; Albert, K.; Dalluge, J. J. *Anal. Chem.* **2000**, *72*, 5020-5026.

(154) Pierce, A. R.; Graham, H. N.; Glassner, S.; Madlin, H.; Gonzalez, J. G. *Anal. Chem.* **1969**, *41*, 298-302.

(155) Watanabe, M.; Ayugase, J. *J. Agric. Food. Chem.* **2009**, *57*, 6438-6442.

(156) Cooper, K. A.; Campos-Gimenez, E.; Alvarez, D. J.; Nagy, K.; Donovan, J. L.; Williamson, G. *J. Agric. Food. Chem.* **2007**, *55*, 2841-2847.

(157) Zhang, K.; Zuo, Y. *J. Agric. Food. Chem.* **2004**, *52*, 222-227.

(158) Kofink, M.; Papagiannopoulos, M.; Galensa, R. *Molecules* **2007**, *12*, 1274-1288.

(159) Roy, J. J.; Abraham, T. E.; Abhijith, K. S.; Kumar, P. V.; Thakur, M. S. *Biosens. Bioelectron.* **2005**, *21*, 206-211.

(160) Gomes, S. A.; Nogueira, J. M.; Rebelo, M. J. *Biosens. Bioelectron.* **2004**, *20*, 1211-1216.

(161) Jarosz-Wilkolazka, A.; Ruzgas, T.; Gorton, L. *Enzyme Microb. Technol.* **2004**, *35*, 238-241.

(162) Xie, C.; Li, H.; Li, S.; Wu, J.; Zhang, Z. *Anal. Chem.* **2010**, *82*, 241-249.

(163) Sergeyeva, T. A.; Slinchenko, O. A.; Gorbach, L. A.; Matyushov, V. F.; Brovko, O. O.; Piletsky, S. A.; Sergeeva, L. M.; Elska, G. V. *Anal. Chim. Acta* **2010**, *659*, 274-279.

(164) Hillberg, A. L.; Brain, K. R.; Allender, C. *J. Adv. Drug Delivery Rev.* **2005**, *57*, 1875-1889.

(165) McNiven, S.; Kato, M.; Levi, R.; Yano, K.; Karube, I. *Anal. Chim. Acta* **1998**, *365*, 69-74.

(166) Li, Y.; Zhou, W.; Yang, H.; Wang, X. *Talanta* **2009**, *79*, 141-145.

(167) Lu, Q.; Chen, X.; Nie, L.; Luo, J.; Jiang, H.; Chen, L.; Hu, Q.; Du, S.; Zhang, Z. *Talanta* **2010**, *81*, 959-966.

(168) Liao, H. P.; Zhang, Z. H.; Li, H.; Nie, L. H.; Yao, S. Z. *Electrochemi. Acta* **2004**, *49*, 4101-4107.

(169) Piacham, T.; Josell, A.; Arwin, H.; Prachayasittikul, V.; Ye, L. *Anal. Chim. Acta* **2005**, *536*, 191-196.

(170) Gonzalez, G. P.; Hernando, P. F.; Alegria, J. S. D. *Biosens. Bioelectron.* **2008**, *23*, 1754-1758.

(171) Moreno-Bondi, M. C.; Navarro-Villoslada, F.; Benito-Pena, E.; .Urraca, J. L. *Anal. Chem.* **2008**, *4*, 316-340.

(172) Chen, P.; Vittal, R.; Nien, P.; Liou, G.; Ho, K. *Talanta* **2010**, *80*, 1145-1151.

(173) Kan, X.; Zhao, Q.; Zhang, Z.; Wang, Z.; Zhu, J. *Talanta* **2008**, *75*, 22-26.

(174) Song, X.; Li, J.; Wang, J.; Chen, L. *Talanta* **2009**, *80*, 694-702.

(175) Richter, A.; Gibson, U. J.; Nowichi, M.; Belbruno, J. *J. Appl. Polym. Sci.* **2006**, *101*, 2919-2926.

(176) Gonzalez, G. P.; Hernando, P. F.; Alegria, J. S. *Anal. Chim. Acta* **2006**, *557*, 179-183.

(177) Yang, X.; Wu, D.; Du, Z.; Li, R.; Chen, X.; Li, X. *J. Agric. Food. Chem.* **2009**, *57*, 3431-3435.

(178) Wang, P.; Hu, W.; Su, W. *Anal. Chim. Acta* **2008**, *615*, 54-62.

(179) Liu, G.; lin, Y. *Anal. Chem.* **2005**, *77*, 5894-5901.

(180) Perry, L. G.; Thelen, G. C.; Ridenour, W. M.; Callaway, R. M.; Paschke, M. W. *J. Chem. Ecol.* **2007**, *33*, 2337-2344.

(181) Wang, Y.; Chen, Q.; Zeng, X. *Biosens. Bioelectron.* **2010**, *25*, 1356-1362.

(182) Bhavsar, K.; Fairchild, A.; Alonas, E.; Bishop, D. K.; La-Belle, J. T.; Sweeney, J.; Alford, T. L.; Joshi, L. *Biosens. Bioelectron.* **2009**, *25*, 506-509.

(183) Hossain, S. M. Z.; Luckham, R. E.; Smith, A. M.; Lebert, J. M.; Davies, L. M.; Pelton, R. H.; Filipe, C. D. M.; Brennan, J. D. *Anal. Chem.* **2009**, *81*, 5474-5483.

(184) Soelberg, S. D.; Stevens, R. C.; Limaye, A. P.; Furlong, C. E. *Anal. Chem.* **2009**, *81*, 2357-2363.

(185) Jane, A.; Dronov, R.; Hodges, A.; Voelcker, N. H. *Trends Biotechnol.* **2009**, *27*, 230-239.

(186) Vaddiraju, S.; Burgess, D. J.; Jain, F. C.; Papadimitrakopoulos, F. *Biosens. Bioelectron.* **2010**, *24*, 1557-1562.

(187) Alexander, C.; Andersson, H. S.; Anderson, L. I.; Ansell, R. J.; Kirsch, N.; Nicholls, I. A.; O'Mahony, J.; Whitcombe, M. J. *J. Mol. Recognit.* **2006**, *19*, 106-180.

(188) Hirayama, K.; Sakai, Y.; Kameoka, K.; Noda, K.; Naganawa, R. *Sens. Actuators B* **2002**, *86*, 20-25.

(189) Dickert, F. L.; Forth, P.; Lieberzeit, P. A.; Voigt, G. *J. Anal. Chem.* **2000**, *366*, 802-806.

(190) Lai, E. P. C.; Fafara, A.; Vander-Noot, V. A.; Kono, M.; Polsky, B. *Can. J. Chem.* **1996**, *76*, 265-273.

(191) Bengtsson, H.; Ross, U.; Andersson, L. I. *Anal. Commun.* **1997**, *34*, 233-235.

(192) Sergeyeva, T. A.; Piletsky, S. A.; Brovko, A. A.; Slinchenko, E. A.; Sergeeva, L. M.; Panasyuk, T. L.; El'Skaya, A. V. *Analyst* **1999**, *124*, 331-334.

(193) Panasyuk-Delaney, T.; Mirsky, V. M.; Ulbricht, M.; Wolfbeis, O. S. *435* **2001**.

(194) Liu, X. Y.; Li, C. Y.; Wang, C. F.; Li, T.; Hu, S. H. *J. Appl. Polym. Sci.* **2006**, *101*, 2222-2227.

(195) Liu, Y.; Song, Q. J.; Wang, L. *Microchem. J.* **2009**, *91*, 222-226.

(196) Rostovtsev, V. V.; Green, L. G.; Fokin, V. V.; Sharpless, K. B. *Angew Chem Int Ed* **2002**, *41*, 2596-2599.

(197) Devaraj, N. K.; Miller, G. P.; Ebina, W.; Kakaradov, B.; Collman, J. P.; Kool, E. T.; Chidsey, C. E. D. *J. Am. Chem. Soc.* **2005**, *127*, 8600-8601.

(198) Zirbs, R.; Kienberger, F.; Hinterdorfer, P.; Binder, W. H. *Langmuir* **2005**, *21*, 8414-8421.

(199) Chang, L.; Li, Y.; Chu, J.; Qi, J.; Li, X. *Anal. Chim. Acta* **2010**, *680*, 65-71.

(200) Zill, A. T.; Zimmerman, S. C. *Isr. J. Chem.* **2009**, *49*, 71-78.

(201) Porter, M. D.; Bright, T. B.; Allara, D. L.; Chidsey, C. E. D. *J. Am. Chem. Soc.* **1987**, *109*, 3559-3568.

(202) Gu, C.; Xu, H.; Park, M.; Shannon, C. *Langmuir* **2009**, *25*, 410-414.

(203) Kantarovich, K.; Tsarfati, I.; Gheber, L. A.; Haupt, K.; Bar, I. *Anal. Chem.* **2009**, *81*, 5686-5690.

(204) Kantarovich, K.; Belmont, A.; Haupt, K.; Bar, I.; Gheber, L. A. *Appl. Phys. Lett.* **2009**, *94*, 194103/1-194103/3.

(205) Kostrewa, S.; Emgenbroich, M.; Klockow, D.; Wulff, G. *Macromol. Chem. Phys.* **2003**, *204*, 481-487.

(206) Gehan, H.; Fillaud, L.; Felidj, N.; Aubard, J.; Lang, P.; Chehimi, M. M.; Mangeney, C. *Langmuir* **2010**, *26*, 3975-3980.

(207) Wang, L.; Tian, Y.; Ran, Q.; Hu, Z.; Xu, J.; Xian, Y.; Ru, P.; Jin, L. *Electrochem. Commun.* **2009**, *11*, 339-342.

(208) Yoo, B. K.; Joo, S. *J. Colloid Interface Sci.* **2007**, *311*, 491-496.

(209) Bard, A. J.; Faulkner, L. R. *Electrochemical Methods: Fundamentals and Applications, 2nd ed.*, 2001.

(210) Peng, J.; Gao, Z. *Anal. Bioanal. Chem.* **2006**, *384*, 1525-1532.

(211) World Health Organization, I. I. P. o. C. S., Health and Safety Guide, 1996, No. 101.

(212) Wilson, R.; Johansson, M. K. *Chem. Commun.* **2003**, *21*, 2710-2711.

(213) Xu, X.; Shreder, K.; Iverson, B. L.; Bard, A. J. *J. Am. Chem. Soc.* **1996**, *118*, 3656-3660.

(214) Ollino, M.; Cherry, W. R. *Inorg. Chem.* **1985**, *24*, 1417-1418.

(215) Navon, G.; Sutin, N. *Inorg. Chem.* **1974**, *13*, 2159-2164.

(216) Demas, J. N.; Addington, J. W. *J. Am. Chem. Soc.* **1976**, *98*, 5800-5806.

(217) Xia, X.; Ding, Z.; Liu, J. *Photochem. Photobiol. A: Chem.* **1995**, *88*, 81-84.

(218) Clark, C. D.; Debad, J. D.; Yonemoto, E. H.; Mallouk, T. E.; Bard, A. J. *J. Am. Chem. Soc.* **1997**, *119*, 10525-10531.

(219) Demas, J. N.; Admson, A. W. *J. Am. Chem. Soc.* **1973**, *95*, 5159-5168.

(220) Keizer, J. *J. Am. Chem. Soc.* **1983**, *105*, 1494-1498.

(221) Eggins, B. R. In *Chem. Sens. Biosens.* 2002, p 53.

(222) Sulub, R.; Martinez-Millan, W.; Smit, M. A. *Int. J. Electrochem. Sci.* **2009**, *4*, 1015-1027.